SEISMIC PERFORMANCE ASSESSMENT

OF

ORTAKÖY V409 VIADUCT

by

Ali Cem ÖZTÜRK

B.S., Civil Engineering, Yıldız Technical University, 2003

Submitted to Kandilli Observatory and Earthquake Research Institute

in partial fulfillment of the requirements for the degree of

Master of Science

Graduate Program in Earthquake Engineering

Boğaziçi University

2007

SEISMIC PERFORMANCE ASSESSMENT

OF

ORTAKÖY V409 VIADUCT

APPROVED BY:

Prof. Dr. M. Nuray Aydınoğlu …….

(Thesis Supervisor)

Prof. Dr. Mustafa Erdik …….

Prof. Dr. Zekeriya Polat …….

DATE OF APPROVAL:

This study is dedicated to my mother, my father and my dear sister. Without their endless support, patience and faith on me, this achievement could not be possible.

ACKNOWLEDGEMENTS

I would like to express my sincere gratitude to Professor M. Nuray AYDINOĞLU for his assistance in the preparation of this thesis. It has been pleasure for me to know and be able to have a chance to work with such a unique engineer.

I would like to thank to Professor Mustafa ERDİK and Professor Zekeriya POLAT for their precious time. I would also like to thank deeply to all the academicians and staff of Earthquake Engineering Department of KOERI.

I wish to express my special thanks to Ph.D candidates Göktürk ÖNEM, U. Utku CELEP and Yavuz KAYA for sharing their knowledge.

My brother Değer ERKEK had an endless support. My dear friends H. Cem YENİDOĞAN, B. Tolga CANDAN, Mustafa K. GÜNAY and Musa BODUROĞLU's valuable interpretations and assistance mean a lot to me.

I am deeply grateful to the Project Manager, Tadahiro KODA and the Chief Engineer, Melih TURFAN of Japan Bridge and Structure Institute, Inc. (JBSI) for their understanding.

I want to express my sincere gratitude to Mine ÇETİN, for her encouragement and endless support during my study, rather than spending time with her.

ABSTRACT

SEISMIC PERFORMANCE ASSESSMENT OF ORTAKÖY V409 VIADUCT

The Ortakoy V409 carries 1st Peripheral Highway and has constructed in 1973. The V409 is the last approach viaduct of First Bosphorous Bridge and has a specific role on transportation of İstanbul. The existing condition, which is investigated on site, clearly shows that there are significiant damages like corrosions and etc. at whole structure due to lack of maintenance. The existing condition of structure has been evaluated by inelastic analysis method. In this dissertation, in part 1 the general descriptions have tried to be explained. In part 2; The existing conditions like dimensions and etc. have stated according to the site investigations and existing drawings. In the following part; the methods that were used in calculations explained. In part 4 the modelling procedure with the appropriate softwares and the loads that were applied in analyses have exhibited. In the final part the conclusions have stated. As a result of the time history analyses, like mentioned above, the viaduct is vulnearable due to deficiencies of ductility and detailing concepts. Existing sections can not resist the shear forces and moments occured during the earthquakes.

ÖZET

ORTAKÖY V409 VİYADÜĞÜNÜN SİSMİK PERFORMANS DEĞERLENDİRMESİ

Birinci Çevre yolunu Boğaziçi Köprüsüne bağlayan Ortaköy V409 viyadüğü 1973 yılında inşaa edilmiştir. Boğaziçi Köprüsüne son bağlantı noktası olan Ortaköy V409 viyadüğü İstanbul için oldukça önemli bir role sahiptir. Sahada yapılan incelemelere göre mevcut durumda yapının tümünde bakımsızlık ve diğer etkiler nedeniyle oluşan korozyon gibi ciddi hasarlar açıkça görülmektedir. Viyadüğün mevcut durumu elastik olmayan çözüm yöntemleri tarafından belirlenmiştir. Bu tezde, Bölüm 1'de viyadükle ilgili genel açıklamalar yapılmaya çalışılmıştır. Bölüm 2'de, mevcut durumda boyut ve benzeri ölçülerin belirlenmesi için saha muayeneleri ve kullanılan çizimler dikkate alınmıştır. Bir sonraki bölümde, hesaplamada uygulanan yöntemler, 4. bölümde ise modelin oluşturulması aşamasında kullanılan uygun bilgisayar programları ile analiz aşamasında etkiyen yükler kısaca açıklanmıştır. Son bölümde ise sonuçlar yer almaktadır. Zaman tanım alanında yapılan doğrusal olmayan çözümleme aşamasında daha öncede belirtildiği gibi V409 viyadüğü zayıftır. Mevcut kesitler, deprem sırasında olusacak olan kesme kuvveti ve momentleri karşılayamamaktadır.

TABLE OF CONTENTS

LIST OF FIGURES

LIST OF TABLES

LIST OF SYMBOLS / ABBREVIATIONS

*A*0	Effective area for torsion
Al	Area of longitudinal reinforcement for torsion
Ash	Area of shear-friction reinforcement
At	Area of transverse reinforcement for torsion
Av	Area of transverse reinforcement in the direction of shear force applied
bw	Width of section
d	Effective section depth
f_c	Compressive strength of concrete
fy	Yield strength of reinforcement
H	Column height
Mn	Nominal flexural strength
Mo	Over-strength moment capacity of plastic hinge
ph	Perimeter of the area within transverse torsion reinforcement
s	Spacing of transverse reinforcement
Td	Design torsion force
Tn	Nominal torsional strength
Vc	Contribution of concrete to shear capacity
Vd	Design shear force
Vn	Nominal shear strength
Vs	Contribution of shear reinforcement to shear capacity

Vsf	Shear-friction capacity
φ	Strength reduction factor
φo	Over-strength factor for plastic hinges
μ	Friction coefficient

ABYYHY	Afet Bölgelerinde Yapılacak Yapılar Hakkında Yönetmelik
ARS	Acceleration Response Spectra
DRS	Displacement Response Spectra
PC	Prestressed concrete
RC	Reinforced concrete

1. INTRODUCTION

1.1. General Description

Earthquakes do not only cause big amount of deaths but also cause financial problems for the countries. Actually, the most dramatic and memorable images of earthquake damages are structural collapses. There are many studies have been done to understand the physical meaning of earthquakes and the behaviors of structures. Many researchers deals with the effects of earthquakes on people and their environment and they have been studying methods of reducing the earthquake induced damages. Over the years, considerable developments have been made in earthquake resistant design of structures. The seismic design requirements in building codes have continued to improve with the help of new studies in this field. Earthquake resistant design has moved from an emphasis on structural strength to emphasis on both strength and ductility. Seismic structural systems must possess significant ductility capacity.

Earthquake disasters were forced engineers to focus on new numerical methods. First of all, conservative methods were preferred to use in the analysis in the past. One of the most common analysis is equivalent earthquake load method. The objective of this method is to apply the dynamic load as a static load to the structure. The static load which has to be applied on structure is found with the help of response spectrum concept. Response spectrum concept have been studied for three or four decades.

Nowadays, by the development of computer technology and increases in engineering knowledge, new analysis methods were established instead of conservative methods. These methods named as inelastic analysis. In the inelastic analysis; a kinematically admissible plastic mechanism is chosen. The mechanism chosen should be such that the necessary overall displacement ductility can be

developed with the smallest inelastic rotation demands with the plastic hinges, parts of a structure intended to remain elastic in all events are designed so that under maximum feasible actions corresponding overstrength in the plastic hinges and inelastic deformations should occur in those regions. The actions originating from plastic hinges are those associated overstrength of these regions. The required strength of all other regions is then in excess of strength demand corresponding to the overstrength relevant plastic hinges.

Bridges are one of the essential elements in transportation projects since the beginning of modern ages. With the evolution of engineering approaches, the design and construction criteria's have changed considerably. As the importance of the parameters 'travel time between two points' and 'continual operation' increased in transportation, it became necessary to design the bridges appropriate to the site characteristics by means of challenging geometries, seismic durability, aesthetic considerations. The simplicity of the bridges has become a challenge in constructional engineering not allowing any design and detailing mistakes. The effects of local soil conditions on ground motions and provide guidance for the development of site-specific design.

Furthermore, damages in bridges can take many forms depending on the ground motion, site conditions, structural configurations and specific details of the bridge. Those different forms of damages have experienced during the past earthquakes. Especially, after 1971 San Fernando earthquake which caused remarkable damage over the highway bridges is a milestone for the specialized bridge engineers. Because of the 1971 San Fernando earthquake, first attempts to make some ductile design and detailing requirements had been applied. Ductile behavior of bridge elements are essential for the design of philosophy. For instance, if the elements are not ductile brittle failure due to deficiencies in shear design can occur. Also it is important to do confinement reinforcements in stems. Usually collapses of bridges are not due to primary damages in superstructure.

Nevertheless, the 1989 Loma Prieta and the 1994 Northridge earthquakes in California and the 1995 Kobe earthquake in Japan which occurred in the urbanized cities and major damage of bridges was observed. Until those earthquakes many of the designs for bridges had been done according to pre-1970 requirements which rely on the working stress methodology. These two earthquake not only caused modifications of seismic design but also made necessary to focus on evaluation and retrofit of existing bridges. Beside sufficient strength capacity beyond elastic limits have to be taken into consideration to evaluate the seismic performance. A capacity design approach is likely to assure predictable and satisfactory inelastic response under conditions for which even sophisticated dynamic analyses techniques can yield no more than crude estimates (Paulay and Priestley, 1993). Retrofitting and performance based design are beyond the scope of this thesis.

Türkiye is located in an active seismic zone and most of the major earthquakes occurred in Turkey have been generated by the North Anatolian Fault (NAF). Because of this reason, the studies that were conducted about mitigating the effects of earthquakes have a significant impacts in Türkiye. Kocaeli (17.08.1999) and the Duzce (12.11.1999) earthquakes occurred in highly populated regions in Türkiye.

Ortaköy V409 viaduct is one of the lifeline highway bridges together with V408 viaduct, connecting first peripheral highway to the 1st Bosphorus bridge. The main purpose of this study is to do the seismic assessment of the V409 regarding to ABYYHY (ABYYHY, 1998). Also it is essential to understand the behavior of the viaduct and make some suggestions to avoid the collapse of V409 viaduct.

2. DESCRIPTION OF THE BRIDGE

2.1. General Information

Ortakoy Viaducts are approaches to The First Bosphorous Bridge which are constructed in 1973 undertaken by the control of General Directorate of Highways. V409, V408 and V411 viaducts are the approach viaducts and located European side of Istanbul. These 3 Viaducts were constructed as two separate frames by expansion joints from the middle and carries very high critical role in 1st Peripheral Highway. Figure 1.1 shows the general locations of the viaducts.

Table 2.1. Ortakoy Viaducts general specifications

Ortakoy V408	9 Spans, Approach Viaduct	414 m (1 Expansion Joint, 16 Piers)
Ortakoy V409	8 Spans, Approach Viaduct	360 m (1 Expansion Joint , 14 Piers)
Ortakoy V411	6 Spans, Approach Viaduct	270 m (1 Expansion Joint , 10 Piers)

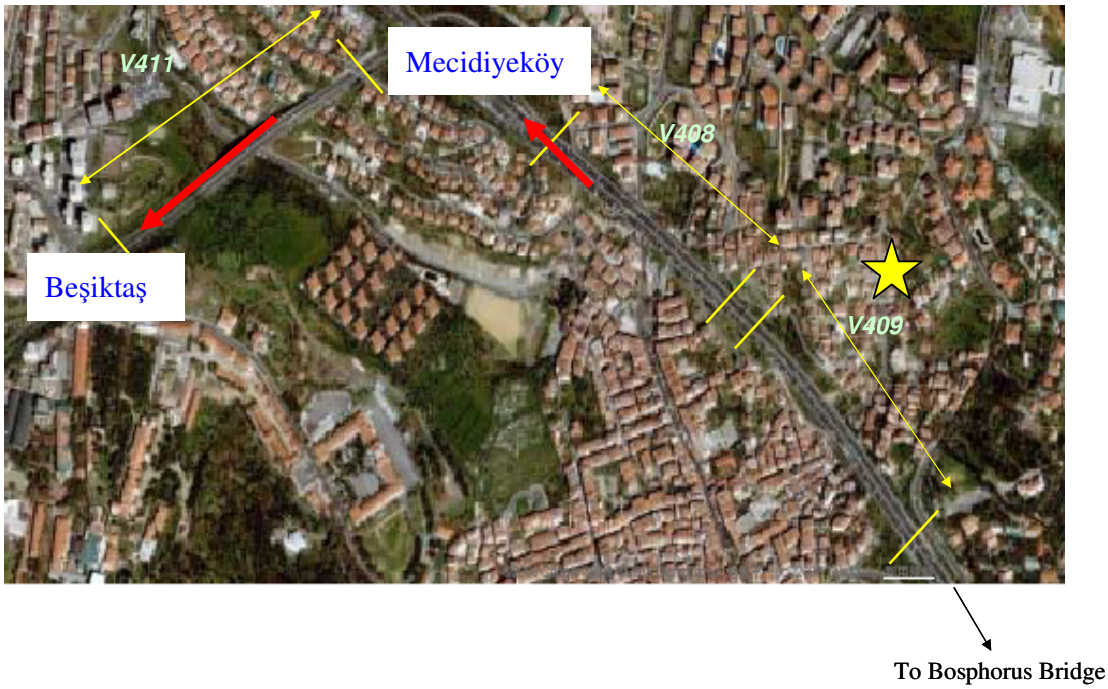

Figure 2.1. Location of Ortakoy Approach Viaducts

2.2. Ortakoy V409 Viaduct Description

Ortakoy V409 carries 1st Peripheral Highway and has constructed in 1973. The viaduct is carrying opposite direction of traffic with 3 lines, crosses Ortakoy in width and supplies the first approach to the First Bosphorus Bridge. Figure 2.1 shows the general view of the viaduct. Structural elements named from Ortakoy Viaduct 408 to First Bosphorus Bridge like A1 (Abutment 1), P1 (Pier 1) , P2, P3, P4, P5, P6, P7 and A2.

The Viaduct is totally 360 m long bridge with prestressed concrete superstructure. Superstructure is consisting of eight equal spans supported by elastomeric bearings, placed under every girder, to the piers and abutments. There are ten prestressed girders in longitudinal direction for each span which are connected by solidarizations to provide continuity and cap beams in each transverse direction axes. Figure 3.17 shows the typical solidarization detail. Length of the each span is 45m. The Viaduct has constructed as two separate frames by expansion joint. Expansion

joint is at Pier 4. Side view, expansion joint, cap beam and typical girder sections stated in Figure 3.7, 3.9, 3.11, 3.12 respectively.

Deck width is 31 meter and it has connected with cast-in-situ concrete plates to the girders with the thickness of 20cm. between girder flanges, as shown in Figure 3.10

Every axis consist of two hollow sectioned pier, total 7 x 2 = 14 Piers. The approximate height of the piers are 8 to 25 meters. Pier sections 1.67-1.86 and 5.12-5.18 meters. All Pier foundations analyzed as two seperate foundation according to the site investigation and existing drawings. Foundation dimensions are about 12m x8m x3m. for all piers. Figure 3.18 shows the typical foundation detail.

Viaduct abutments are seat type named as A1 and A2 according to the existing drawings. The superstructure has connected to the abutment by solidarization similar with the girders. Also, girders supported to the abutment by elastomeric bearings in both sides. Figure 3.6, 5.22 show the abutment.

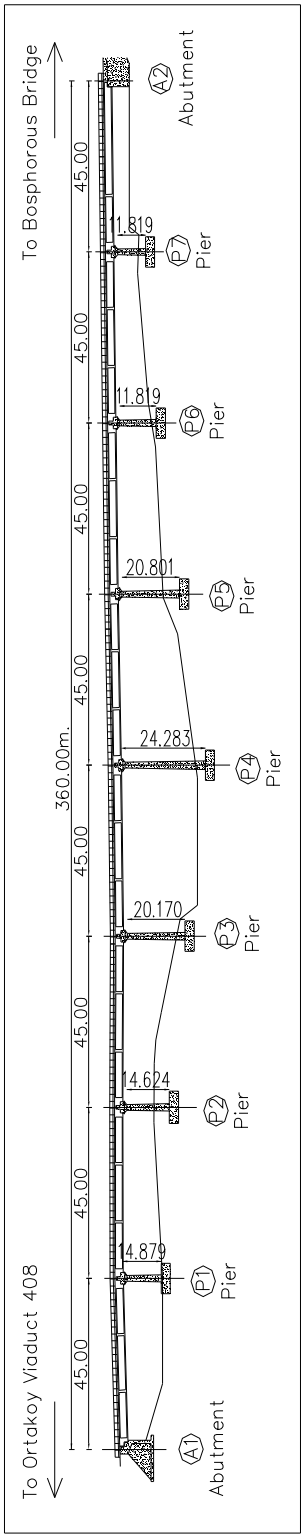

Figure 2.2. Side view drawing of Ortakoy V409 Viaduct

3. EXISTING CONDITION OF ORTAKOY V409 VIADUCT

3.1. Site Investigation

In the analysis, data was used according to the site investigation and existing drawings. The site investigations are necessary to make assumptions during the analysis. In different times; site has been visited, some of existing drawings have been obtained and information was collected. Altough the structure was built 35 years ago, the situation is very bad. Lack of maintenance and other effects cause corrosions at all of the structure. Cracks and diameter losses can be easily observed.

Figure 3.1. Side view picture of Ortakoy V409 Viaduct

Figure 3.2. Corrosion at top of pier

Figure 3.3. Corrosion at cross beam

Figure 3.4. Corrosion at girder side

Figure 3.5. PC beams

Figure 3.6. A2 abutment

3.2. Dimensions of the Viaduct

The dimensions of the viaducts has been taken from the site investigations and existing drawings. Characteristics of the Ortakoy 409 Viaduct shown below.

- Characteristics of the Viaduct

- Span length : 45m.

- Span number: 8

- Pier number : 7

- Total length : 45x8=360m.

- Deck width : 31m.

- Number of girders : 10 at every span

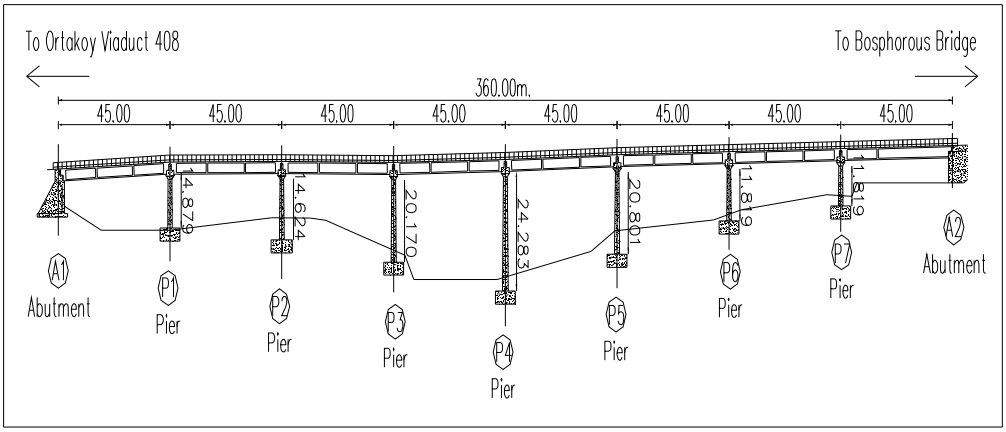

Figure 3.7. Side view drawing

Figure 3.8. There are 10 girders at every span

Figure 3.9. Expansion joint at pier 4

- Dimension of elastomeric bearing : 40x40x8 cm.

- Expansion joint : At P4

- Concrete and Steel classes;

Cap Beam : Concrete Class : B300 (C25)

Re-bar Class : St III (S420)

Pier; Concrete Class : B300 (C25)

Re-bar Class : St I (S220)

3.2.1. Deck

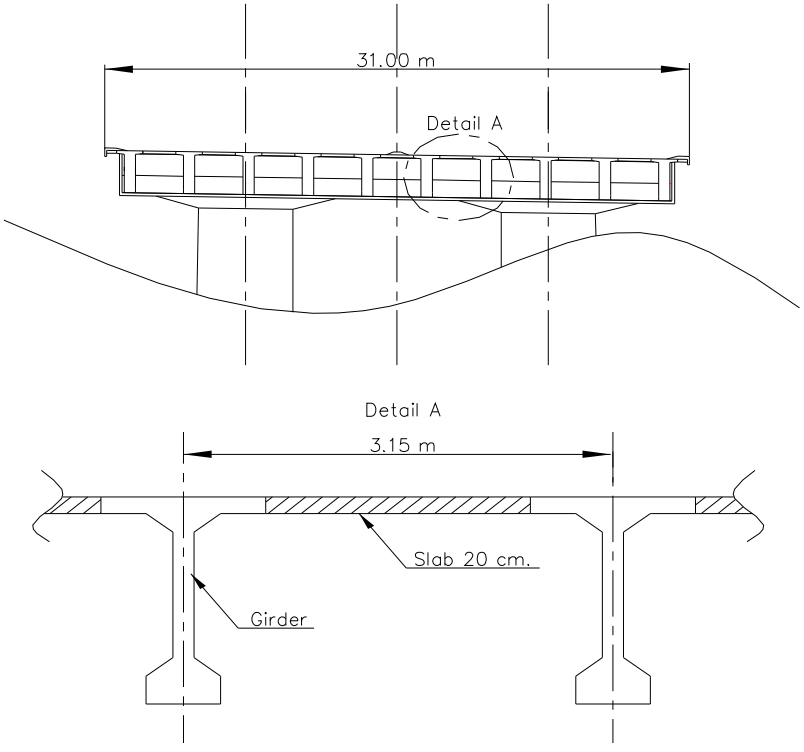

Figure 3.10. Superstructure and slab-girder connection typical section

Deck width is 31 meter and slab has connected with cast-in-situ concrete plates to the girders with the thickness 20cm. between girder flanges.

3.2.2. Cap Beams

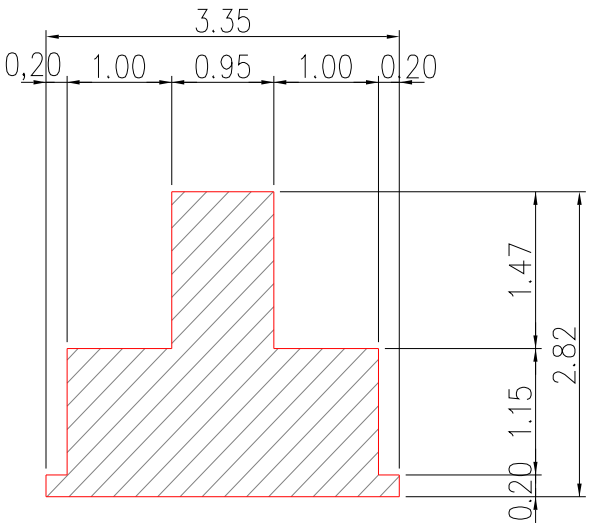

Figure 3.11. Typical cap beam section

3.2.3. Girders

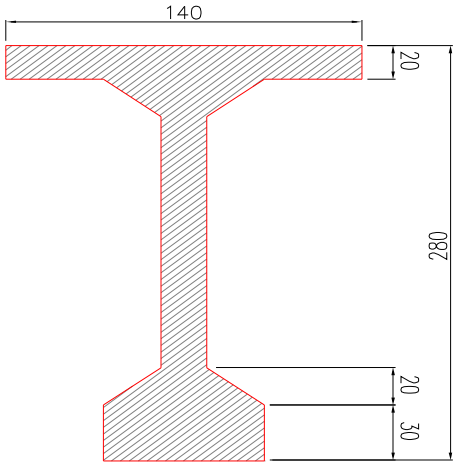

Figure 3.12. Typical girder cross section

3.2.4. Elastomeric Bearings

One of the design tools available to the designer is to isolate the bridge superstructure from the strongest components of ground shaking. A considerable amount of research effort has been directed toward developing effective isolation techniques for both new and existing bridges. Seismic isolation provides the designer with an alternative to the ductile design philosophy and it has a growing importance and novelty in the structures.

Force-deformation of a seismic isolator can be idealized as a bilinear with two key variables: Second slope stiffness and characteristic strength. Moreover, the force deformation relationship can be represented by an effective stiffness based on the secant stiffness and a damping coefficient.

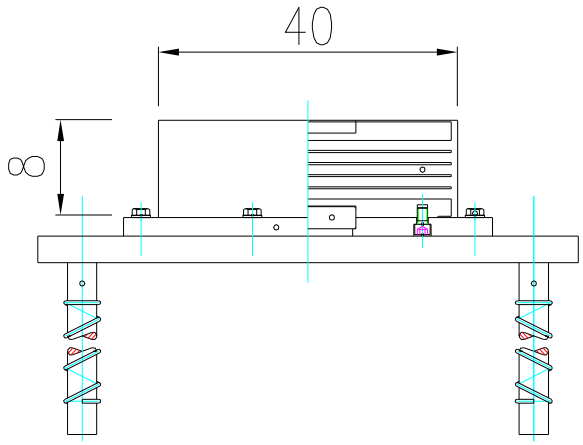

Figure 3.13 Elastomeric bearing

Elastomeric Bearing Dimensions : 40 x 40 x 8cm.

Superstructure consists of equal length spans supported by elastomeric bearings, placed under every girder, to the piers and abutments.

3.2.5. Piers

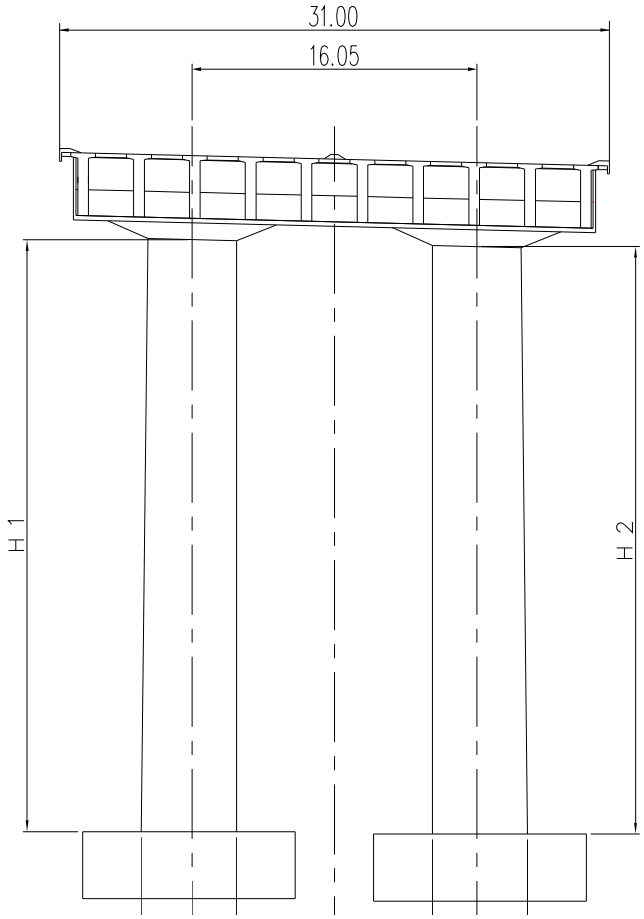

Figure 3.14. Typical pier cross section

Table 3.1. Pier heights

	P1	P2	P3	P4	P5	P6	P7
H1 (m.)	12.82	13.98	20.51	24.05	18.97	12.20	9.05
H2 (m.)	14.88	14.62	20.17	24.28	20.81	11.82	8.18

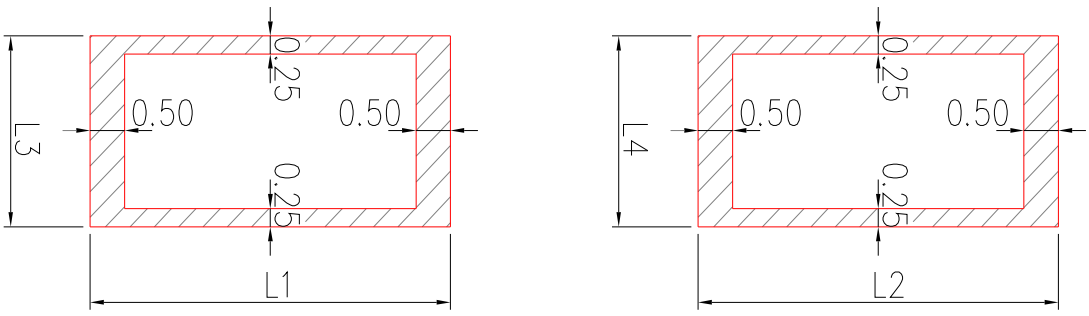

Figure 3.15. Typical pier section

Table 3.2. Pier dimensions

	P1	P2	P3	P4	P5	P6	P7
L1 (m.)	5.12	5.12	5.18	5.14	5.18	5.12	5.12
L2 (m.)	5.12	5.12	5.18	5.14	5.18	5.12	5.12
L3 (m.)	1.67	1.67	1.78	1.86	1.78	1.67	1.67
L4 (m.)	1.67	1.67	1.78	1.86	1.78	1.67	1.67

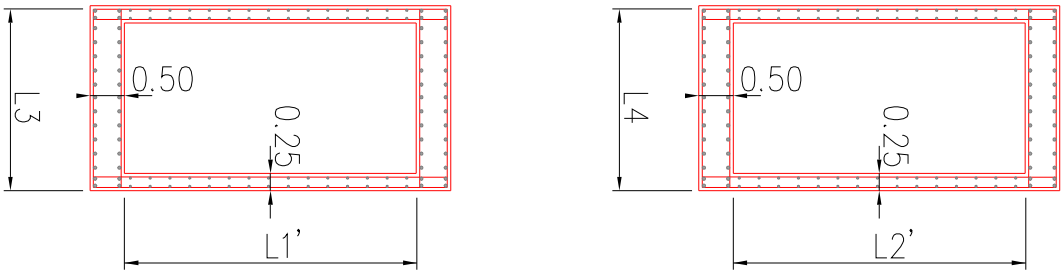

Figure 3.16. Typical re-bar assembling of piers

Table 3.3. Pier rebar (right)

	P1	P2	P3	P4	P5	P6	P7
Level	***Bottom***						
L2'	2x21Φ16	2x21Φ16	2x43Φ18	2x43Φ18	2x43Φ18	2x21Φ16	2x21Φ16
L4	2x21Φ20	2x21Φ20	2x23Φ22	2x25Φ22	2x23Φ22	2x21Φ20	2x21Φ20
Level	***Decreased***						
L2'	2x21Φ16	2x21Φ16	2x22Φ18	2x22Φ18	2x22Φ18	2x21Φ16	2x21Φ16
L4	2x21Φ20	2x21Φ20	2x13Φ22	2x13Φ22	2x13Φ22	2x21Φ20	2x21Φ20
Level	***Top***						
L2'	2x21Φ16	2x21Φ16	2x22Φ18	2x22Φ18	2x22Φ18	2x21Φ16	2x21Φ16
L4	2x11Φ20	2x11Φ20	2x13Φ22	2x13Φ22	2x13Φ22	2x11Φ20	2x11Φ20

Table 3.4. Pier rebar (left)

	P1	P2	P3	P4	P5	P6	P7
Level	***Bottom***						
L1’	2x21Φ16	2x21Φ16	2x43Φ18	2x43Φ18	2x43Φ18	2x21Φ16	2x21Φ16
L3	2x21Φ20	2x21Φ20	2x23Φ22	2x25Φ22	2x23Φ22	2x21Φ20	2x21Φ20
Level	***Decreased***						
L1’	2x21Φ16	2x21Φ16	2x22Φ18	2x22Φ18	2x22Φ18	2x21Φ16	2x21Φ16
L3	2x21Φ20	2x21Φ20	2x13Φ22	2x13Φ22	2x13Φ22	2x21Φ20	2x21Φ20
Level	***Top***						
L1’	2x21Φ16	2x21Φ16	2x22Φ18	2x22Φ18	2x22Φ18	2x21Φ16	2x21Φ16
L3	2x11Φ20	2x11Φ20	2x13Φ22	2x13Φ22	2x13Φ22	2x11Φ20	2x11Φ20

3.2.6. Solidarization

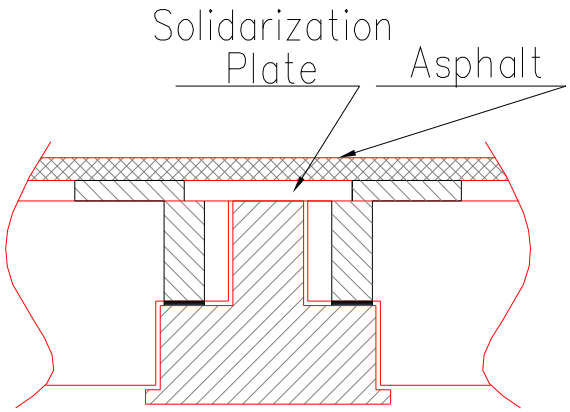

Figure 3.17. Typical solidarization plan

Table 3.5. Solidarization re-bars

	P1	P2	P3	P4	P5	P6	P7
Re-Bar	4Φ32	4Φ32	2Φ32	-	2Φ32	4Φ32	4Φ32
Effective Length (m)	2.50	2.50	2.50	-	2.50	2.50	2.50

3.2.7. Foundations

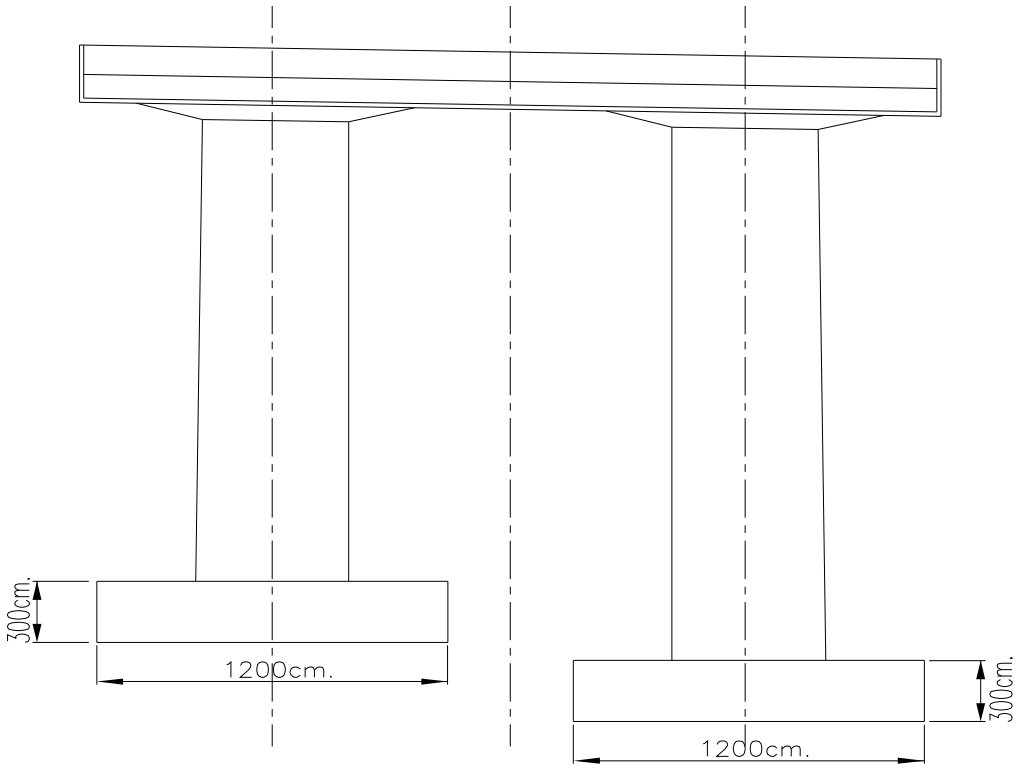

Figure 3.18. Typical foundation

Foundations are separate for each pier. The foundation dimensions are approximately 1200x800x300 for all piers.

4. OVERVIEW OF THE USED MODEL IN THE ANALYSIS

4.1. Response Spectrum Analysis

G. W. Housner was instrumental in the widespread acceptance of the concept of the earthquake response spectrum as a practical means of characterizing ground motions and their effects on structures. Now a central concept in earthquake engineering, the response spectrum provides a convenient means to summarize the peak response of all linear single degree of freedom systems to a particular component of ground motion. It also provides a practical approach to apply the knowledge of structural dynamics to the design of structures and development of lateral force requirements. SDF systems having a fixed damping ratio (ξ), and several such plots for different values of ξ are included to cover the range of damping values encountered in actual structures (Chopra, 1995).

The traditional way to determine the seismic demands to be used in design of bridges is the elastic or modified elastic acceleration response spectrum method, which has many limitations (Priestley, 1995).

Response spectrum analysis is a statistical type of analysis for the determination of the likely response of a structure to seismic loading.

The dynamic equilibrium equations associated with the response of a structure to ground motion are given by :

$$\mathrm{K}\ u(t) + \mathrm{C}\ \dot{u}(t) + \mathrm{M}\ \ddot{u}(t) = m_x\ \ddot{u}_{gx}\ (\mathrm{t}) + m_y\ \ddot{u}_{gy}\ (\mathrm{t}) + m_z\ \ddot{u}_{gz}\ (\mathrm{t})$$

Where K is the stiffness matrix; C is the proportional damping matrix; M is the diagonal mass matrix; u, $\dot{u}$, and $\ddot{u}$ are the relative displacements, velocities and

accelerations with respect to the ground; m_x , m_y and m_z are the unit acceleration loads and $\ddot{u}_{gx}$, $\ddot{u}_{gy}$ and $\ddot{u}_{gz}$ are the components of uniform ground acceleration.

Response spectrum analysis seeks the likely maximum response to these equations rather than the full time history. The earthquake ground acceleration in each direction is given as a digitized response spectrum curve of pseudo-spectral acceleration response versus period of the structure.

Even though accelerations may be specified in three directions, only a single, positive result is produced for each response quantity. These response quantities include displacements, forces and stresses. Each computed result presents a statistical measure of the likely maximum magnitute for that response quantity. The actual response can be expected to vary within a range from this positive value to its negative.

No correspondence between two different response quantities is available. No information is available as to when this extreme value occurs during the seismic loading, or as to what the values of other response quantities are at that time.

Elastic response spectrum analysis (ERSA), including the uniform load method and multimode dynamic analysis method, is a lineer elastic spectral analysis with the appropriate response spectrum and an adequate number of modes considered to capture a minimum of 90% mass participation.

In response spectrum analysis, effective stiffness of the components should be used in order to obtain realistic evaluation of the structure's period and displacement demands. The effective stiffness include the effects of concrete cracking, reinforcement and axial load for concrete components.

For ductile concrete pier members, effective moments of inertia I_{eff} should be based on crack section properties and can be determined from the initial slope of the M-ϕ curve between the origin and the first yield point of the of reinforcement.

For conventionally reinforced concrete box girders superstructures, I_{eff} can be estimated between 0.5 and 0.75 times I_{gross} the moment of inertia of a gross section.

4.1.1. Elastic Design Spectrum

One of the most important applications of the theory of structural dynamics is in analyzing the response of structures to ground shaking caused by an earthquake.

The design spectrum should satisfy certain requirements because it is intended for the design of new structures, or the seismic safety evaluation of existing structures to resist future earthquakes.

The design spectrum should, in a general sense be representative of ground motions recorded at the site during past earthquakes. If none have been recorded at the site the design spectrum should be based on ground motions recorded at other sites under similar conditions. The factors that one tries to match in the selection include the magnitude of the earthquake, the distance of the site from the earthquake fault, the fault mechanism, the geology of the travel path of seismic waves from the source to the site, and the local soil conditions at the site. While this approach is feasible for some parts of the world, such as California and Japan, where numerous ground motion records are available, in many other regions it is hampered by the lack of a sufficient number of such records.

The design spectrum based on statistical analyses of response spectra for the ensemble of ground motions.

4.2. Non-Linear Time History Analysis

In the non linear time history analysis method, an inelastic model of the structure is subjected at least three strong ground motion (ABYYHY, 1998).

The most sophisticated level of analysis available to the designer for the purpose of predicting design forces and displacements under seismic attack is dynamic inelastic time history analysis. This involves stepwise solution in the time domain of the multi-degree-of freedom equations of motion representing the design earthquake. It requires one or more design accelerograms representing the design earthquake. Since spectral response will depend on the strengths and stiffnesses of the various structural elements of the building, which will generally be known at the preliminary stages of a design, it is unsuitable for defining design force levels (Wilson, 2002).

Time History analysis is used to determine the dynamic response of a structure to a arbitrary loading. (Elnashai and McClure, 1996). Response quantities are computed as a function of a time.

For the earthquake time history analysis of bridge models, three analysis tools are available:

1- step-by-step integration in the domain, 2- superposition of normalized modal time histories in the domain and 3- evaluation of frequency dependent response contributions with transformation to and superposition in the domain. Since little design information can be gained from linear elastic time history analyses with a specific earthquake ground motion input. methods 2 and 3, which are in their general form limited to the linear elastic domain due to the inherent reliance on the principle of superposition. (Priestley *et al*., 1996)

The dynamic equilibrium equations to be solved are given by;

$$\mathrm{K}\ u(t) + \mathrm{C}\dot{u}(t) + \mathrm{M}\ \ddot{u}(t) = \mathrm{r}(\mathrm{t});$$

Where K is the stiffness matrix; C is the proportional damping matrix; M is the diagonal mass matrix; u, $\dot{u}$, and $\ddot{u}$ are the relative displacements, velocities and accelerations of the structure and r is the applied load. If the load includes ground acceleration the displacements, velocities and accelerations are relative to this ground motion.

The main value of dynamic inelastic analysis is a research tool, investigating generic rather than specific response . It may also be considerable value in verifying anticipated response of important structures after detailed design to forces and displacements defined by less precise analytical methods (Paulay and Priestley, 1993).

The bridge behavior under seismic excitation should be understood well and a preliminary elastic analysis may be useful to have an idea about the seismic behavior to have a healthy comments on the results. Another but a major problem is the selection of the appropriate accelerograms for nonlinear time history analyses, which are affected by the source mechanism, travel path geology and the local soil conditions. This problem becomes more complicated if a scaling procedure is necessary since there is not an agreement on this subject (Elnashai and McClure, 1996).

5. MODELLING THE VIADUCT

All section dimensions and material specifications has identified by site investigations and existing drawings which are explained in Chapter 3 and Chapter 4.

For the exact behavior of the structure; materials, section capacities and some auxiliary interactions such as Moment-Curvatures and Axial Load-Moment Interactions were calculated in Xtract version 2.6 (XTRACT, 2002). Also, the structure including its all geometrical and numerical features were modeled by SAP2000 Version 10 (SAP2000, 1998).

Modelling process was the crucial stage of this assessment. For instance, every pier, girder and cap beam are defined to the software by mostly the known data. However, sometimes –as mentioned earlier- due to insufficient resources some assumptions were made. Superstructure forming period was also important because of its dense distribution, consisting of two different forms which will be explained in detail at the following stages.

Generally, most conditions were tried to be implemented to the model as exactly they are. It is one of the reasons to find out better results. Nevertheless, this cause some problems such as solving the system, especially during time history analysis.

5.1. Materials

5.1.1. Confined Concrete

For most of the concrete elements, there are transversal reinforcements surrounding the longitudinal ones. These reinforcements can be mostly spiral or rectangular. Thus, even both of them used to surround the longitudinal reinforcement and containing some concrete which remains inside its surrounding zone. This

increase the level of concrete strength.

In addition to that, we have lack of proper data so that the confinement was assumed to be rare.

The section concrete is C25 according to the existing drawings. And Specifications have identified as follows;

28-Day Compressive strength: $f'_c = 25$ Mpa

Tension strength: $f_t = 0$ MPa

Modulus of elasticity: $E_c = 23\ 700$ MPa

Crushing strain: $\varepsilon_{cu} = 0.00643$

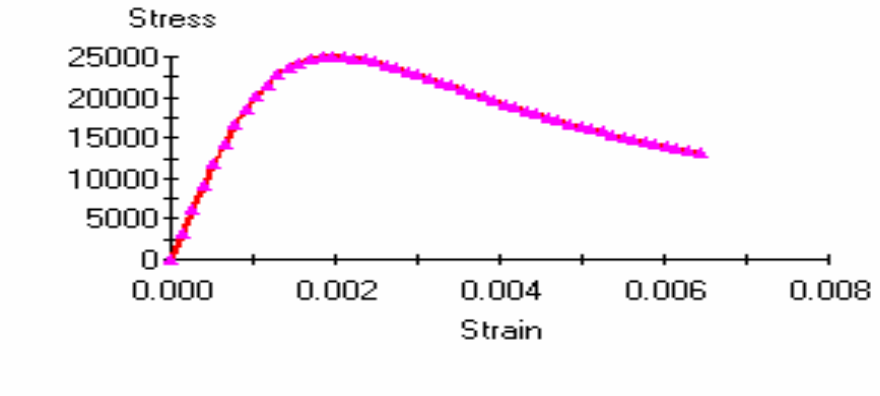

Figure 5.1. Confined concrete Xtract graphic

5.1.2. Unconfined Concrete

In unconfined concrete transverse reinforcement is not used and when an axial load applied on an unconfined section it will act like an element under compression. When the strain value of an unconfined concrete exceeds the strain value that corresponds to its maximum stress the cover section will be crushed and then will be spalled.

The cover concrete is C25 according to the existing drawings. And the thickness of the cover is 5 cm. And the values have taken form the Specifications as follows;

28-Day Compressive Strength: $f'_c = 25$ MPa

Modulus of elasticity: $E_c = 23\ 700$ MPa

Crushing strain: $\varepsilon_{cu} = 0.004$

Spalling strain: $\varepsilon_{sp} = 0.005$

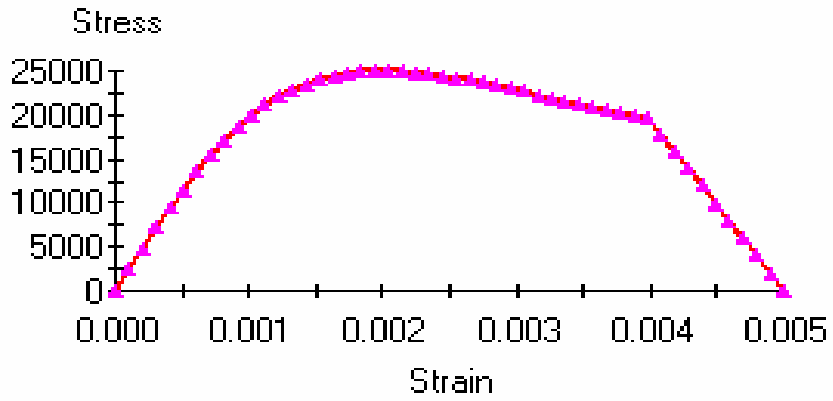

Figure 5.2. Unconfined concrete Xtract graphic

5.1.3. Steel

The steel type is S220 according to the existing drawings. And specifications have identified as follows;

Yield stress: $f_y = 220$ MPa

Fracture stress: $f_{su} = 340$ MPa

Modulus of elasticity: $E_s = 200\ 000$ MPa

Strain at onset of strain hardening: $\varepsilon_{sh} = 0.00115$

Failure strain: $\varepsilon_{su} = 0.015$

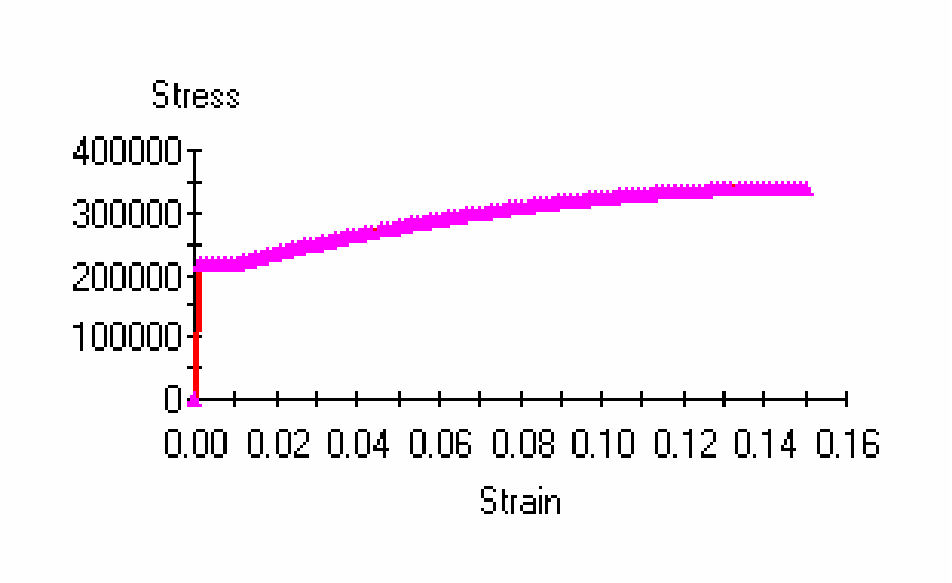

Figure 5.3. Steel Xtract graphic (S 220)

The steel type is S420 according to the existing drawings and specifications have identified as follows;

Yield stress: $f_y = 420$ MPa

Fracture stress: $f_{su} = 500$ MPa

Modulus of elasticity: $E_s = 200\ 000$ MPa

Strain at onset of strain hardening: $\varepsilon_{sh} = 0.008$

Failure strain: $\varepsilon_{su} = 0.09$

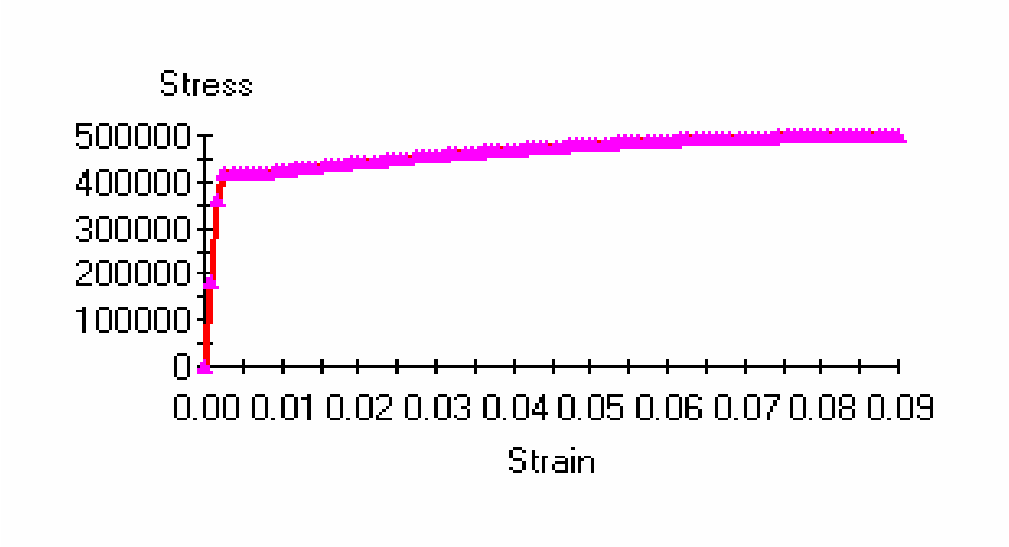

Figure 5.4. Steel Xtract graphic (S 420)

5.2. Superstructure

The superstructure is modeled by using frame elements for decks and girders, shell elements for deck.

There are 7 piers and 8 spans at the viaduct. Every span and cross beam have divided in to 22 pieces in the longitudinal direction, 11 pieces in transverse direction.

5.2.1. Superstructure Weight Calculation

Girder Load = 10 x 0.9264 m^2 x 25 kN/m^3 = 231.6 kN/m

Slab Load = 31 m x 0.20 m x 25 kN/m^3 = 155 kN/m

Border Load = (1.20 m + 1.20 m) x 0.27 m x 25 kN/m^3 = 16.2 kN/m

Asphalt Cover Load = 31 m x 0.06 m x 23 kN/m^3 = 42.78 kN/m

Railing Load = 6 x 1 kN/m = 6 kN/m

Total **= 451.58 kN/m**

Cross beam weight;

(2 x 9) x 2.55 m x 2.42 m x 0.25 m x 25 kN/m^3 = 694.24 kN

For L = 45 m,

W_{DL} = (451.58 kN/m x 45 m) + 694.24 kN = 21015 kN / Span

γ_{GIRDER} = 21015 kN / (0.9264 m^2 x 42.05 m) = 539.50 kN/m^3 per span

In every span there are 10 girders. Thus,

γ_{GIRDER} = 539.50 / 10 = 54 kN/m^3

5.3. Elastomeric Bearings

Elastomeric bearings have been modeled by using nonlinear springs elements

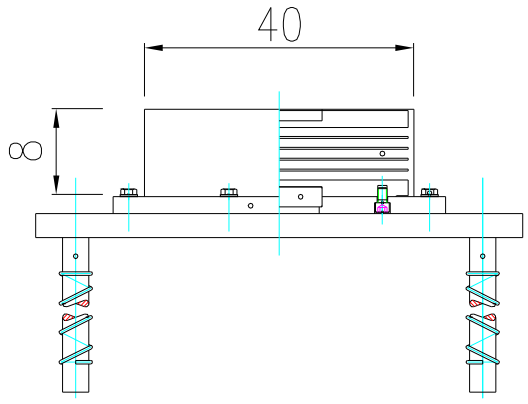

Figure 5.5. Elastomeric bearing

Elastomeric Bearing Dimensions : 40 x 40 x 8cm.

Elastomeric bearings stiffnesses have calculated according to Gumba (Gumba, 2003) which shown below;

$k_b = GA / h_{eff}$

k_b = Elastomeric Bearings

G = Shear Modulus

A = Bearing Area

h_{eff} = Effective Height

Where;

G = Shear Modulus has taken 1.0 MPa.

A = Bearing Area = 0.40 x 0.40 = 0.16

h_{eff} = Effective Height; Has taken 1.5cm lower than the original height of the bearing according to Gumba = 8 – 1.5 = 6.5

So;

$k_b = GA / h_{eff}$ = (1000 x 0.16) / (0.065) = 2462 KN/m.

5.4. Piers

Piers have been modeled by using frame elements. Plastic hinges have assigned on neccessary points. For plastic hinge properties, the sections have defined to the Xtract program (XTRACT, 2002).

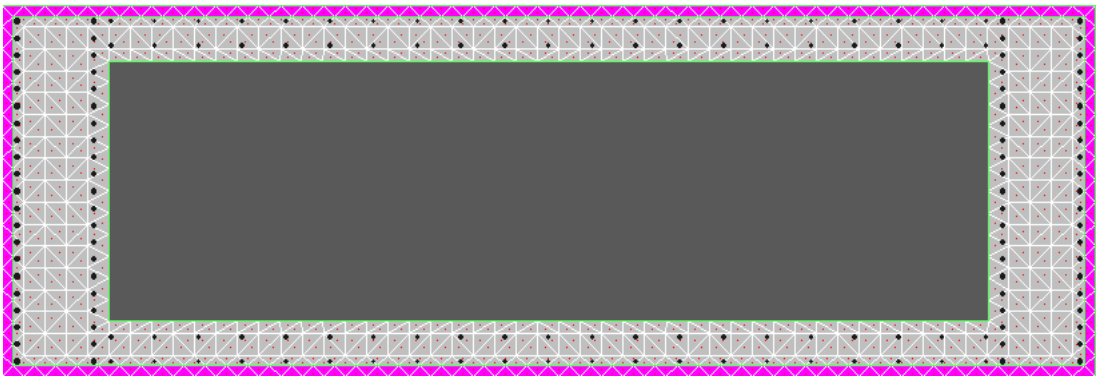

Figure 5.6. Typical pier section Xtract view

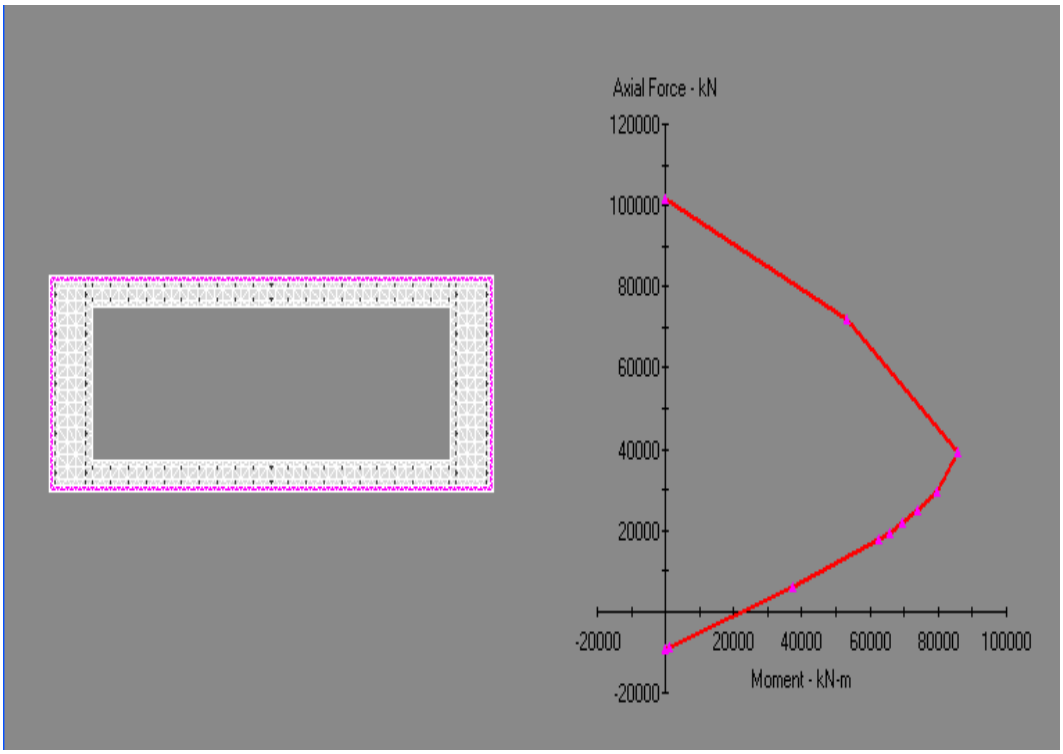

Figure 5.7 Typical pier P-M diagram Xtract view

5.4.1. Plastic Hinge Lengths

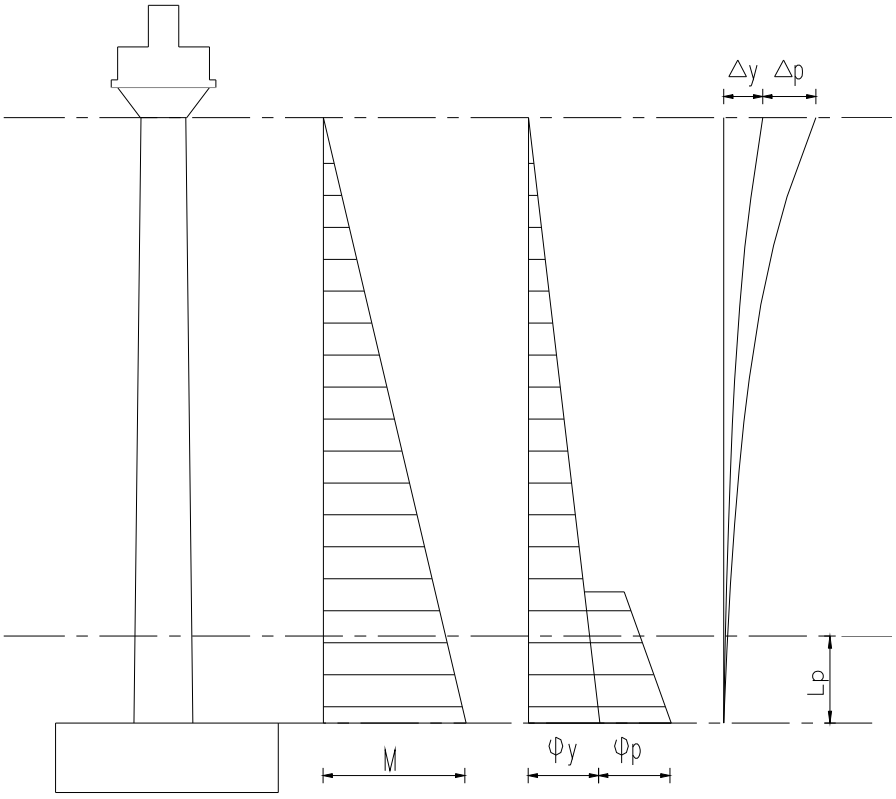

Figure 5.8. Hinge mechanism cantilever systems

Plastic Hinge lengths were calculated due to California Department of Transportation 7.6.2 (Caltrans, 1999) and defined to Sap2000 Program (SAP2000, 1998).

$$L_p = 0.08xL + 0.022xF_{ye}xd_{bl} \geq 0.044xF_{ye}xd_{bl}$$

L : Pier Height

Fye : Yield Strength

Dbl : Re-Bar Diameter

Lp : Hinge Length

Table 5.1. Hinge lengths according to Caltrans

Axis	L	F_{ye}	D_{bl}	$L_{p\ (needed)}$		$L_{p\ (minimum)}$	
	(mm)	(MPa)	(mm)	(mm)		(mm)	
P1-L	**12816**	**220**	**16**	1102,72	≥	154,88	**O.K**
P1-R	**14879**	**220**	**16**	1267,76	≥	154,88	**O.K**
P2-L	**13981**	**220**	**16**	1195,92	≥	154,88	**O.K**
P2-R	**14624**	**220**	**16**	1247,36	≥	154,88	**O.K**
P3-L	**20513**	**220**	**16**	1718,48	≥	154,88	**O.K**
P3-R	**20170**	**220**	**16**	1691,04	≥	154,88	**O.K**
P4-L	**24047**	**220**	**18**	2010,88	≥	174,24	**O.K**
P4-R	**24283**	**220**	**18**	2029,76	≥	174,24	**O.K**
P5-L	**18973**	**220**	**16**	1595,28	≥	154,88	**O.K**
P5-R	**20801**	**220**	**16**	1741,52	≥	154,88	**O.K**
P6-L	**12201**	**220**	**16**	1053,52	≥	154,88	**O.K**
P6-R	**11819**	**220**	**16**	1022,96	≥	154,88	**O.K**
P7-L	**9054**	**220**	**16**	801,76	≥	154,88	**O.K**
P7-R	**8175**	**220**	**16**	731,44	≥	154,88	**O.K**

Table 5.2. Selected hinge lengths

	P1	P2	P3	P4	P5	P6	P7
Lp (m)	1.20	1.20	1.70	2.00	1.70	1.00	0.80

5.4.2. P-M and Moment-Curvature Values

Values have taken from Xtract analysis results and defined to the Sap2000 program. The values shown below ;

All values defined to the excel program and followings graphs have obtained.Most tables and Values enclosed. The changing sections shown as follows.

5.4.2.1. P-M Section-Loading Tables and Diagrams due to Changing Section.

Table 5.3. An example of a P-M table (for P1)

P	Mxx	P	Mxx	Myy	P	Myy
P1267	**P1267**	**P1267**	**P1267**	**P1267**	**P1267**	**P1267**
PM0	PM0	PM45	PM45	PM45	PM90	PM90
kN	kN-m	kN	kN-m	kN-m	kN	kN-m
101,700.00	0.00	101,700.00	0.00	0.00	101,700.00	0.00
68,990.00	20,350.00	76,070.00	4,841.00	40,940.00	71,840.00	53,340.00
41,960.00	30,410.00	36,780.00	7,264.00	77,190.00	39,060.00	85,740.00
34,840.00	29,150.00	23,340.00	7,219.00	66,030.00	29,560.00	79,760.00
31,030.00	27,730.00	15,680.00	7,253.00	53,660.00	24,710.00	73,920.00
28,410.00	26,470.00	10,240.00	7,104.00	43,230.00	21,710.00	69,350.00
26,250.00	25,290.00	6,383.00	6,637.00	35,420.00	19,600.00	65,710.00
24,350.00	24,170.00	3,580.00	6,066.00	29,550.00	17,920.00	62,590.00
10,890.00	15,290.00	-5,287.00	2,447.00	9,958.00	6,198.00	37,190.00
-9,084.00	335.40	-9,470.00	37.31	131.20	-8,995.00	1,314.00
-9,523.00	0.00	-9,523.00	0.00	0.00	-9,523.00	0.00

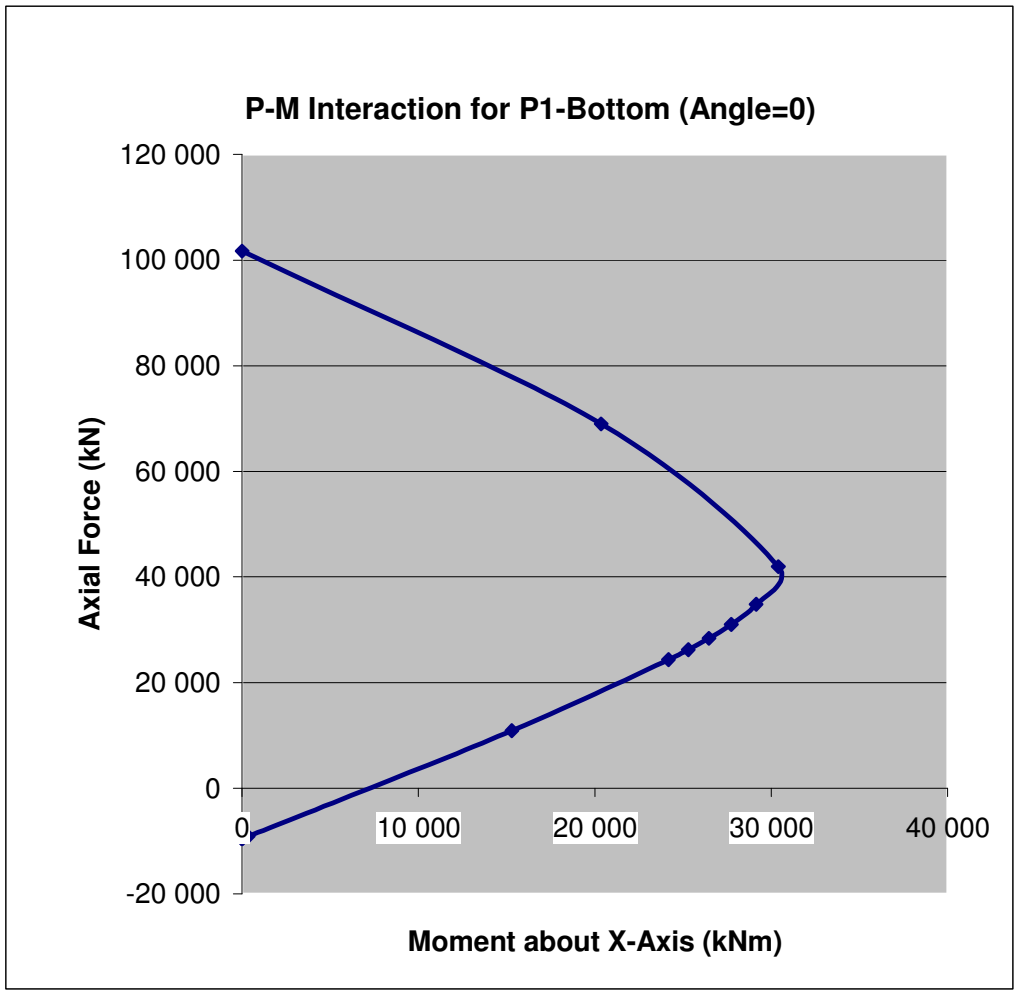

Figure 5.9. P-M graph of P1-bottom section at 0 angle in u1 direction

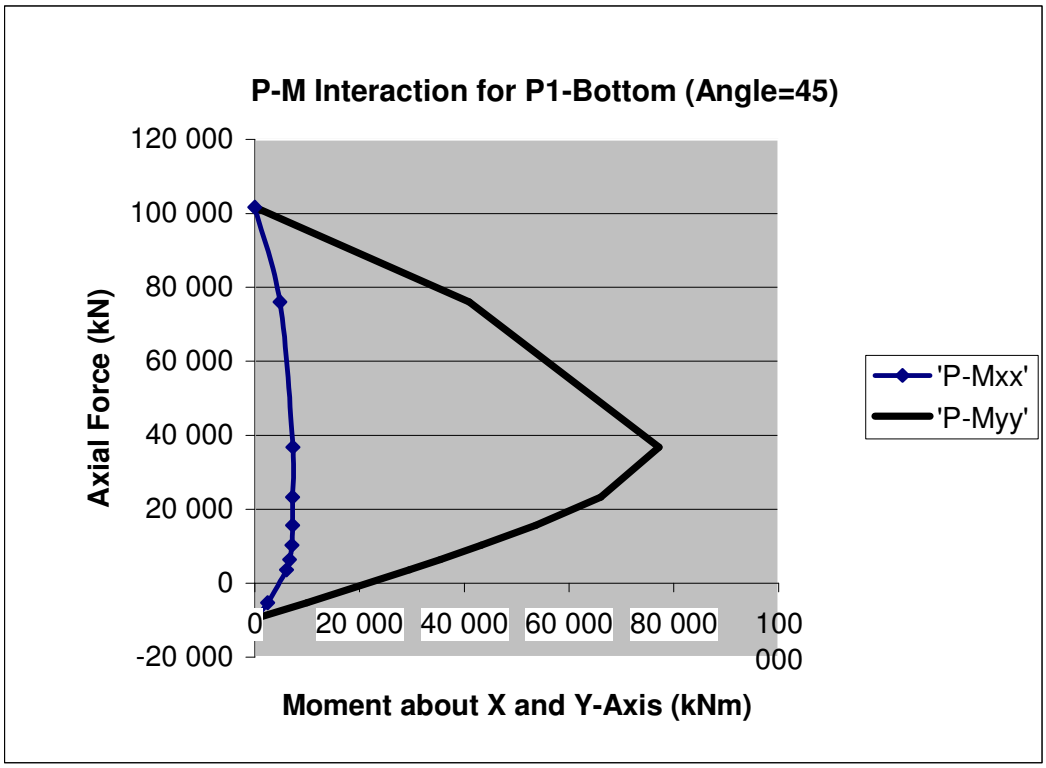

Figure 5.10. P-M graph of P1-bottom section at 45 angle both in u1 and u2

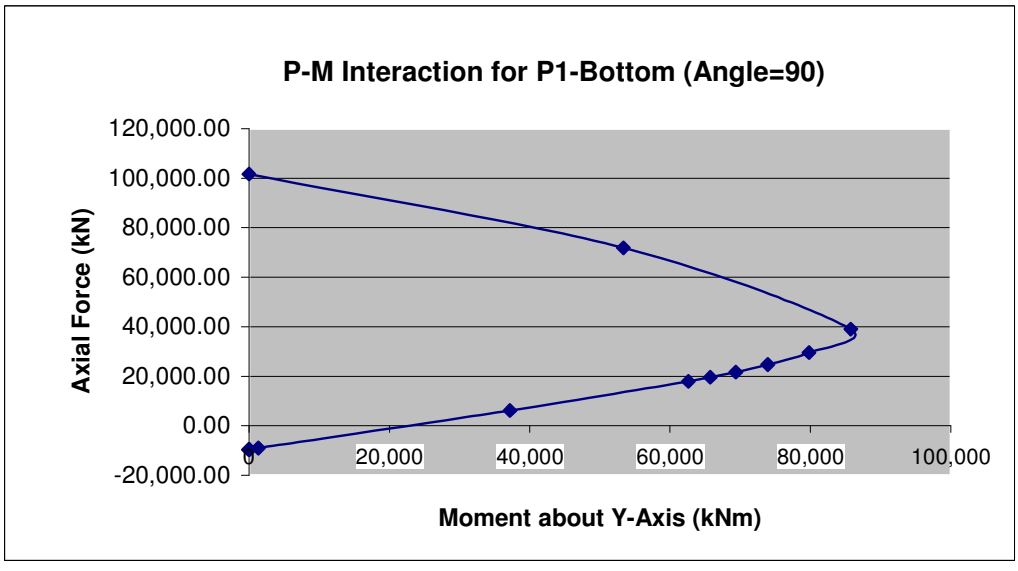

Figure 5.11. P-M graph of P1-bottom section at 90 angle in u2 direction

Table 5.4. An example of a P-M table (for P3)

P	Mxx	P	Mxx	Myy	P	Myy
P3	P3	P3	P3	P3	P3	P3
PM0	PM0	PM45	PM45	PM45	PM90	PM90
kN	kN-m	kN	kN-m	kN-m	kN	kN-m
113,600.00	4.55	113,600.00	4.55	0.00	113,600.00	0.00
77,050.00	25,660.00	85,580.00	6,630.00	45,150.00	80,410.00	60,530.00
43,800.00	40,600.00	39,510.00	10,930.00	88,420.00	41,970.00	100,500.00
35,580.00	39,100.00	22,100.00	10,890.00	76,490.00	29,880.00	94,630.00
31,230.00	37,350.00	12,240.00	10,760.00	61,530.00	23,740.00	87,830.00
28,370.00	35,850.00	5,632.00	10,190.00	49,400.00	19,930.00	82,320.00
26,240.00	34,560.00	1,120.00	9,277.00	40,540.00	17,270.00	77,890.00
24,350.00	33,330.00	-2,160.00	8,339.00	33,830.00	15,190.00	74,100.00
8,993.00	21,850.00	-12,240.00	3,303.00	11,840.00	1,468.00	44,480.00
-16,320.00	748.60	-17,250.00	-50.02	188.70	-16,620.00	1,748.00
-17,320.00	0.00	-17,320.00	0.00	0.00	-17,320.00	0.00

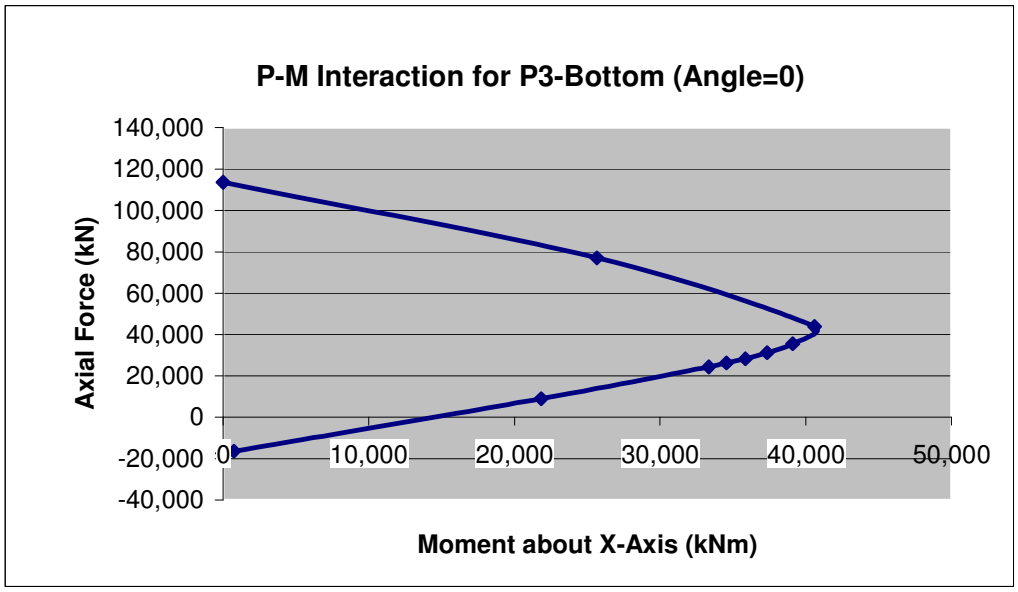

Figure 5.12. P-M graph of P3-bottom section at 0 angle in u1 direction

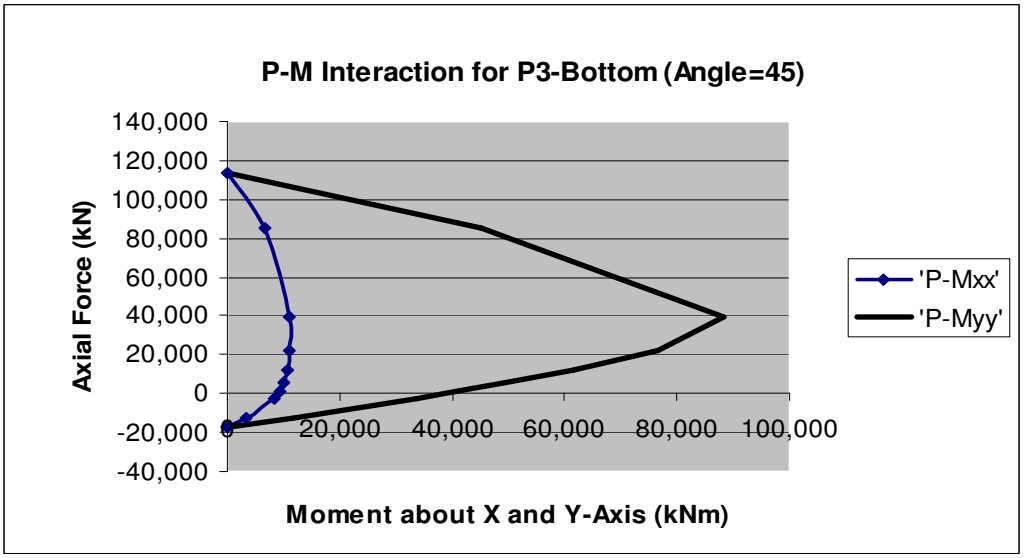

Figure 5.13. P-M graph of P3-bottom section at 45 angle both in u1 and u2

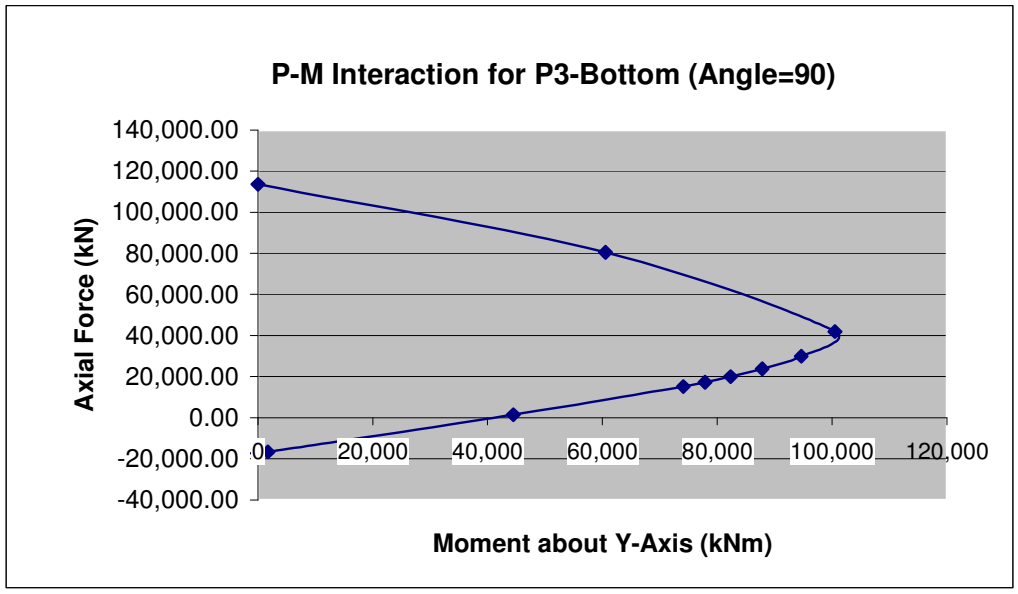

Figure 5.14. P-M graph of P3-bottom section at 90 angle in u2 direction

Table 5.5. An example of a P-M table (for P4)

P	Mxx	P	Mxx	Myy	P	Myy
P4	P4	P4	P4	P4	P4	P4
PM0	PM0	PM45	PM45	PM45	PM90	PM90
kN	kN-m	kN	kN-m	kN-m	kN	kN-m
114,200.00	0.00	114,200.00	0.00	0.00	114,200.00	0.00
77,590.00	25,640.00	86,010.00	6,636.00	45,550.00	80,780.00	61,050.00
43,760.00	40,810.00	39,500.00	10,970.00	89,840.00	41,930.00	101,900.00
35,230.00	39,320.00	22,030.00	10,940.00	77,870.00	29,840.00	96,100.00
30,730.00	37,540.00	12,100.00	10,840.00	62,760.00	23,700.00	89,290.00
27,780.00	36,000.00	5,406.00	10,290.00	50,440.00	19,890.00	83,790.00
25,590.00	34,680.00	807.30	9,403.00	41,380.00	17,230.00	79,360.00
23,630.00	33,410.00	-2,549.00	8,480.00	34,500.00	15,150.00	75,570.00
8,498.00	22,110.00	-12,800.00	3,436.00	12,100.00	1,311.00	45,690.00
17,000.00	857.50	-17,920.00	55.13	172.70	-17,230.00	1,900.00

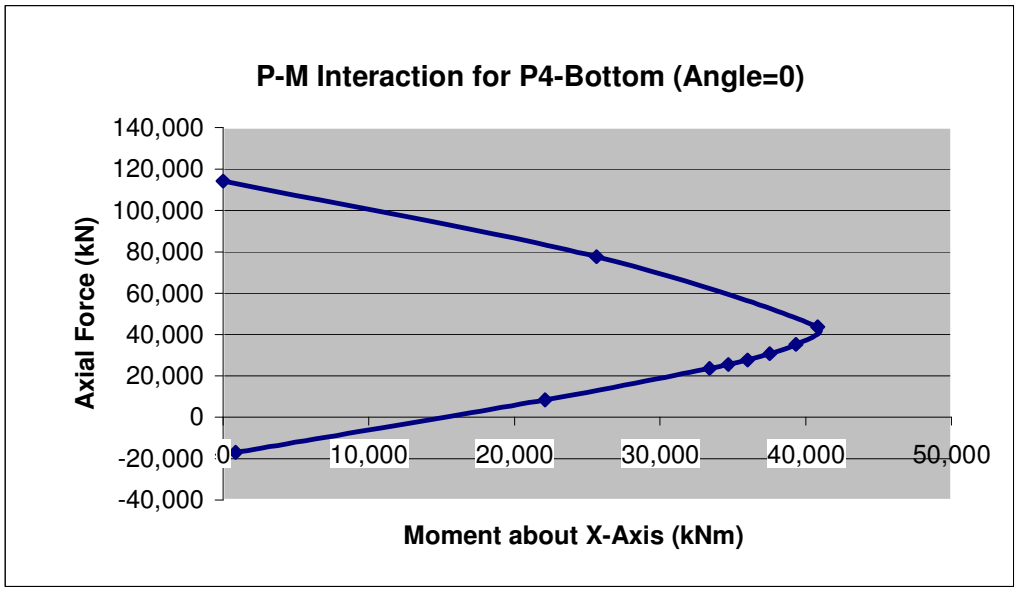

Figure 5.15. P-M graph of P4-bottom section at 0 angle in u1 direction

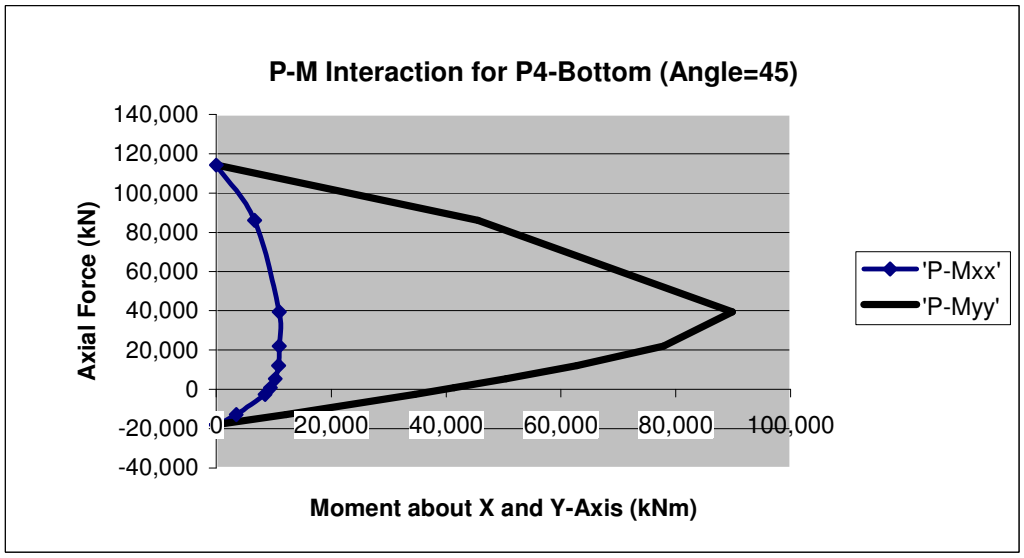

Figure 5.16. P-M graph of P4-bottom section at 45 angle both in u1 and u2

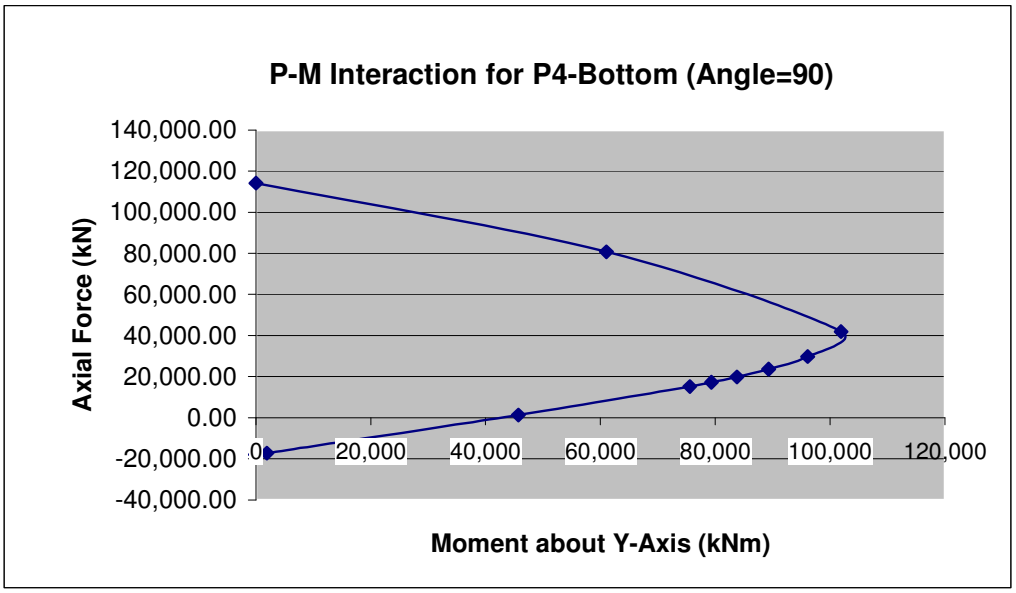

Figure 5.17. P-M graph of P4-bottom section at 90 angle in u2 direction

5.4.2.2. Moment-Curvature Tables and Diagrams due to Changing Section.

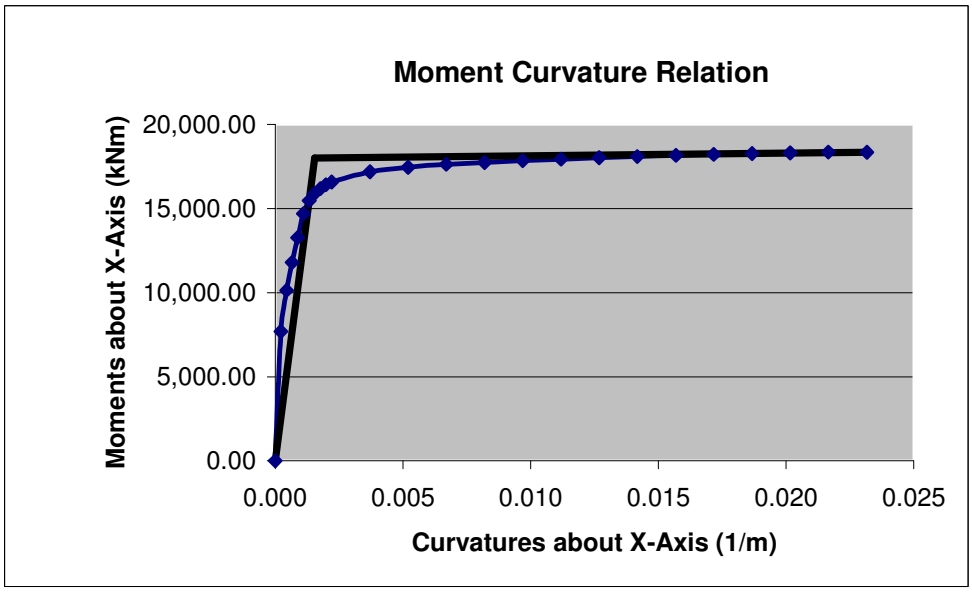

Figure 5.18. Moment-Curvarture of P1-bottom about x-axis (1/m)

Table 5.6. Moment-Curvature values in u1 and u2 directions for p1-bottom

Kxx	**Mxx**	**Kyy**	**Myy**
P1267	P1267	P1267	P1267
Kxx-M33	Mxx-M33	Myy-M22	Myy-M22
1/m	kN-m	1/m	kN-m
0.0000	0	0.0000	0
0.0002	7,691.00	0.0001	20,860.00
0.0004	10,140.00	0.0001	29,280.00
0.0007	11,790.00	0.0002	35,090.00
0.0009	13,280.00	0.0003	40,220.00
0.0011	14,700.00	0.0004	45,080.00
0.0013	15,460.00	0.0004	47,550.00
0.0015	15,890.00	0.0005	48,840.00
0.0018	16,190.00	0.0006	49,780.00
0.0020	16,410.00	0.0006	50,520.00
0.0022	16,580.00	0.0007	51,060.00
0.0037	17,190.00	0.0010	52,500.00
0.0052	17,450.00	0.0013	53,200.00
0.0067	17,630.00	0.0016	53,620.00
0.0082	17,740.00	0.0019	53,890.00
0.0097	17,840.00	0.0022	54,080.00
0.0112	17,930.00	0.0025	54,230.00
0.0127	18,020.00	0.0028	54,360.00
0.0142	18,090.00	0.0031	54,560.00
0.0157	18,160.00	0.0034	54,760.00
0.0172	18,220.00	0.0037	54,980.00
0.0187	18,270.00	0.0040	55,160.00
0.0202	18,310.00	0.0043	55,330.00
0.0217	18,360.00	0.0046	55,490.00
0.0232	18,340.00	0.0067	56,460.00

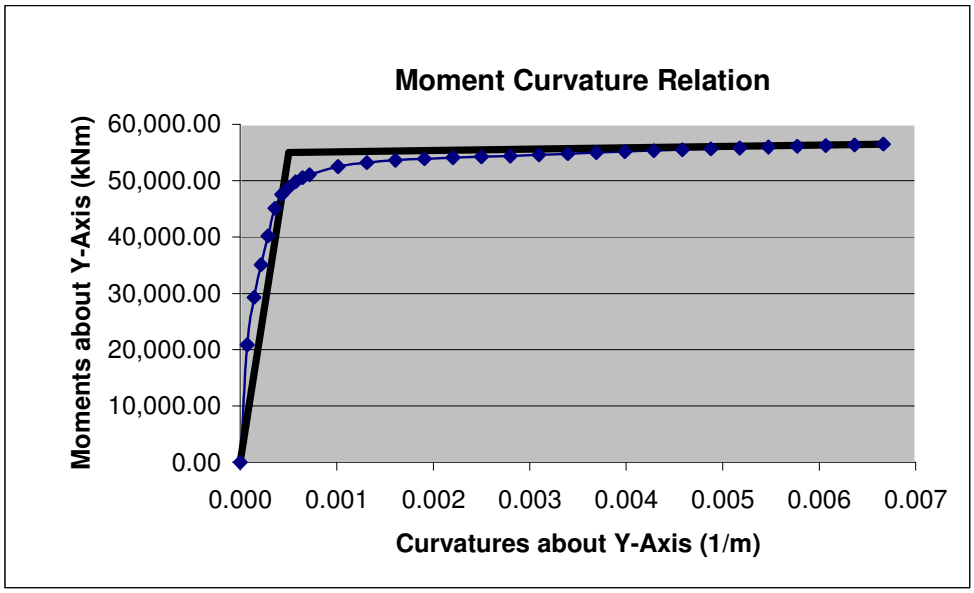

Figure 5.19. Moment-Curvarture of P1-bottom about y-axis (1/m)

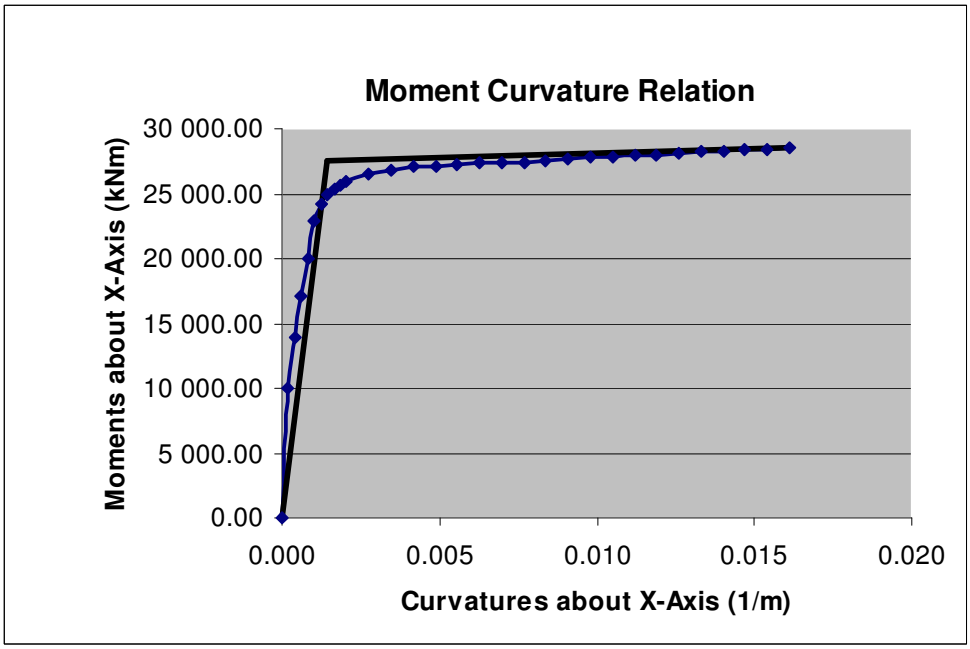

Figure 5.20. Moment-Curvature of P3-bottom about x-axis (1/m)

Table 5.7. Moment-Curvature values in u1 and u2 directions for p3-bottom

Kxx	**Mxx**	**Kyy**	**Myy**
P3	P3	P3	P3
Mxx-M33	Mxx-M33	Myy-M22	Myy-M22
1/m	kN-m	1/m	kN-m
0.0000	0	0.0000	0
0.0002	9,986.00	0.0001	26,060.00
0.0004	13,930.00	0.0002	37,980.00
0.0006	17,080.00	0.0002	46,690.00
0.0008	20,050.00	0.0003	54,600.00
0.0010	22,940.00	0.0004	62,150.00
0.0012	24,240.00	0.0005	66,710.00
0.0014	24,880.00	0.0005	69,450.00
0.0016	25,340.00	0.0006	71,450.00
0.0019	25,680.00	0.0007	72,980.00
0.0021	25,940.00	0.0008	74,100.00
0.0028	26,510.00	0.0009	75,850.00
0.0035	26,830.00	0.0011	77,030.00
0.0042	27,040.00	0.0013	77,850.00
0.0049	27,170.00	0.0014	78,460.00
0.0056	27,270.00	0.0016	78,900.00
0.0063	27,340.00	0.0018	79,210.00
0.0070	27,400.00	0.0019	79,460.00
0.0077	27,460.00	0.0021	79,660.00
0.0084	27,550.00	0.0023	79,790.00
0.0091	27,660.00	0.0024	79,880.00
0.0098	27,760.00	0.0026	79,930.00
0.0105	27,860.00	0.0028	79,950.00
0.0112	27,960.00	0.0029	79,960.00
0.0119	28,040.00	0.0031	79,940.00
0.0126	28,130.00	0.0033	79,910.00
0.0133	28,210.00	0.0034	79,820.00
0.0140	28,280.00	0.0036	79,650.00
0.0161	28,490.00	0.0038	79,310.00

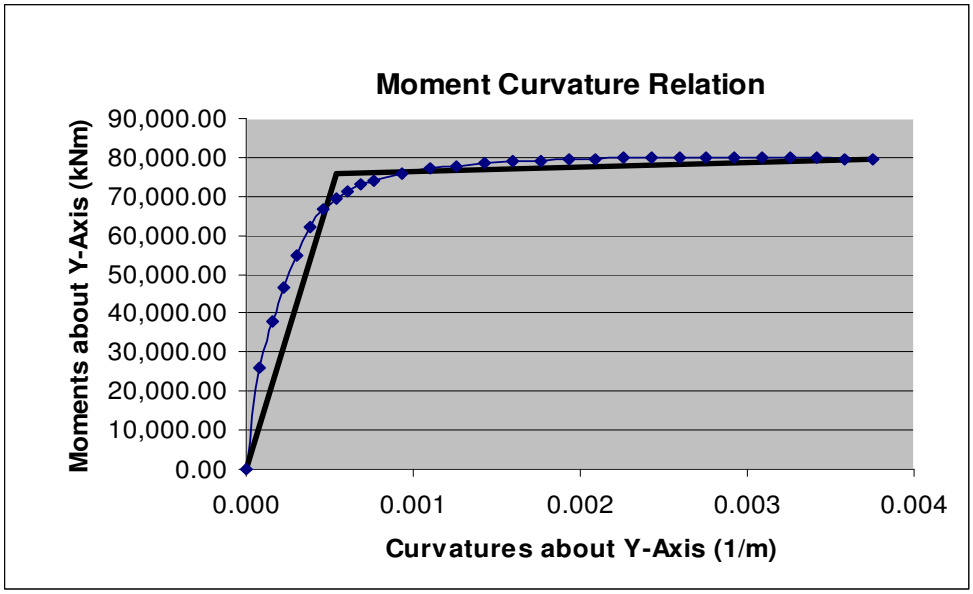

Figure 5.21. Moment-Curvature of P3-bottom about y-axis (1/m)

5.5. Solidarizations

Solidarization rebars have been modeled by using nonlinear springs (plastic (wen)).

It is assumed that full lengths of the solidarization rebars can not be effective while transferring stresses to the deck slab concrete. This is called the shear lag effect, which results in decreasing stresses with increasing distance from the side of the deck slab. Hence effective lengths are used in the calculation of axial stiffness of rebars (Celep, 2001).

As stated in Section-X the number of solidarization rebars anchoraged to girder flanges and to slabs between girders decrease with increasing distance from the abutments.Each rebar group is represented with a single nonlinear spring including the number of rebars in the group. Axial stiffness (k_r) and yield strengths (P_y) of rebar groups can be calculated by using:

$$k_r = \frac{nEA}{L_{eff}}$$

$$P_y = nf_yA$$

E : Young's modulus of steel = 210000 MPa

n : Number of rebars = 2, 4

A: Re-bar area = Ø32, 8.04 cm^2

L_{eff} : Effective length = 250 cm

f_y : Yield Stress 420, 500 MPa

k_1 = 4 x ((210000 x 8,04) / 250) x 10^1 = 270144 kN/m

k_2 = 2 x ((210000 x 8,04) / 250) x 10^1 = 135072 kN/m

For non-linear case;

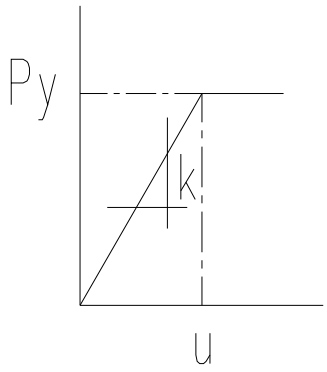

Post yield stiffness = 0.001

Yield exponent = 20 - 30

S420 ;

$Py_1 = 4 \times 420 \times 8{,}04 \times 10^2 \times 10^{-3} = 1350{,}72$ kN

U = 2.50 x 0,002 = 0,005 m

$k_1 = 1350{,}72 / 0{,}005 = 270144$ kN/m

$Py_2 = 2 \times 420 \times 8{,}04 \times 10^2 \times 10^{-3} = 675{,}36$ kN

U = 2.50 x 0,002 = 0,005 m

$k_2 = 675{,}36 / 0{,}005 = 135072$ kN/m

S500 ;

$Py_1 = 4 \times 500 \times 8{,}04 \times 10^2 \times 10^{-3} = 1608$ kN

U = 2.50 x 0,002 = 0,005 m

$k_1 = 1608 / 0{,}005 = 321600$ kN/m

$Py_2 = 2 \times 500 \times 8{,}04 \times 10^2 \times 10^{-3} = 804$ kN

U = 2.50 x 0,002 = 0,005 m

$k_2 = 804 / 0{,}005 = 160800$ kN/m

5.6. Abutments

Abutments have been modeled by using fictive frame elements have with nonlinear springs, combined to the girders with the connection through four bars (solidarization) with diameters of 32 mm. According to the existing drawings ; yield and ultimate strengths of the rebars are 500 MPa and 550 MPa respectively.

Figure 5.22. Abutment

5.7. Determining Earthquake Data

Before even the structural form of the bridge is determined, the designer should consider the constraints imposed by site seismicity. Potential for liquefaction, slumping of existing or modified slopes, ground dislocation if the bridge crosses an existing fault, geographical amplification of ground motion and potential for nosynchronous motion should be determined (Priestley *et al.*, 1996).

Table 5.8. The characteristics of Kocaeli, Landers, Cape Mendocino, Westmorland, Loma Prieta and North Palm Springs earthquakes

1)

Kocaeli, Turkey 1999/08/17	**Station: Arcelik**
Magnitude: M (7.4) Ml ( ) Ms (7.8)	Data Source: KOERI
Distance (km):	Site conditions:
Closest to fault rupture (17.0)	Geomatrix or CWB (B)
Hypocentral ( )	USGS (B)
Closest to surface projection of rupture (17.0)	

	Selected Component

Record/Component	HP (Hz)	LP (Hz)	PGA (g)	PGV (cm/s)	PGD (cm)
KOCAELI/ARCDWN	0.08	50	0.086	8.6	5.52
KOCAELI/ARC000	0.07	50	0.218	17.7	13.64
KOCAELI/ARC090	0.04	50	0.149	39.5	35.57

2)

Kocaeli, Turkey 1999/08/17	**Station: Goynuk**
Magnitude: M (7.4) Ml ( ) Ms (7.8)	Data Source: ERD
Distance (km):	Site conditions:
Closest to fault rupture (35.5)	Geomatrix or CWB (B)
Hypocentral ( )	USGS ( )
Closest to surface projection of rupture (35.5)	

Record/Component	HP (Hz)	LP (Hz)	PGA (g)	PGV (cm/s)	PGD (cm)
KOCAELI/GYN-UP	0.1	30	0.114	11.5	7.59
KOCAELI/GYN000	0.15	30	0.132	8.8	3.05
KOCAELI/GYN090	0.1	25	0.119	10.5	3.94

3)

Landers 1992/06/28 11:58	**Station: 12149 Desert Hot Springs**
Magnitude: M (7.3) Ml ( ) Ms (7.4)	Data Source: CDMG
Distance (km):	
Closest to fault rupture (23.2)	Geomatrix or CWB (D)
Hypocentral ( )	USGS (B)
Closest to surface projection of rupture (22.5)	

Record/Component	HP (Hz)	LP (Hz)	PGA (g)	PGV (cm/s)	PGD (cm)
LANDERS/DSP-UP	0.07	23	0.167	9.9	3.71
LANDERS/DSP000	0.07	23	0.171	20.2	13.87
LANDERS/DSP090	0.07	23	0.154	20.9	7.78

4)

Cape Mendocino 1992/04/25 18:06	Station: 89486 Fortuna - Fortuna Blvd
Magnitude: M (7.1) Ml ( ) Ms (7.1)	Data Source: CDMG
Distance (km):	Site conditions:
Closest to fault rupture (23.6)	Geomatrix or CWB (D)
Hypocentral ( )	USGS (B)
Closest to surface projection of rupture (13.7)	

	Selected Component

Record/Component	HP (Hz)	LP (Hz)	PGA (g)	PGV (cm/s)	PGD (cm)
CAPEMEND/FOR-UP	0.07	23	0.049	5.8	3.72
CAPEMEND/FOR000	0.07	23	0.116	30	27.59
CAPEMEND/FOR090	0.07	23	0.114	21.7	12.79

5)

Westmorland 1981/04/26 12:09	Station: 5051 Parachute Test Site
Magnitude: M (5.8) Ml (5.6) Ms ( )	Data Source: USGS
Distance (km):	Site conditions:
Closest to fault rupture ( )	Geomatrix or CWB (D)
Hypocentral (24.1)	USGS (B)
Closest to surface projection of rupture ( )	

Record/Component	HP (Hz)	LP (Hz)	PGA (g)	PGV (cm/s)	PGD (cm)
WESTMORL/PTS-UP	0.35	35	0.157	11.2	1.78
WESTMORL/PTS225	0.1	30	0.242	39.2	26.88
WESTMORL/PTS315	0.1	33	0.155	26.6	12.97

6)

Loma Prieta 1989/10/18 00:05	Station: 57504 Coyote Lake Dam (Downst)
Magnitude: M (6.9) Ml ( ) Ms (7.1)	Data Source: CDMG
Distance (km):	Site conditions:
Closest to fault rupture (22.3)	Geomatrix or CWB (D)
Hypocentral ( )	USGS (B)
Closest to surface projection of rupture (21.7)	

Record/Component	HP (Hz)	LP (Hz)	PGA (g)	PGV (cm/s)	PGD (cm)
LOMAP/CLD-UP	0.1	30	0.095	9.9	4.51
LOMAP/CLD195	0.1	30	0.16	13	6.11
LOMAP/CLD285	0.1	29	0.179	22.6	13.2

7)

North Palm Springs 1986/07/08 09:20	Station: 22170 Joshua Tree
Magnitude: M (6.0) Ml (5.9) Ms (6.0)	Data Source: CDMG
Distance (km):	Site conditions:
Closest to fault rupture (29.8)	Geomatrix or CWB (C)
Hypocentral ( )	USGS (B)
Closest to surface projection of rupture ( )	

Record/Component	HP (Hz)	LP (Hz)	PGA (g)	PGV (cm/s)	PGD (cm)
PALMSPR/JOS-UP	0.5	36	0.04	3.6	0.6
PALMSPR/JOS000	0.5	30	0.052	3.7	0.75
PALMSPR/JOS090	0.5	24	0.065	3.9	0.48

According to ABYYHY (ABYYHY, 1998), Bent 6.9.2, At least three recorded or simulated accelograms should be used in inelastic time history analysis. But during this process, to understand the exact behavior of the structure there are seven different kind of accelograms are used.

Table 5.9. The characteristics of the selected earthquake records

Earthquake Data	**Number of Time Steps**	**Output Time Steps**	**Total Time (sec)**
ARC 090	6000	0.005	29.995
GYN 090	5096	0.005	25.475
CLD 285	7990	0.005	33.980
JOS 000	5000	0.005	24.995
PTS 315	8000	0.005	39.995
FOR 090	2200	0.02	43.980
DSP 000	2500	0.02	49.980

Gathered data were modified by scaling with an appropriate factor in order to show similar behavior with the chosen response spectrum from ABYYHY (ABYYHY, 1998). During the modification process, Seismosigmal Software (Seismosignal, 2003) was used.

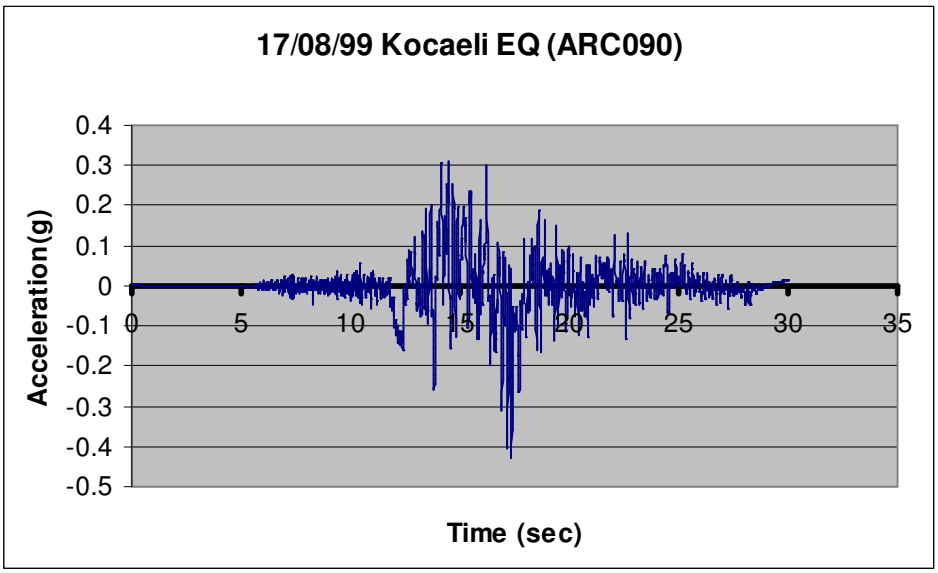

Figure 5.23. Acceleration-time records of Kocaeli (Arcelik 090)

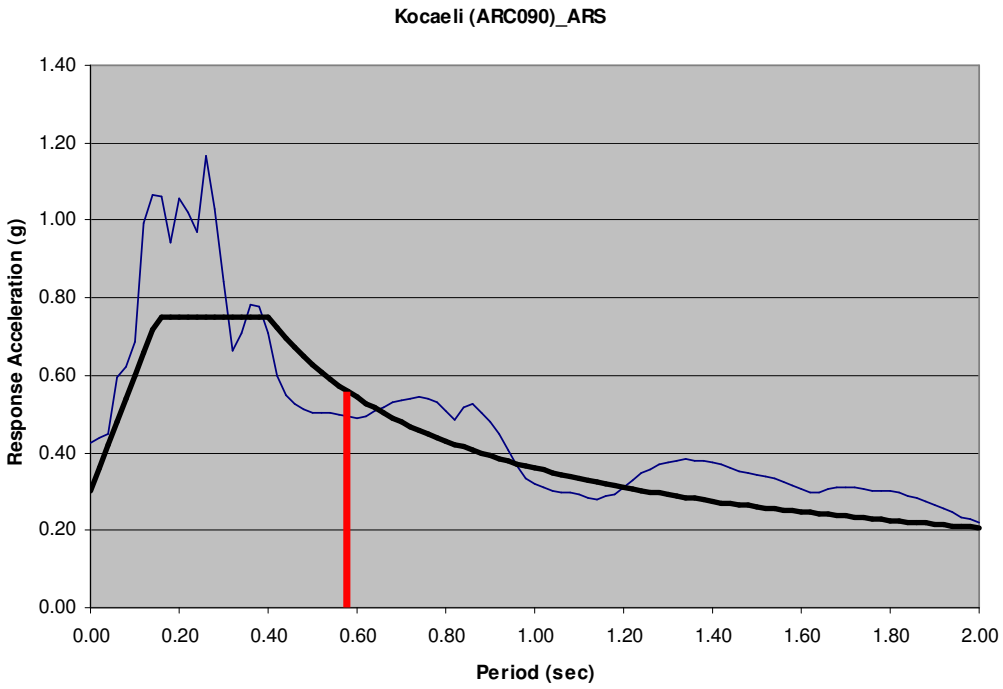

Figure 5.24. Acceleration response spectra of Kocaeli (Arcelik 090)

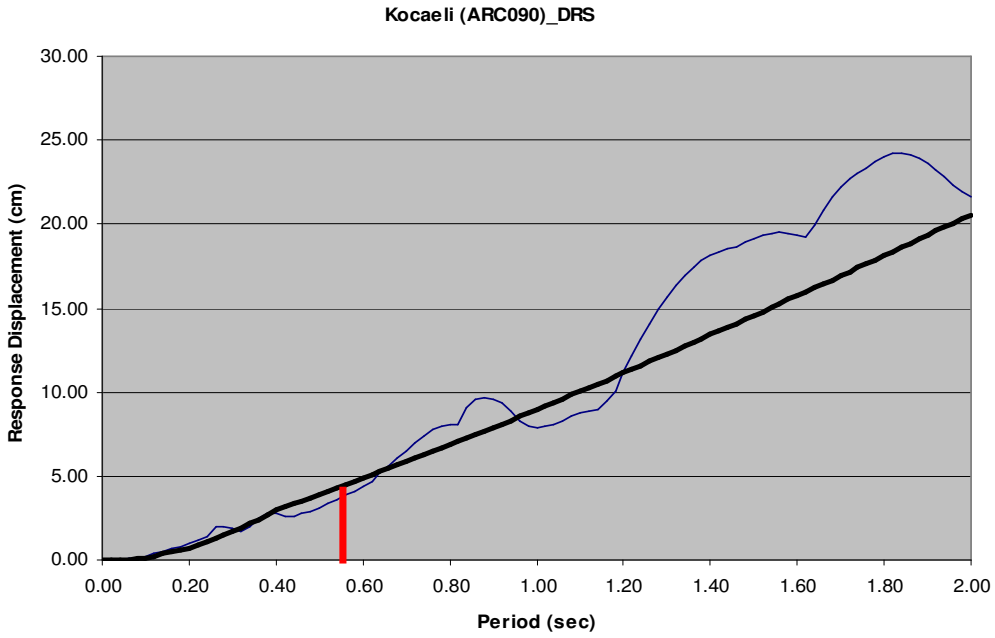

Figure 5.25. Displacement response spectra of Kocaeli (Arcelik 090)

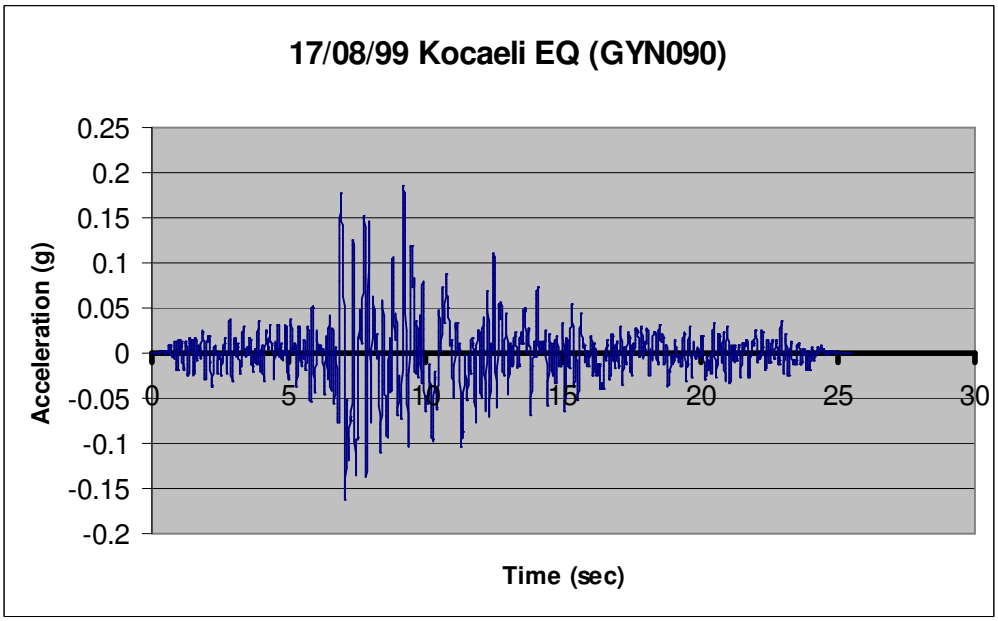

Figure 5.26. Acceleration-time records of Kocaeli (GYN090)

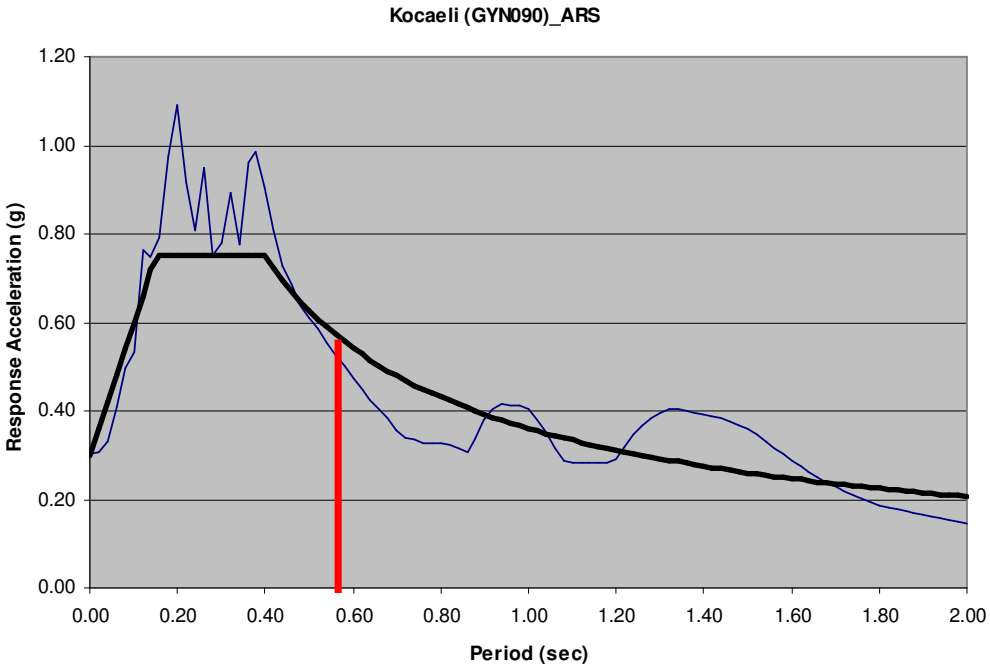

Figure 5.27. Acceleration response spectra of Kocaeli (GYN090)

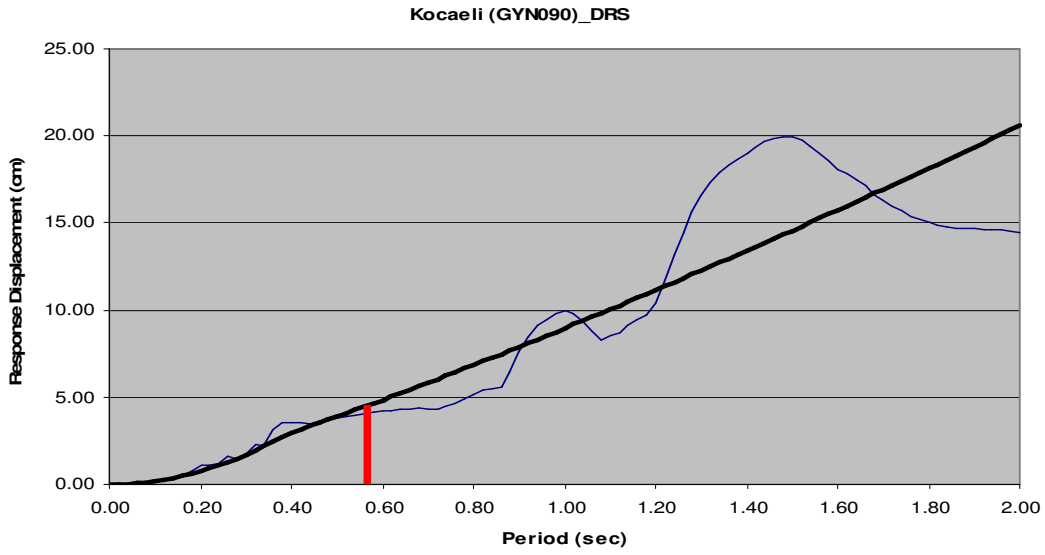

Figure 5.28. Displacement response spectra of Kocaeli (GYN090)

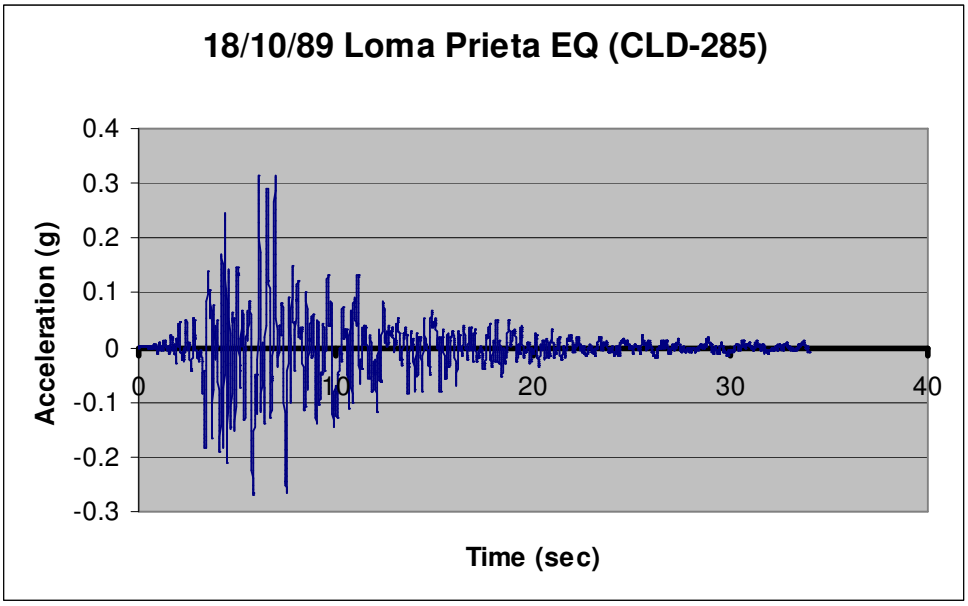

Figure 5.29. Acceleration-time records of Loma Prieta (CLD-285)

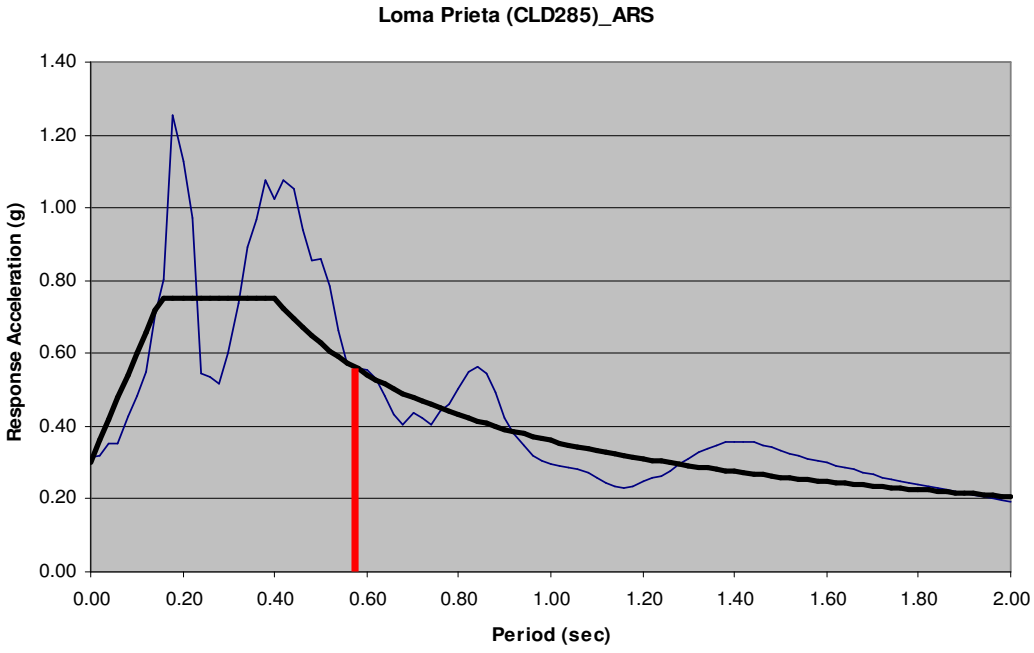

Figure 5.30. Acceleration response spectra of Loma Prieta (CLD-285)

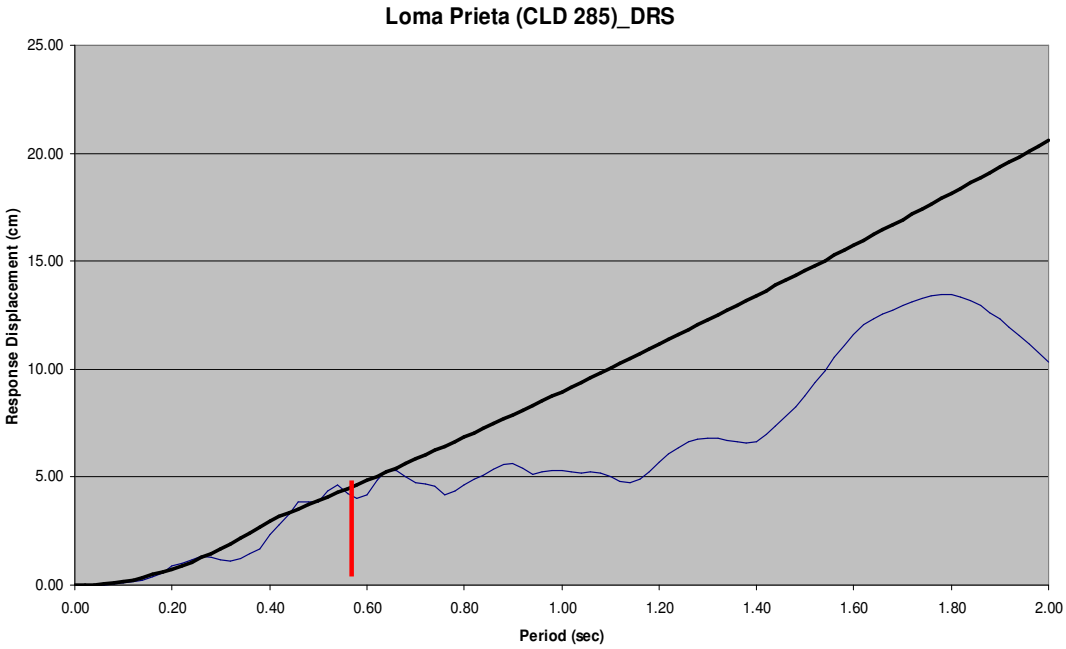

Figure 5.31. Displacement response spectra of Loma Prieta (CLD-285)

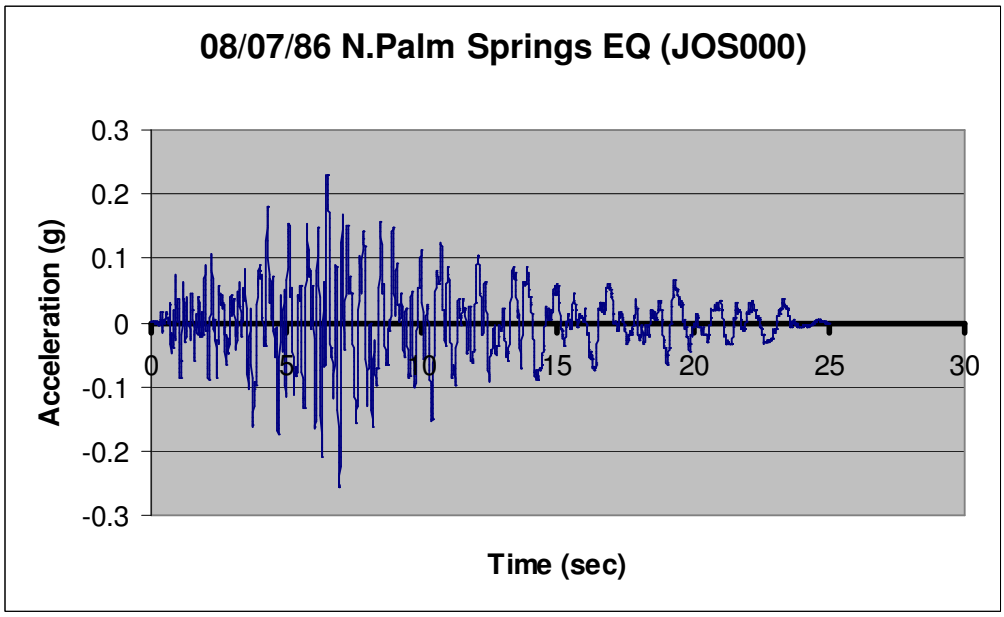

Figure 5.32. Acceleration-time records of N. Palm Springs (J0S000)

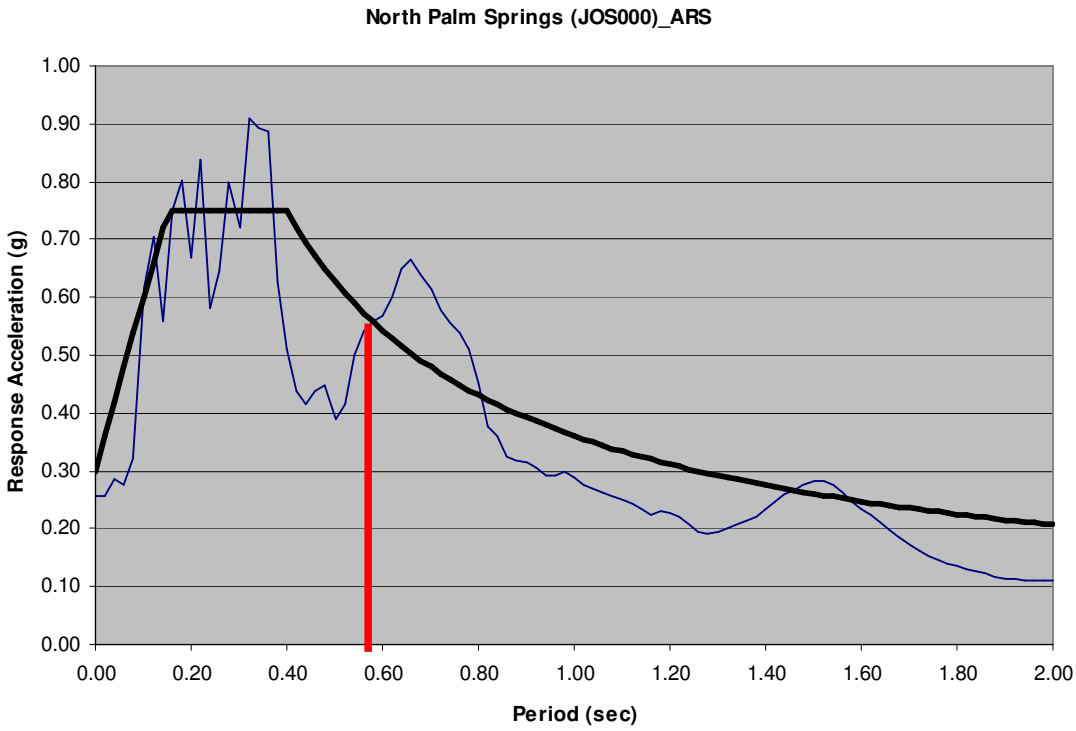

Figure 5.33. Acceleration response spectra of N. Palm Springs (JOS000)

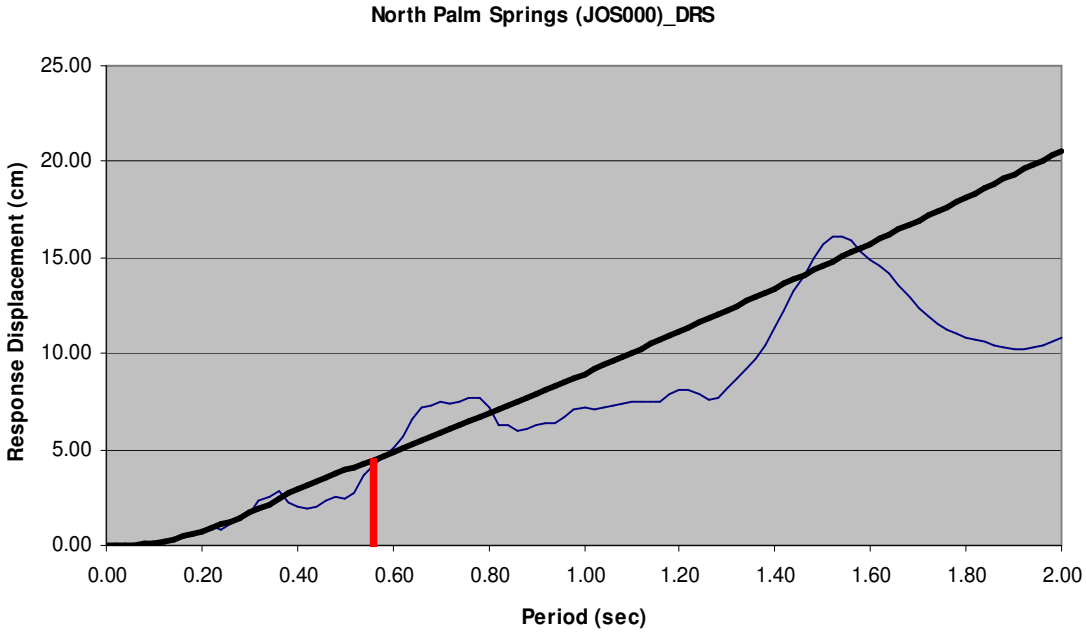

Figure 5.34. Displacement response spectra of N. Palm Springs (JOS000)

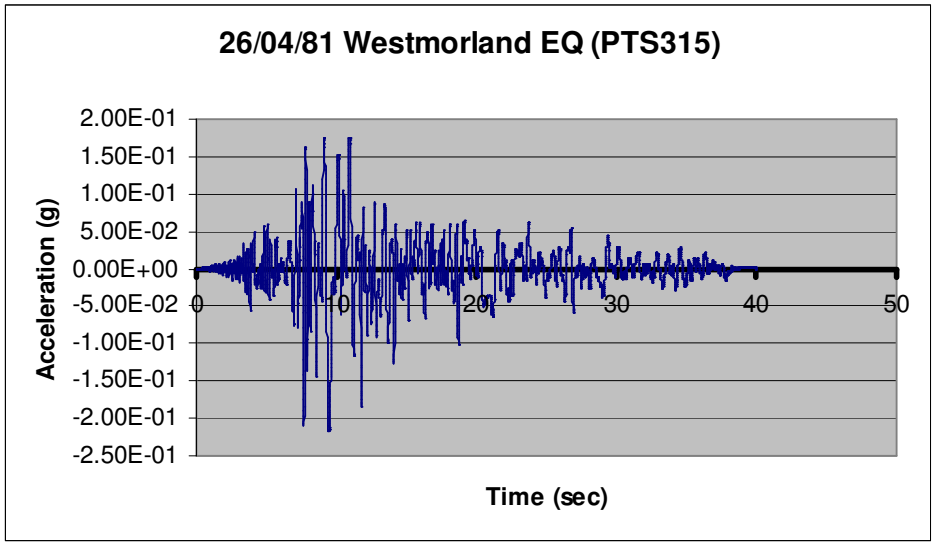

Figure 5.35. Acceleration-time records of Westmorland eq (PTS 315)

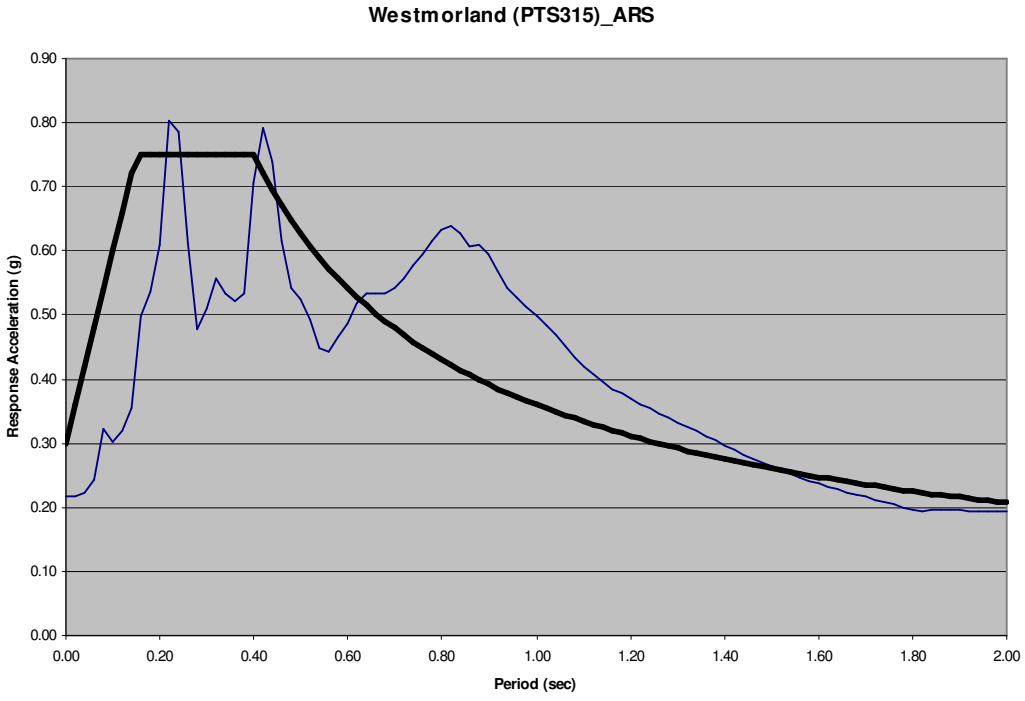

Figure 5.36. Acceleration response spectra of Westmorland eq (PTS 315)

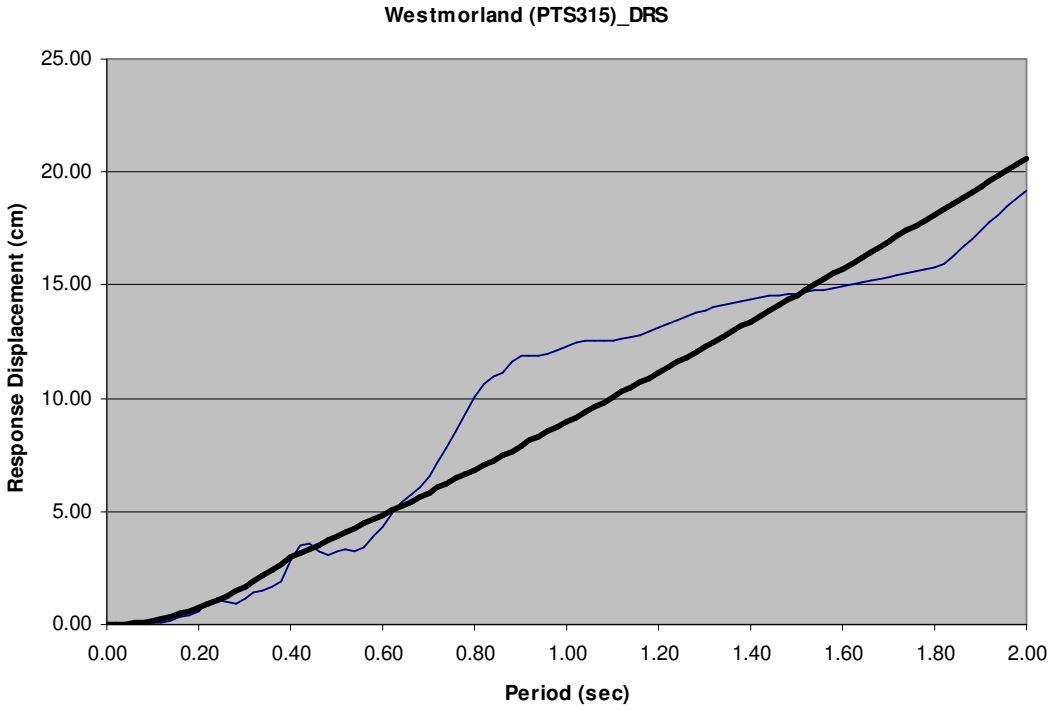

Figure 5.37. Displacement response spectra of Westmorland eq (PTS315)

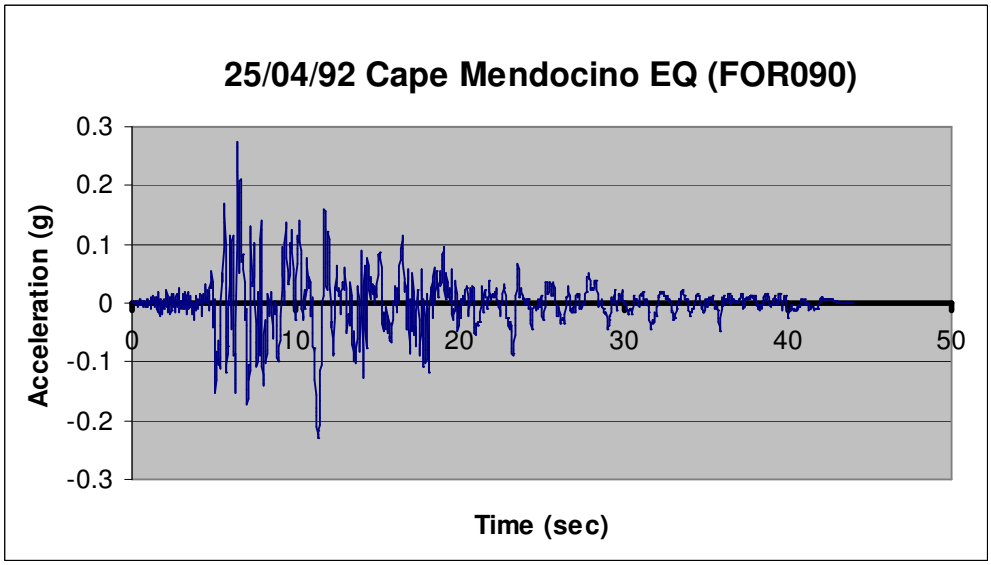

Figure 5.38. Acceleration time records of Cape Mendocino eq (FOR 090)

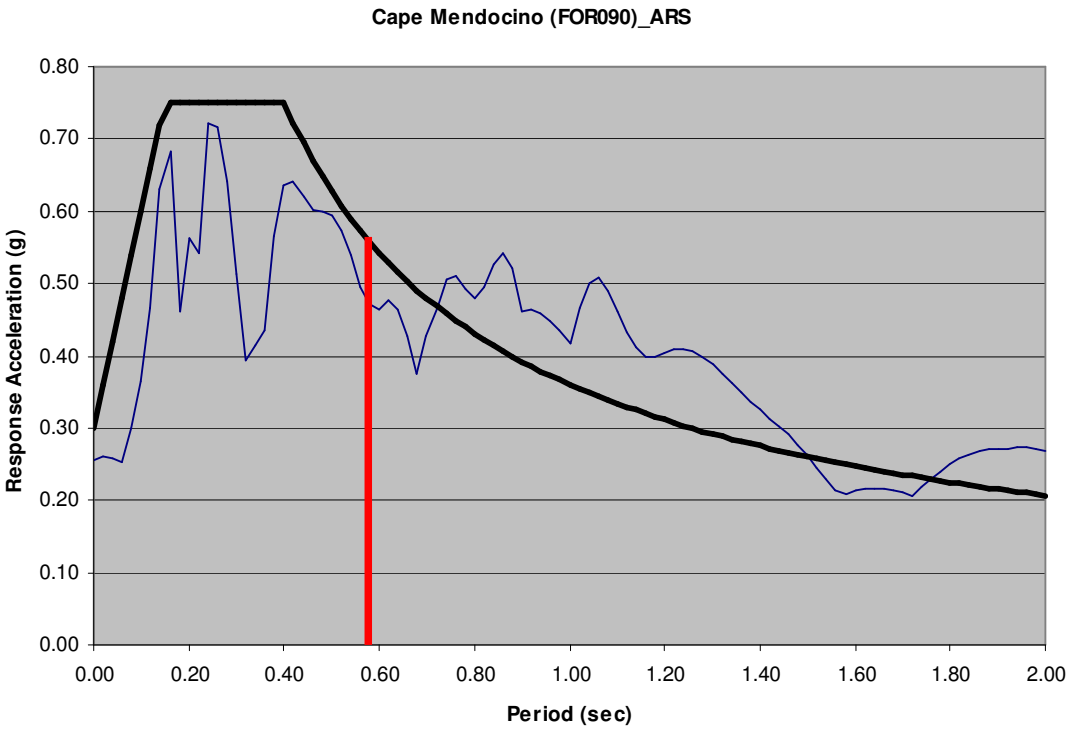

Figure 5.39. Acceleration response spectra of Cape Mendocino eq (FOR 090)

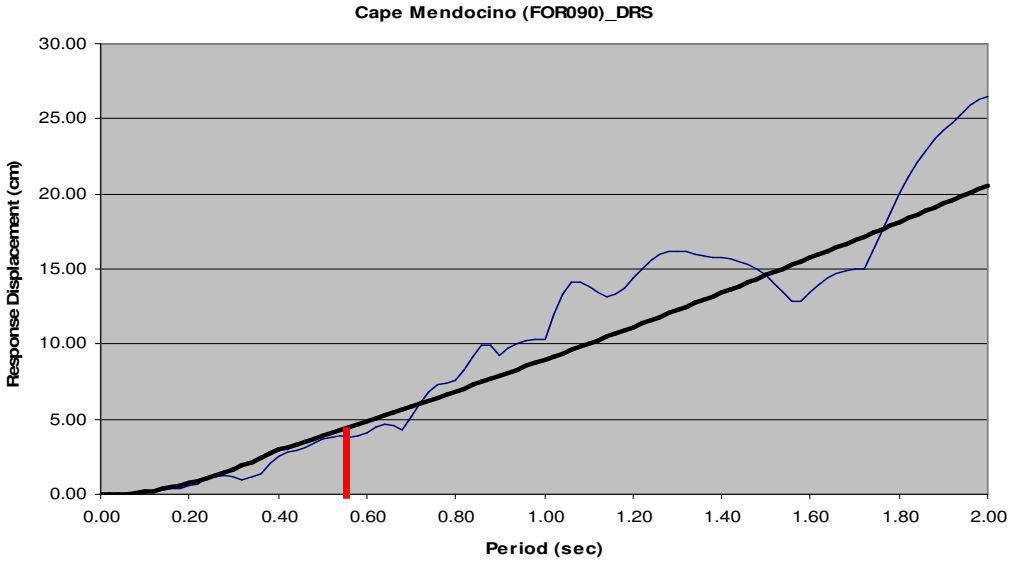

Figure 5.40. Displacement response spectra of Cape Mendocino eq (FOR 090)

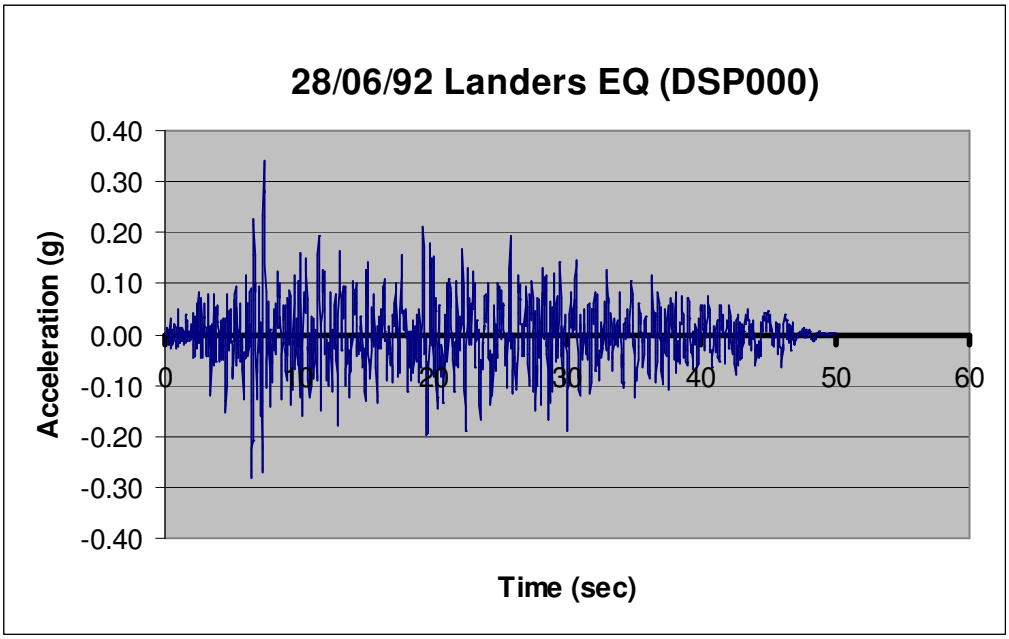

Figure 5.41. Acceleration-time records of Landers eq (DSP 000)

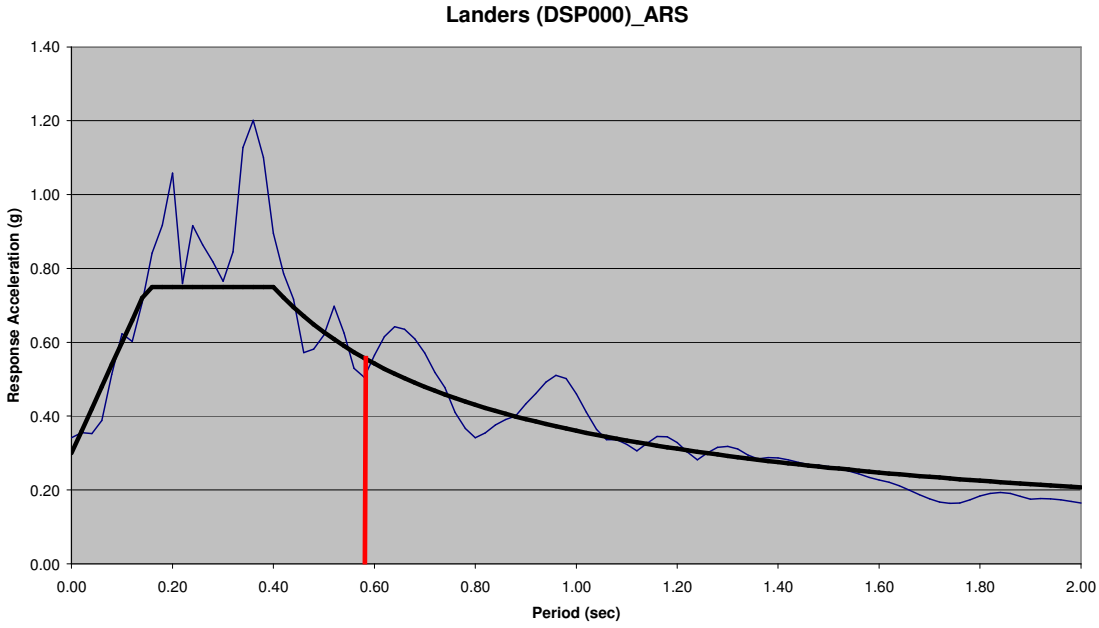

Figure 5.42. Acceleration response spectra of Landers eq (DSP 000)

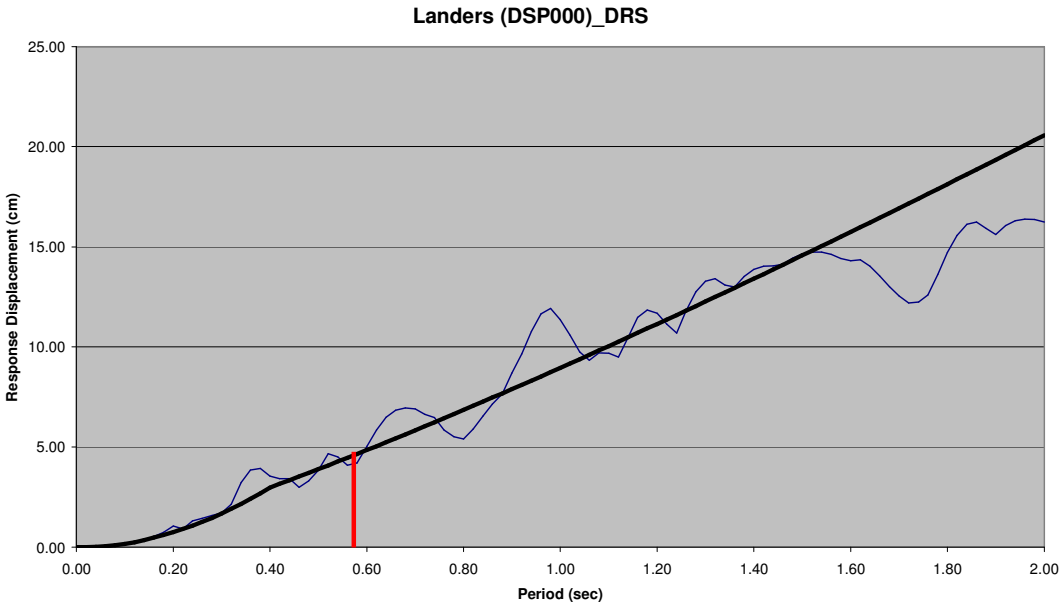

Figure 5.43. Displacement response spectra of Landers eq (DSP 000)

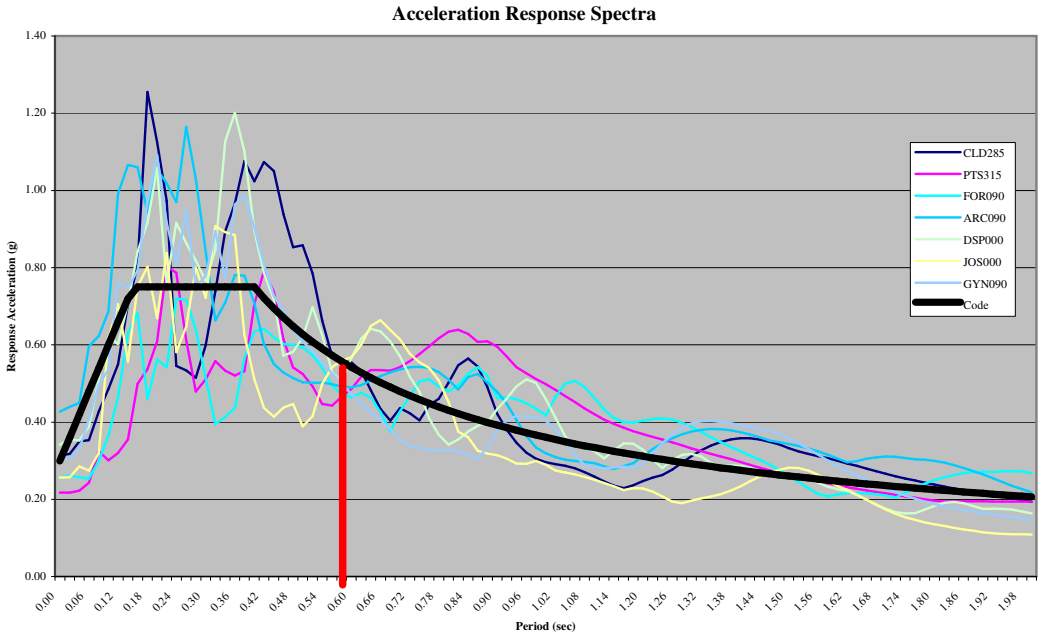

Figure 5.44. Acceleration response spectra

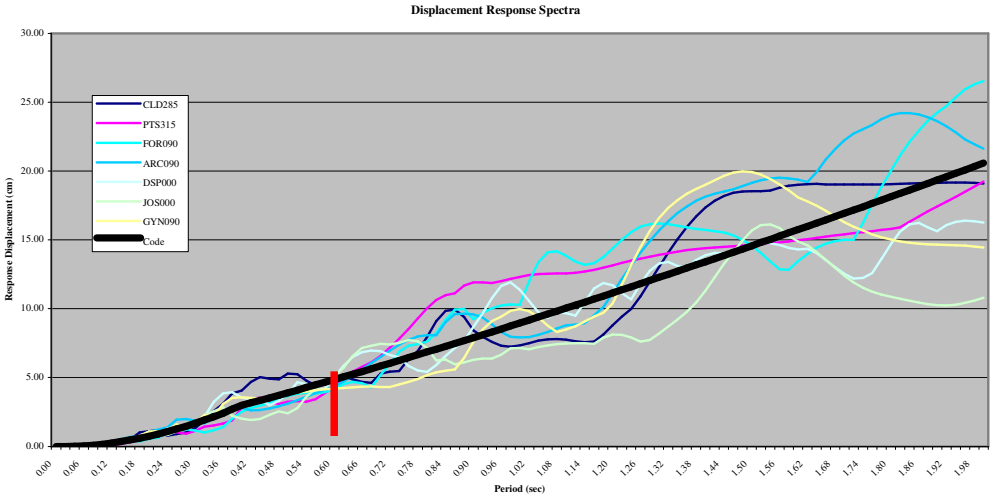

Figure 5.45. Displacement response spectra

5.8. Modal Information

Table 5.10. Modal information

Dominant Direction : Longitudinal			
Mode #	**Period (sec)**	**Circ/Freq (rad/sec)**	**Modal Participating Mass Ratios**
5	0.631	9.96	0.4874
7	0.581	10.81	0.0233
8	0.541	11.62	0.0135
9	0.522	12.04	0.0735
11	0.495	12.71	0.0291
12	0.474	13.25	0.0253
13	0.457	13.75	0.1471
15	0.430	14.63	0.0224
17	0.317	19.81	0.0102
20	0.207	30.40	0.0680
22	0.134	46.82	0.0277
23	0.111	56.64	0.0135
25	0.035	181.31	0.0133
			0.9542

Dominant Direction : Transversal			
Mode #	**Period (sec)**	**Circ/Freq (rad/sec)**	**Modal Participating Mass Ratios**
1	1.365	4.60	0.551
3	0.704	8.92	0.135
15	0.347	18.10	0.039
16	0.335	18.78	0.014
19	0.248	25.37	0.050
21	0.170	36.86	0.045
22	0.142	44.28	0.022
23	0.102	61.44	0.043
24	0.073	86.50	0.011
25	0.028	227.97	0.030
			0.9399

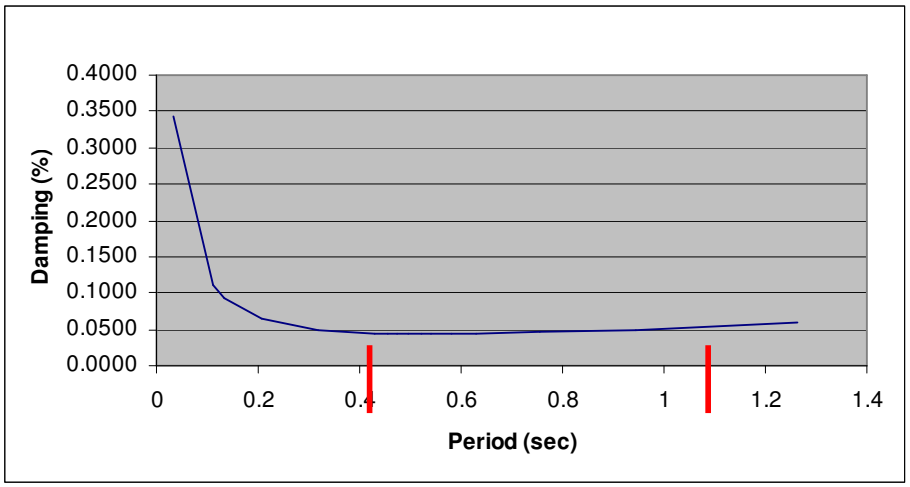

Figure 5.46. Rayleigh damping ratio - longitudinal direction

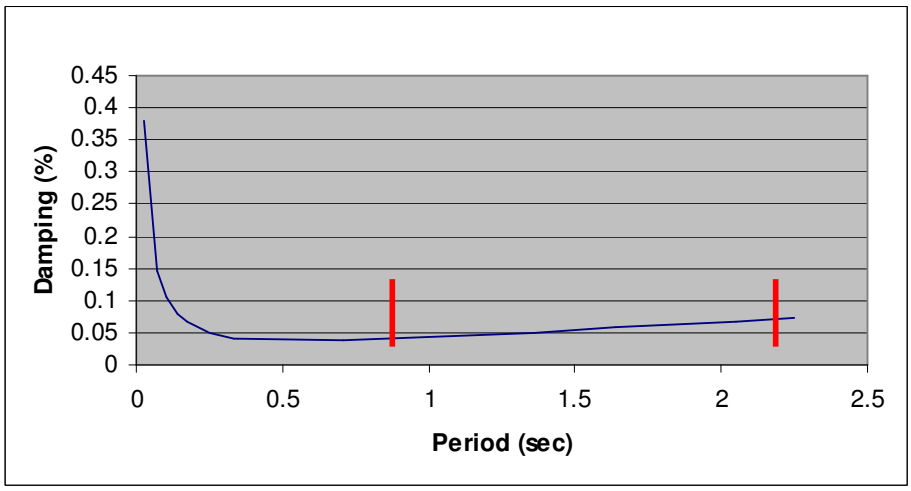

Figure 5.47 Rayleigh damping ratio- tranverse direction

In time history analysis, as shown in Figure 3.4, 3.5, mass participating rations are condensed between 0.3-1.0 sec for - longitudinal direction and between 0.7-2.0 sec for transversal direction.

5.9. Bearing Displacement Values

Table 5.11. Elastomeric bearing displacement values in longitudinal direction

Pier 1	U (m)
ARC090	0.04193
GYN090	0.01779
CLD285	0.04136
JOS000	0.02316
PTS315	0.03503
FOR090	0.03365
DSP000	0.03760

Pier 2	U (m)
ARC090	0.04493
GYN090	0.02011
CLD285	0.03897
JOS000	0.02560
PTS315	0.03343
FOR090	0.03227
DSP000	0.03338

Pier 3	U (m)
ARC090	0.05302
GYN090	0.03744
CLD285	0.05641
JOS000	0.05753
PTS315	0.05560
FOR090	0.04679
DSP000	0.06142

Pier 4	U (m)
ARC090	0.06580
GYN090	0.04821
CLD285	0.07560
JOS000	0.08186
PTS315	0.07274
FOR090	0.06526
DSP000	0.07453

Pier 5	U (m)
ARC090	0.05298
GYN090	0.04162
CLD285	0.06289
JOS000	0.06246
PTS315	0.06408
FOR090	0.05318
DSP000	0.06293

Pier 6	U (m)
ARC090	0.04129
GYN090	0.01429
CLD285	0.03256
JOS000	0.01633
PTS315	0.04317
FOR090	0.02412
DSP000	0.03538

Pier 7	U (m)
ARC090	0.04938
GYN090	0.01903
CLD285	0.02822
JOS000	0.02331
PTS315	0.05752
FOR090	0.03653
DSP000	0.03697

Table 5.12. Elastomeric bearing displacement values in transversal direction

Pier 1	U (m)
ARC090	0.04617
GYN090	0.04195
CLD285	0.05306
JOS000	0.03937
PTS315	0.05306
FOR090	0.04234
DSP000	0.04126

Pier 2	U (m)
ARC090	0.09779
GYN090	0.09622
CLD285	0.09449
JOS000	0.07918
PTS315	0.08701
FOR090	0.07904
DSP000	0.08157

Pier 3	U (m)
ARC090	0.14445
GYN090	0.14719
CLD285	0.13299
JOS000	0.11902
PTS315	0.13430
FOR090	0.12784
DSP000	0.12074

Pier 4	U (m)
ARC090	0.17469
GYN090	0.18835
CLD285	0.18045
JOS000	0.15777
PTS315	0.15876
FOR090	0.15987
DSP000	0.16720

Pier 5	U (m)
ARC090	0.14293
GYN090	0.14556
CLD285	0.13215
JOS000	0.11657
PTS315	0.11675
FOR090	0.11988
DSP000	0.12019

Pier 6	U (m)
ARC090	0.09679
GYN090	0.09567
CLD285	0.09080
JOS000	0.07910
PTS315	0.07897
FOR090	0.07988
DSP000	0.08007

Pier 7	U (m)
ARC090	0.04652
GYN090	0.04202
CLD285	0.04947
JOS000	0.03937
PTS315	0.04422
FOR090	0.04419
DSP000	0.04190

The capacity, effective length, of each bearing is 6.5 cm (Gumba GmbH, 2003). The tables are in both longitudinal and transversal direction that show any failure of bearings under given earthquakes. Thus, the values, in the table, which are more than 0.065 means the failure.

5.10. Occurred Plastic Hinges

Table 5.13. Plastic hinge locations

Earthquake	Pier 1	Pier 2	Pier 3	Pier 4	Pier 5	Pier 6	Pier 7
ARC090	None	None	None	2	None	None	None
GYN090	None	None	None	4	None	None	None
CLD285	None	None	None	3	None	None	None
JOS000	None	None	None	1	None	None	None
PTS315	None	None	None	2	None	None	None
FOR090	None	None	None	3	None	None	None
DSP000	None	None	None	2	None	None	None

After calculation it is observed that plastic hinges occurred under every earthquake record loading , at P4 only.

As shown in the below tables, when the moment value exceeds the yield moment, plastic hinge will be occurred.

Plastic hinges occurred at P4 for all earthquakes.

Table 5.14. Strain values for CLD285-u2

Strain Values (CLD285 U2 Record)

Pier No.	**Effective Yield Moment** *(kNm)*	**Moment** *(kNm)*	**Rotation** *(plastic)* *(radians)*	**Plastic Hinge Length** (m)	**Curvature** *(plastic)* *(1/m)*	**Curvature** *(elastic)* *(1/m)*	**Curvature** *(total)* *(1/m)*	**Reinf. Strain** *(total)*	**Confined Concrete Strain** *(total)*	**Unconf. Concrete Strain** *(total)*
P4L-Top	38000	39198.34	0.008728	2.0	0.004364	0.000404	0.004768	**0.02212**	0.001737	0.001977
P4R-Top	37350	37611.00	0.005494	2.0	0.002747	0.000403	0.003150	0.01445	0.001248	0.001468
P4L-Bottom	60650	65937.60	0.010814	2.0	0.005407	0.000433	0.005840	**0.02639**	0.002829	0.003123

The strain values of the confined concrete and unconfined concrete are within the serviceability limits. However, for P4L-top and P4L-bottom parts, the strain values of the reinforcement fiber exceeds the serviceability limits. Thus, it is a critical situation for the pier.

Table 5.15. Strain values for DSP000-u2

Strain Values (DSP000 U2 Record)

Pier No.	Effective Yield Moment *(kNm)*	Moment *(kNm)*	Rotation *(plastic)* *(radians)*	Plastic Hinge Length (m)	Curvature *(plastic)* *(1/m)*	Curvature *(elastic)* *(1/m)*	Curvature *(total)* *(1/m)*	Reinforcement Strain *(total)*	Confined Concrete Strain *(total)*	Unconfined Concrete Strain *(total)*
P4L-Top	36750	37218.03	0.003092	2.0	0.001546	0.000403	0.001949	0.008736	0.001017	0.001115
P4R-Top	36250	37431.89	0.007716	2.0	0.003858	0.000402	0.004260	0.01976	0.001552	0.001766

The strain values of the the reinforcement fiber, confined concrete and unconfined concrete are within the serviceability limits. Thus, it is not a critical situation for the pier.

Table 5.16. Strain values for JOS000-u2

Strain Values (JOS000 U2 Record)

Pier No.	Effective Yield Moment *(kNm)*	Moment *(kNm)*	Rotation *(plastic)* *(radians)*	Plastic Hinge Length (m)	Curvature *(plastic)* *(1/m)*	Curvature *(elastic)* *(1/m)*	Curvature *(total)* *(1/m)*	Reinforcement Strain *(total)*	Confined Concrete Strain *(total)*	Unconfined Concrete Strain *(total)*
P4L-Top	37000	37636.32	0.004726	2.0	0.002363	0.000403	0.002766	0.01262	0.00122	0.001359

The strain values of the the reinforcement fiber, confined concrete and unconfined concrete are within the serviceability limits. Thus, it is not a critical situation for the pier.

Table 5.17. Strain values for ARC090-u2

Strain Values (ARC090 U2 Record)

Pier No.	Effective Yield Moment *(kNm)*	Moment *(kNm)*	Rotation *(plastic)* *(radians)*	Plastic Hinge Length (m)	Curvature *(plastic)* *(1/m)*	Curvature *(elastic)* *(1/m)*	Curvature *(total)* *(1/m)*	Reinforcement Strain *(total)*	Confined Concrete Strain *(total)*	Unconfined Concrete Strain *(total)*
P4L-Top	37250	37990.22	0.005804	2.0	0.002902	0.000403	0.003305	**0.01518**	0.001356	0.001523
P4L-Bottom	60480	63685.12	0.006522	2.0	0.003261	0.000433	0.003694	**0.01652**	0.001961	0.002147

The strain values of the confined concrete and unconfined concrete are within the serviceability limits. However, for P4L-top and P4L-bottom parts, the strain values of the reinforcement fiber exceeds the serviceability limits. Thus, it is a critical situation for the pier.

Table 5.18. Strain values for PTS315-u2

Strain Values (PTS315 U2 Record)

Pier No.	Effective Yield Moment *(kNm)*	Moment *(kNm)*	Rotation *(plastic)* *(radians)*	Plastic Hinge Length (m)	Curvature *(plastic)* *(1/m)*	Curvature *(elastic)* *(1/m)*	Curvatur *(total)* *(1/m)*	Reinforcemen Strain *(total)*	Confined Concrete Strain *(total)*	Unconfined Concrete Strain *(total)*
P4R-Top	37500	38732.10	0.008648	2.0	0.004324	0.000403	0.004727	**0.02194**	0.001709	0.001946
P4L-Top	36850	38714.26	0.009058	2.0	0.004529	0.000403	0.004932	**0.02292**	0.001752	0.002
P4L-Bottom	60650	62950.33	0.00488	2.0	0.00244	0.000433	0.002873	0.01270	0.001675	0.001820

The strain values of the confined concrete and unconfined concrete are within the serviceability limits. However, for P4R-top and P4L-top parts, the strain values of the reinforcement fiber exceeds the serviceability limits. Thus, it is a critical situation for the pier.

Table 5.19. Strain values for GYN090-u2

Strain Values (GYN090 U2 Record)

Pier No.	**Effective Yield Moment** *(kNm)*	**Moment** *(kNm)*	**Rotation** *(plastic)* *(radians)*	**Plastic Hinge Length** (m)	**Curvature** *(plastic)* *(1/m)*	**Curvature** *(elastic)* *(1/m)*	**Curvature** *(total)* *(1/m)*	**Reinforcement Strain** *(total)*	**Confined Concrete Strain** *(total)*	**Unconfined Concrete Strain** *(total)*
P4L-Top	37500	40157.44	0.0122	2.0	0.0061	0.000403	0.006503	**0.03034**	0.002196	0.002523
P4R-Top	37000	38742.01	0.013448	2.0	0.006724	0.000403	0.007127	**0.03336**	0.002292	0.002650
P4L-Bottom	61000	63104.84	0.004546	2.0	0.002273	0.000433	0.002706	0.01091	0.001624	0.001760
P4R-Bottom	60000	61364..40	0.004306	2.0	0.002153	0.000433	0.002586	0.01141	0.001534	0.001662

The strain values of the confined concrete and unconfined concrete are within the serviceability limits. However, for P4L-top and P4R-top parts, the strain values of the reinforcement fiber exceeds the serviceability limits. Thus, it is a critical situation for the pier.

Table 5.20. Strain values for FOR090-u2

Strain Values (FOR090 U2 Record)										
Pier No.	**Effective Yield Moment** *(kNm)*	**Moment** *(kNm)*	**Rotation** *(plastic)* *(radians)*	**Plastic Hinge Length** (m)	**Curvature** *(plastic)* *(1/m)*	**Curvature** *(elastic)* *(1/m)*	**Curvature** *(total)* *(1/m)*	**Reinforcement Strain** *(total)*	**Confined Concrete Strain** *(total)*	**Unconfined Concrete Strain** *(total)*
P4R-Top	36500	36876.18	0.003316	2.0	0.001658	0.000402	0.002060	0.009272	0.001035	0.001139
P4L-Top	36500	37069.02	0.004786	2.0	0.002393	0.000402	0.002795	0.01278	0.001211	0.01352
P4L-Bottom	60750	62906.39	0.004238	2.0	0.002119	0.000433	0.002552	0.01120	0.001568	0.001696

The strain values of the the reinforcement fiber, confined concrete and unconfined concrete are within the serviceability limits. Thus, it is not a critical situation for the pier.

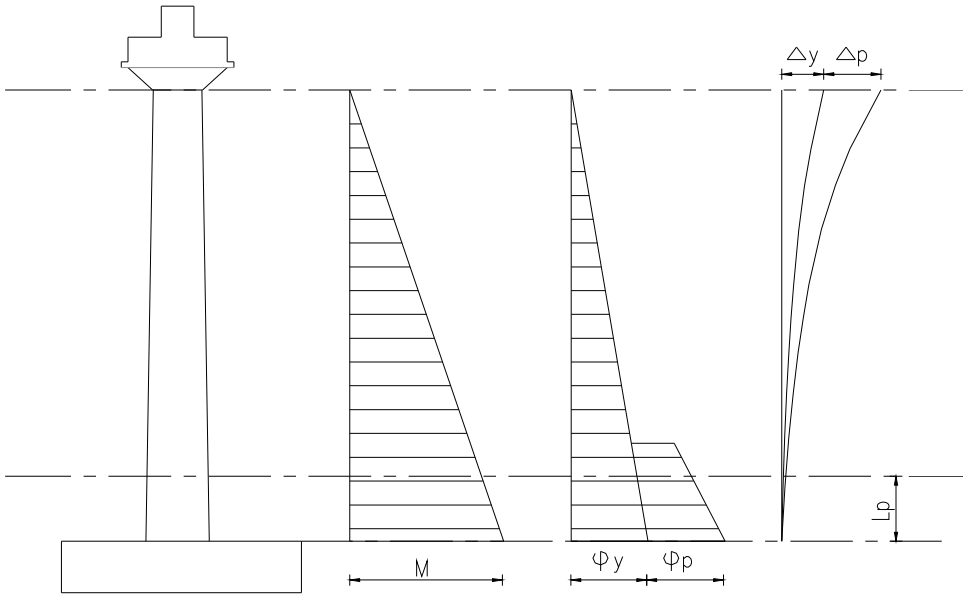

Figure 5.48. Plastic hinge mechanism

Serviceability limit corresponds to a concrete strain, ε_c = 0.004 and a steel strain, ε_s = 0.015, whichever occurs first. Corresponding limit strains are conservatively defined as the damage control strains of a confined and properly detailed section. Damage control limit corresponds to a concrete strain, ε_c = 0.018 and a steel strain, ε_s = 0.060, whichever occurs first.

Table 5.21. Strain limits for concrete and steel

Performance Level	Strain Limits For Concrete, εc	Strain Limits For Steel, εs
Serviceability, S1	0.004	0.015
Damage Control, S2	0.018	0.060

5.11. Solidarization Displacement Values

Table 5.22. Solidarization displacement values in longitudinal direction

Pier 1	U1 (m)
ARC090	0.00892
GYN090	0.00577
CLD285	0.00697
JOS000	0.00810
PTS315	0.01034
FOR090	0.00610
DSP000	0.01079

Pier 2	U1 (m)
ARC090	0.00468
GYN090	0.00416
CLD285	0.00510
JOS000	0.00493
PTS315	0.00481
FOR090	0.00434
DSP000	0.00556

Pier 3	U1 (m)
ARC090	0.01175
GYN090	0.00637
CLD285	0.02139
JOS000	0.01610
PTS315	0.02110
FOR090	0.01161
DSP000	0.01969

Pier 5	U1 (m)
ARC090	0.01044
GYN090	0.00678
CLD285	0.02461
JOS000	0.01528
PTS315	0.02395
FOR090	0.01129
DSP000	0.02251

Pier 6	**U1 (m)**
ARC090	0.02541
GYN090	0.02342
CLD285	0.02900
JOS000	0.02105
PTS315	0.03074
FOR090	0.02675
DSP000	0.02537

Pier 7	**U1 (m)**
ARC090	0.00962
GYN090	0.00625
CLD285	0.00766
JOS000	0.00712
PTS315	0.01107
FOR090	0.00626
DSP000	0.01229

Table 5.23. Solidarization displacement values in transversal direction

Pier 1	U (m)
ARC090	0.01204
GYN090	0.00860
CLD285	0.01075
JOS000	0.01089
PTS315	0.01079
FOR090	0.01081
DSP000	0.01324

Pier 2	U (m)
ARC090	0.00839
GYN090	0.00623
CLD285	0.00719
JOS000	0.01151
PTS315	0.01040
FOR090	0.01030
DSP000	0.01045

Pier 3	U (m)
ARC090	0.01354
GYN090	0.01419
CLD285	0.00982
JOS000	0.01366
PTS315	0.01454
FOR090	0.01114
DSP000	0.02256

Pier 5	U (m)
ARC090	0.01498
GYN090	0.01472
CLD285	0.00979
JOS000	0.01586
PTS315	0.01592
FOR090	0.01498
DSP000	0.02388

Pier 6	U (m)
ARC090	0.01521
GYN090	0.01517
CLD285	0.01520
JOS000	0.015057
PTS315	0.01521
FOR090	0.01505
DSP000	0.01514

Pier 7	U (m)
ARC090	0.01186
GYN090	0.00767
CLD285	0.01076
JOS000	0.00961
PTS315	0.01090
FOR090	0.00954
DSP000	0.01256

Solidarizations have used to provide longitudinal continuity by connecting girders to each other. There are 10 cm gaps between girders and cap beams. Above tables, the longitudinal displacements of solidarizations in both directions are given.

6. RESULTS AND CONCLUSIONS

The main purpose of this study is the seismic performance assessment of Ortakoy V409 Viaduct. The response spectrum, non-linear time history analysis and site investigations clearly shows that; in the existing condition of the viaduct serious problems will occur during a possible earthquake.

According to the analysis, there are two major problems in the viaduct. At Pier 4, under applied earthquakes, column section can not resist the moment force. The strain values of the reinforcement fiber exceeds the serviceability limits. In addition to this, corrosion effects will expedite the damages on sections. This situation will expand the P4 condition to whole structure. As a second major problem, elastomeric bearings will fail in both direction during earthquake. The deflections at elastomeric bearings are more than allowable limits.

In conclusion, retrofitting of the viaduct is necessary. Retrofitting such as, RC Lining, replacement of elastomeric bearings, repairing to avoid corrosions are needed. Also; in order to take further precautions for preventing falling of girders, some devices such as falling down prevention cables can be applied.

APPENDIX A: MOMENT-CURVATURE RELATIONS OF THE PIERS

A.1. Moment-Curvature Relationships of Pier 1

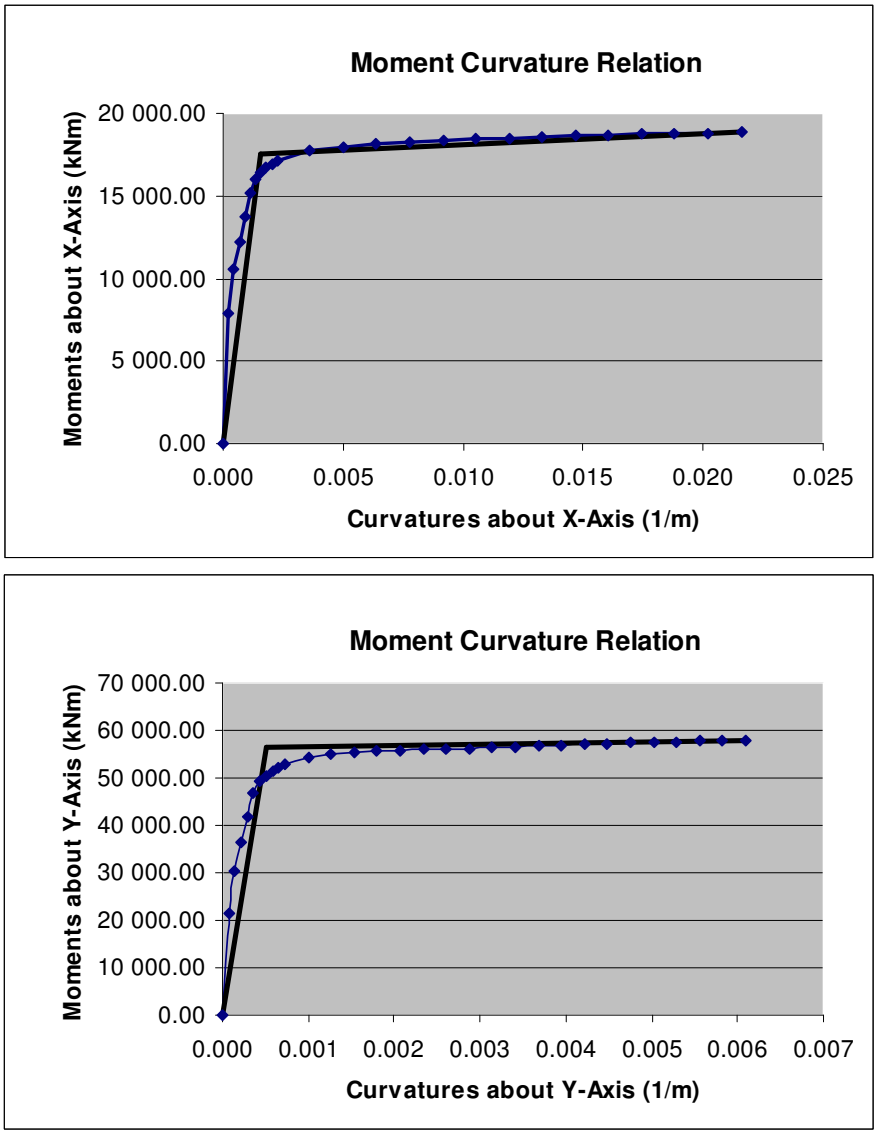

Figure A.1.1. Moment-Curvature relations at the bottom part of Pier 1 in x and y directions

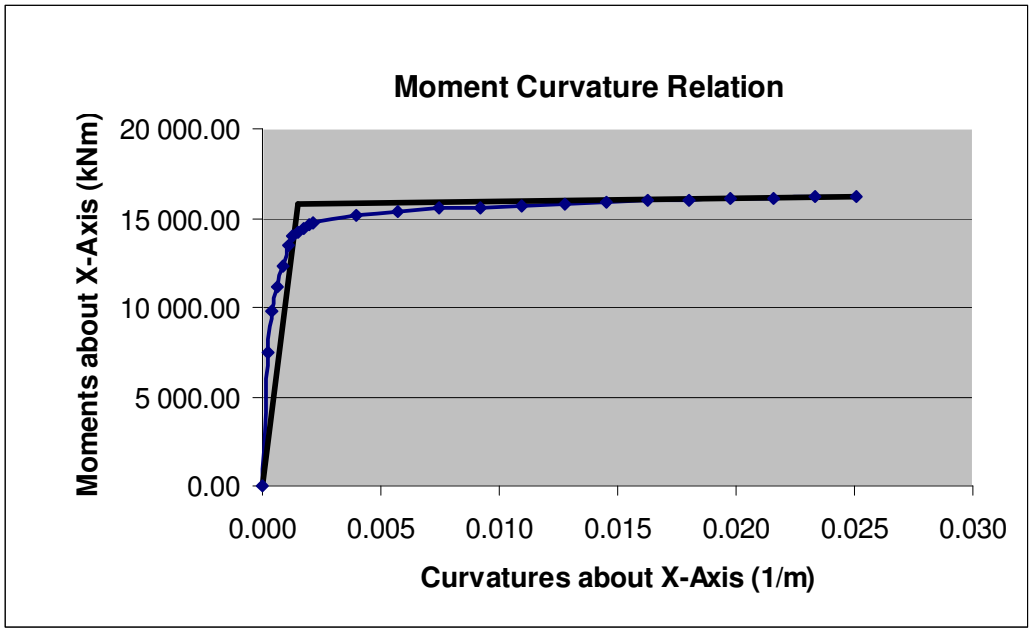

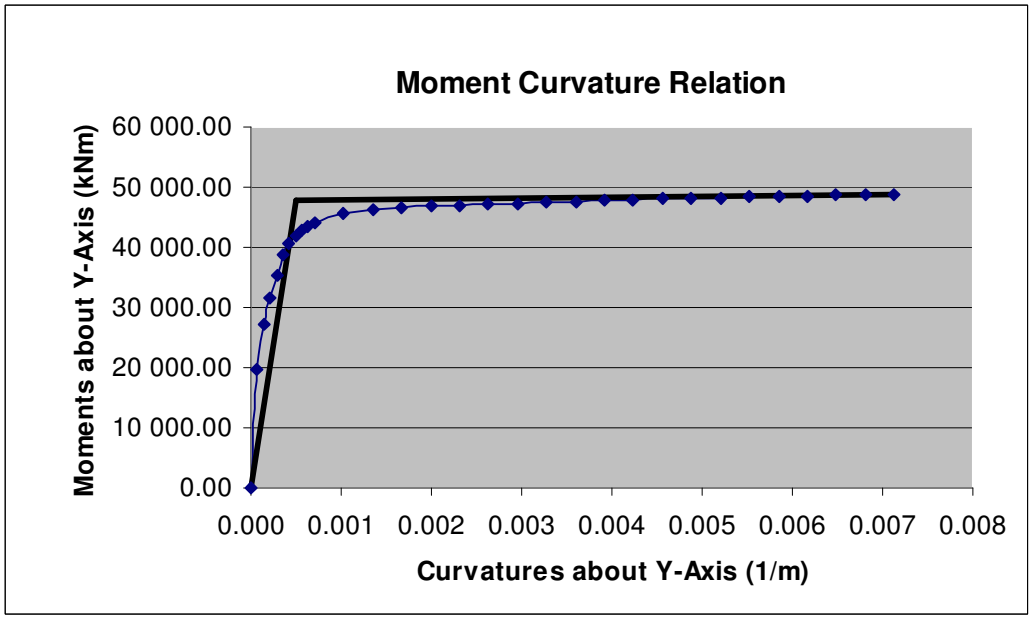

Figure A.1.2. Moment-Curvature relations at the top part of Pier 1 in x and y directions

A.2. Moment-Curvature Relationships of Pier 2

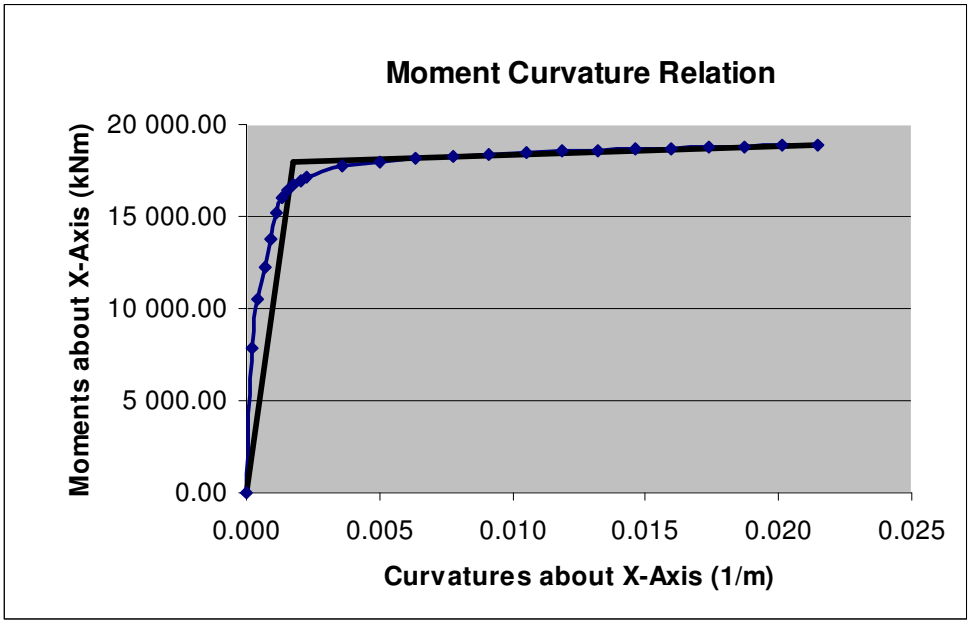

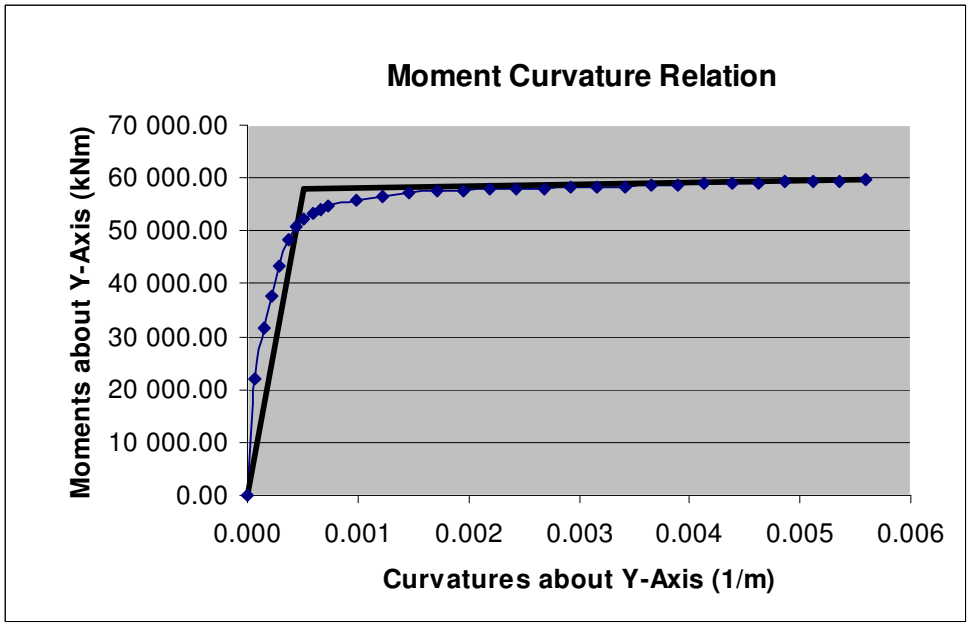

Figure A.2.1. Moment-Curvature relations at the bottom part of Pier 2 in x and y directions

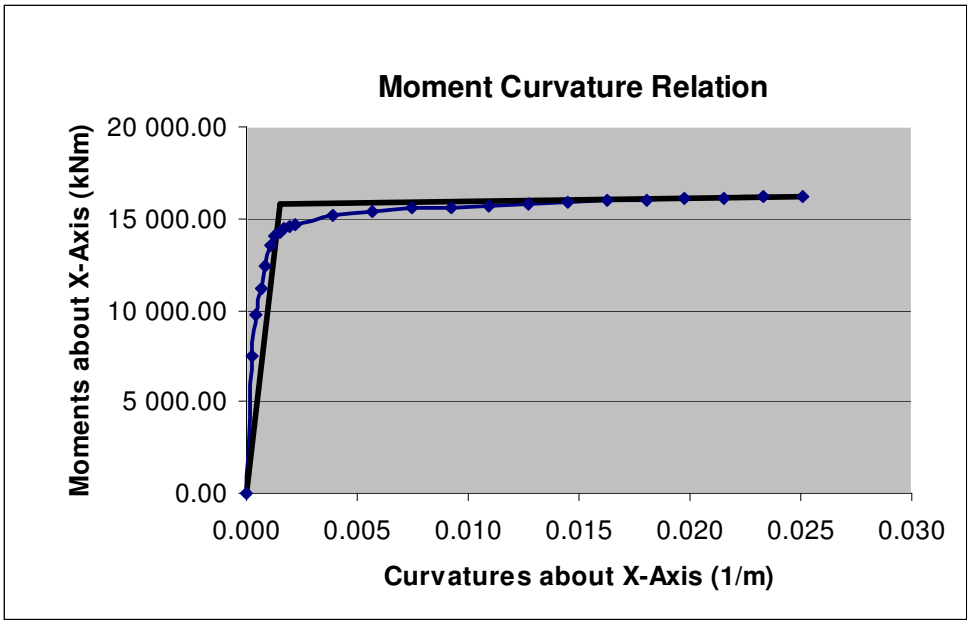

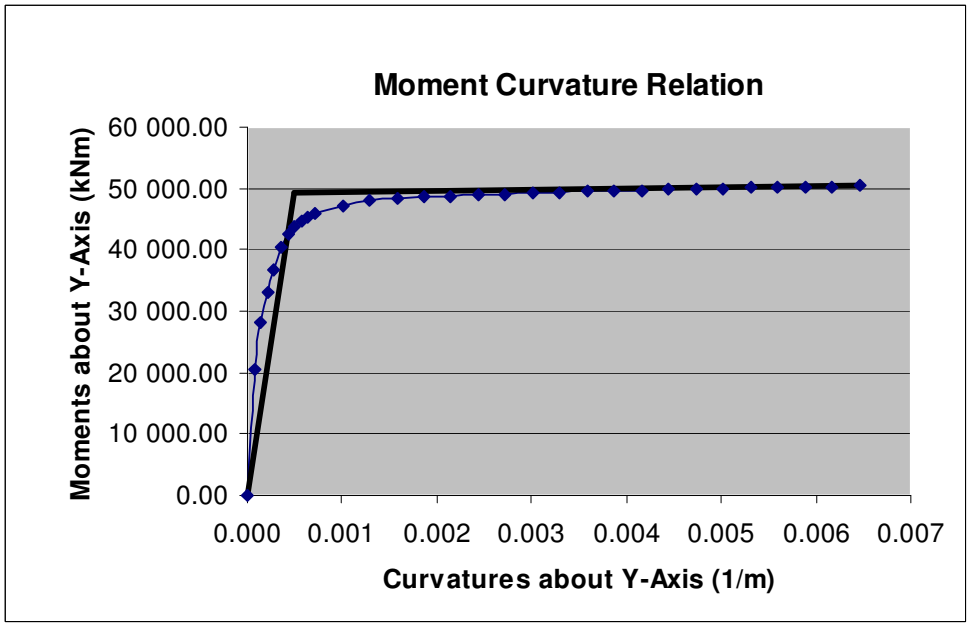

Figure A.2.2. Moment-Curvature relations at the top part of Pier 2 in x and y directions

A.3. Moment-Curvature Relationships of Pier 3

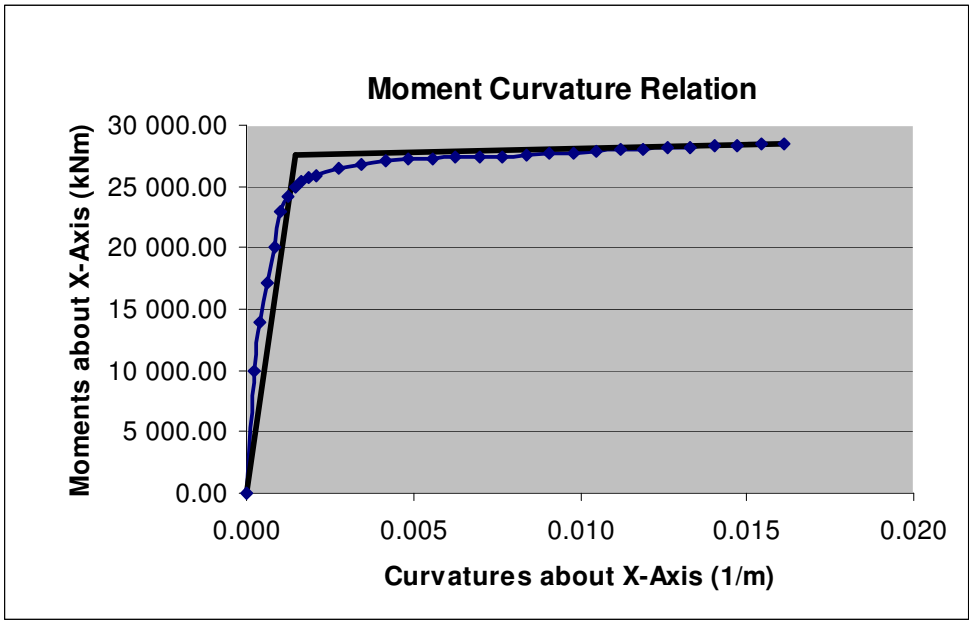

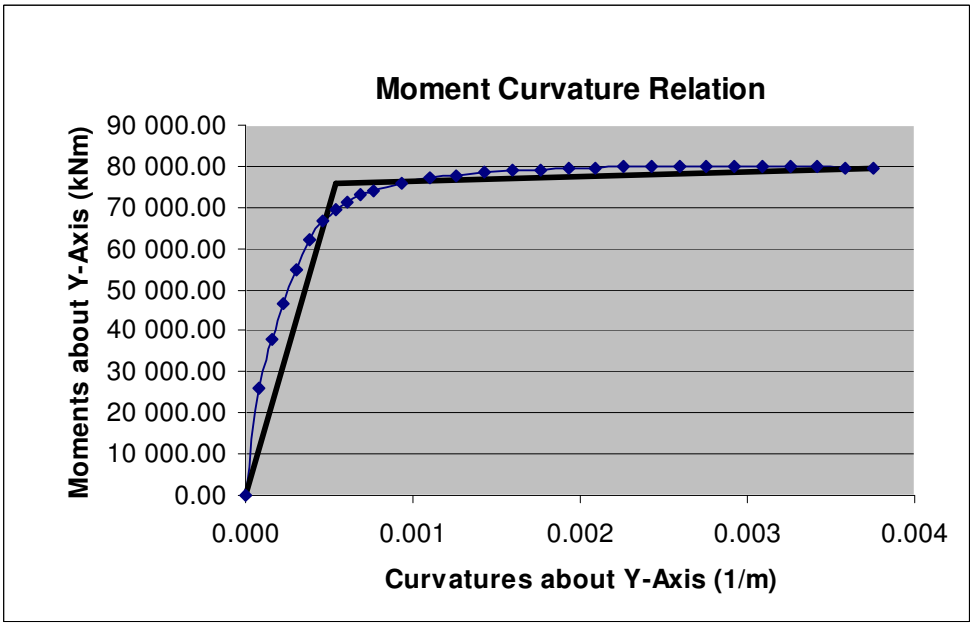

Figure A.3.1. Moment-Curvature relations at the bottom part of Pier 3 in x and y directions

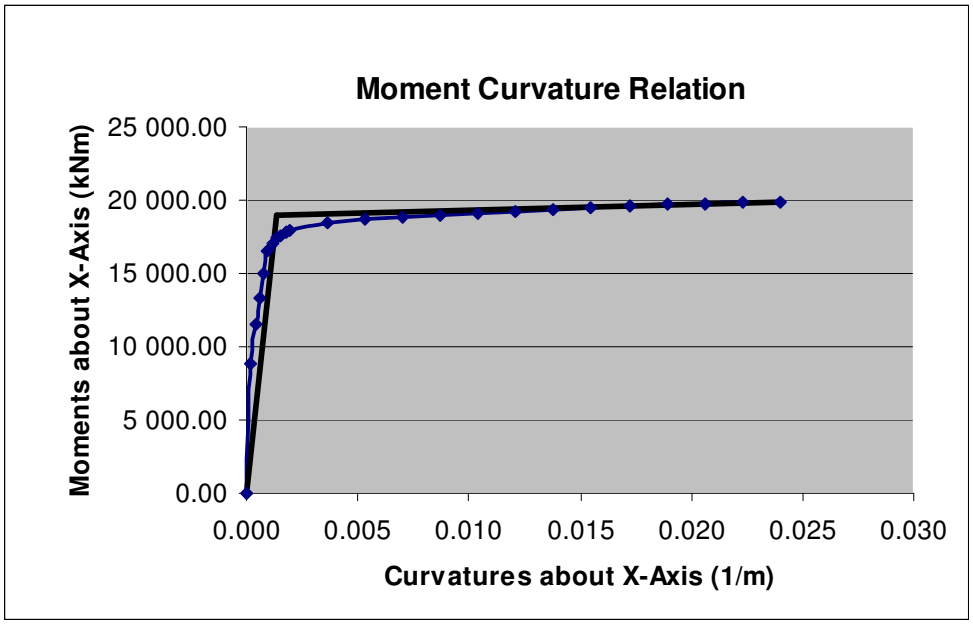

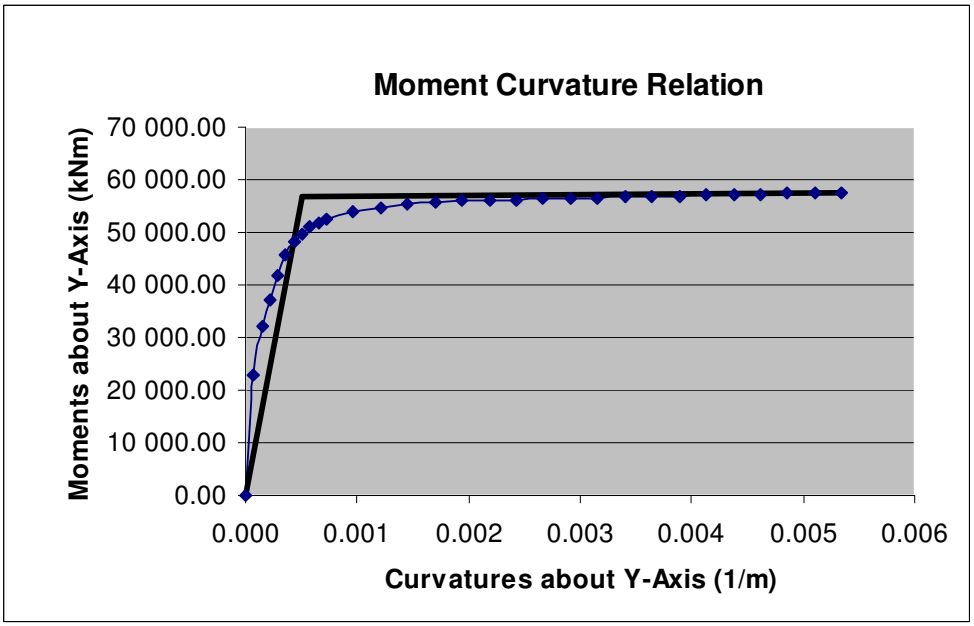

Figure A.3.2. Moment-Curvature relations at the top part of Pier 3 in x and y directions

A.4. Moment-Curvature Relationships of Pier 4

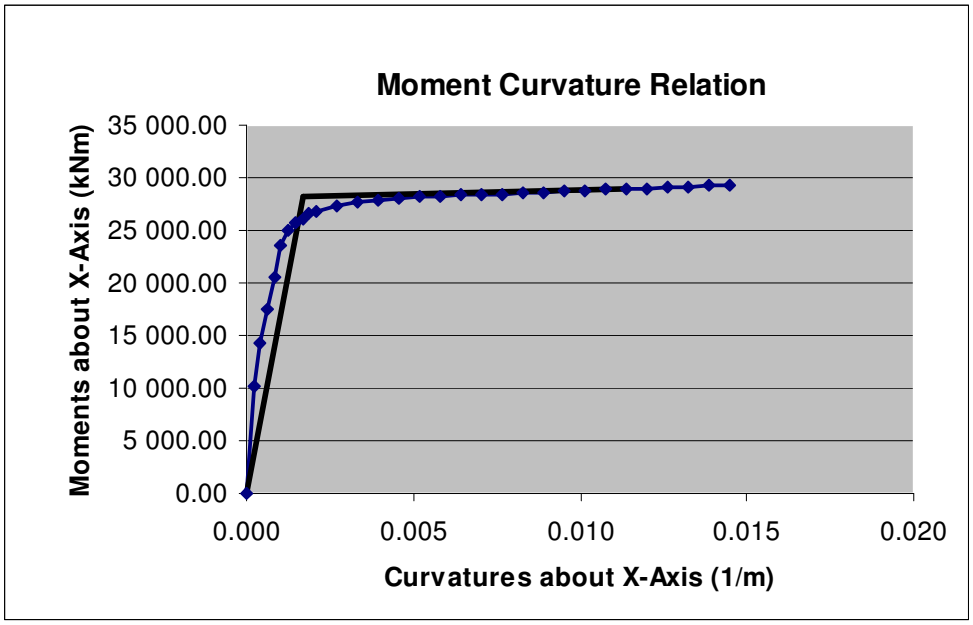

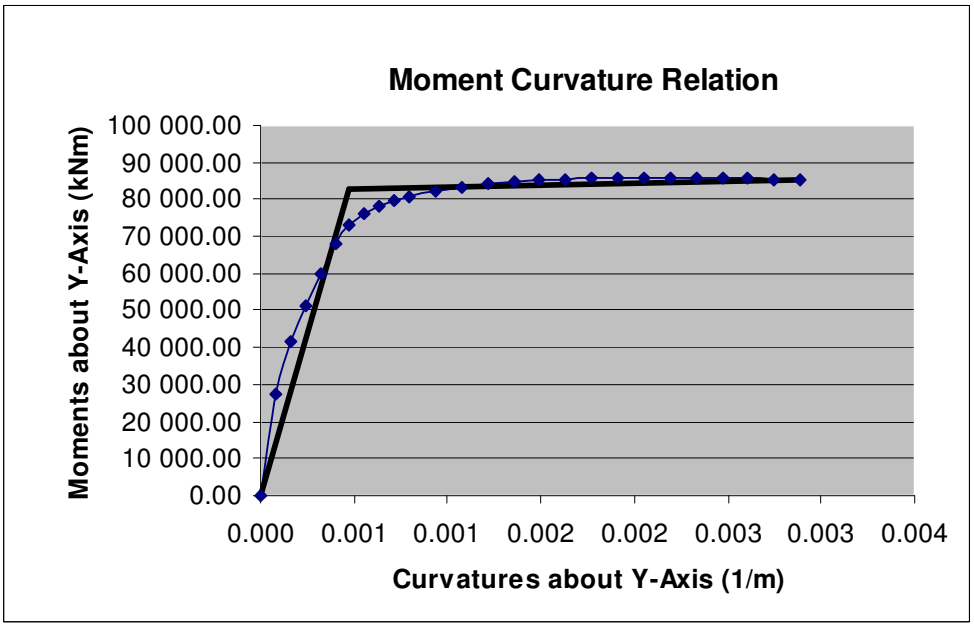

Figure A.4.1. Moment-Curvature relations at the bottom part of Pier 4 in x and y directions

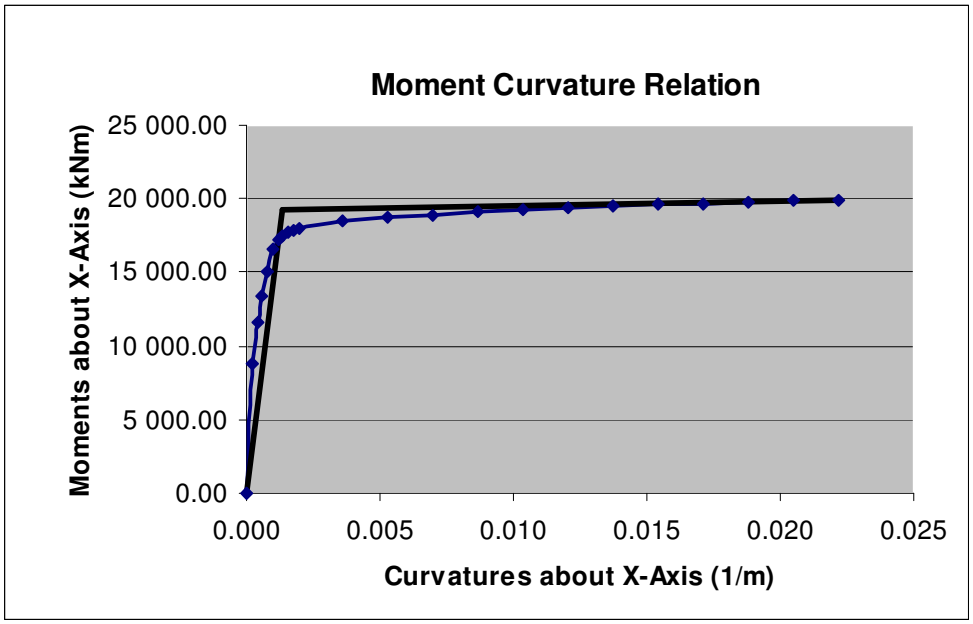

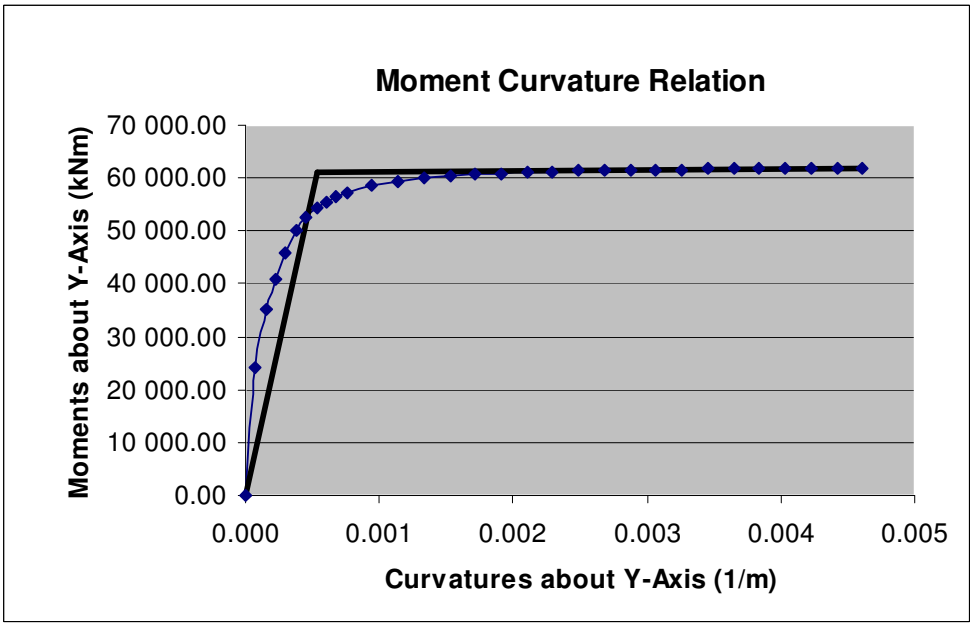

Figure A.4.2. Moment-Curvature relations at the top part of Pier 4 in x and y directions

A.5. Moment-Curvature Relationships of Pier 5

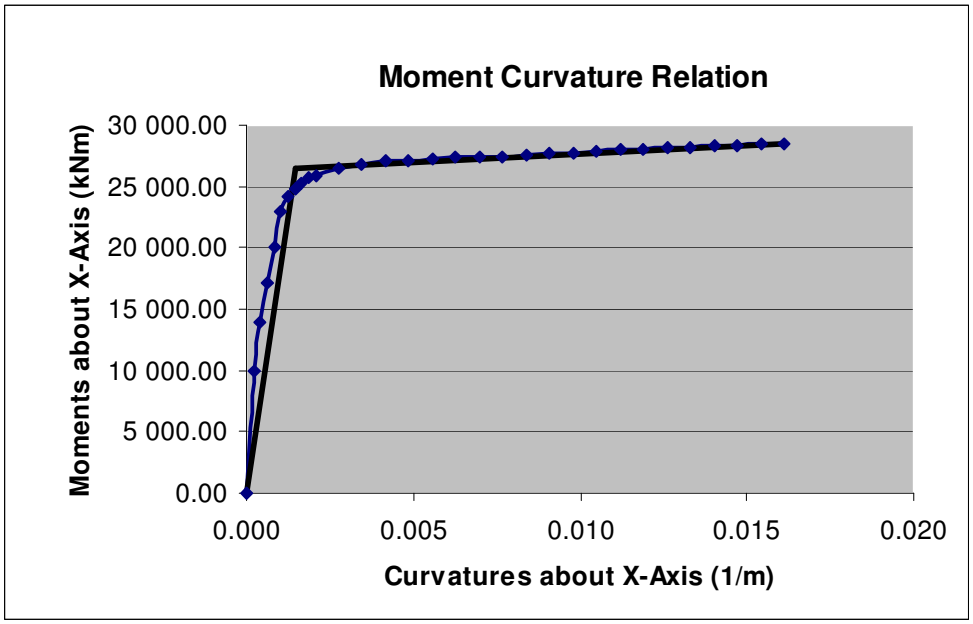

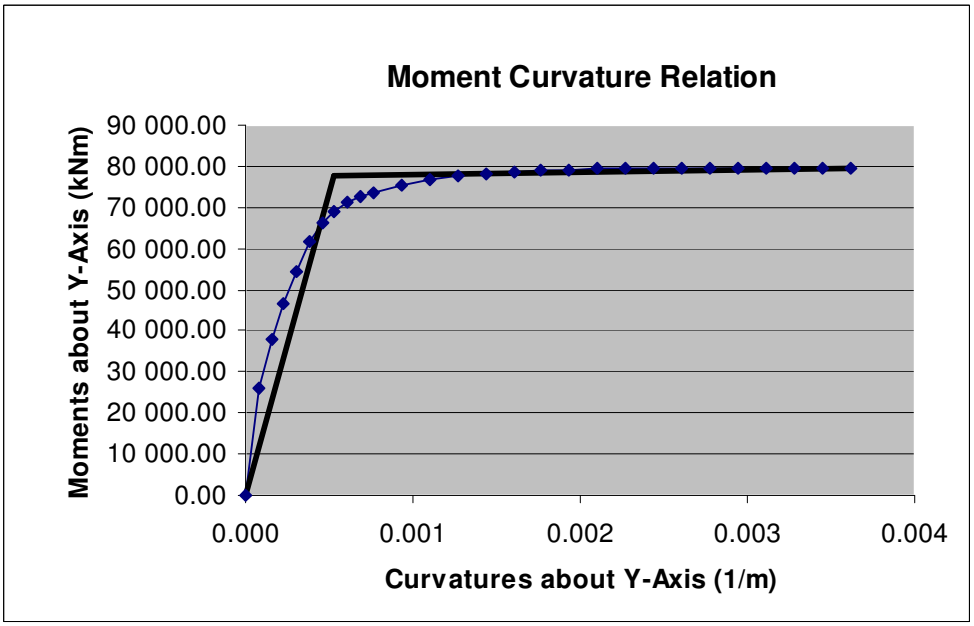

Figure A.5.1. Moment-Curvature relations at the bottom part of Pier 5 in x and y directions

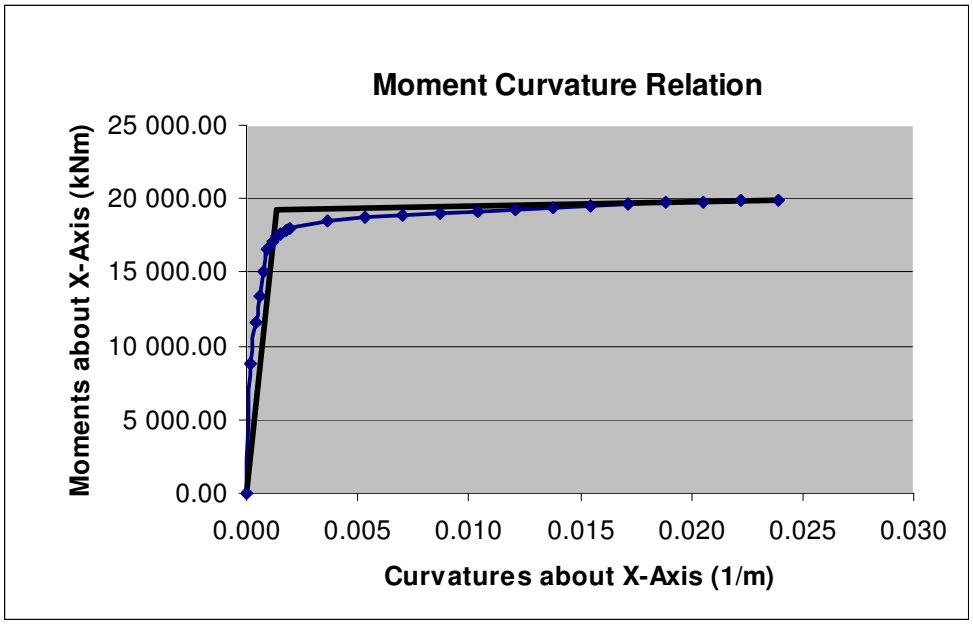

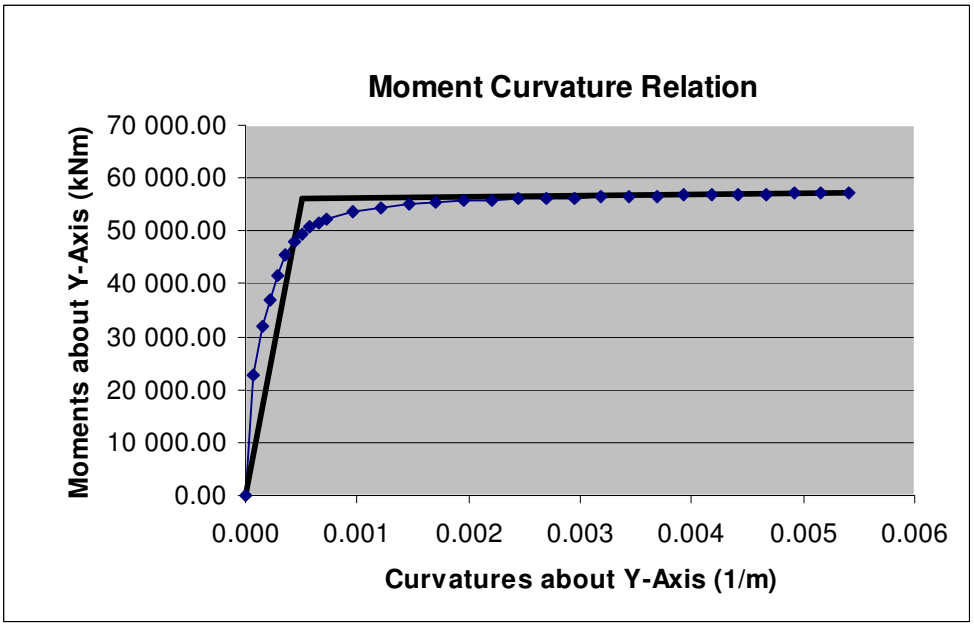

Figure A.5.2. Moment-Curvature relations at the top part of Pier 5 in x and y directions

A.6. Moment-Curvature Relationships of Pier 6

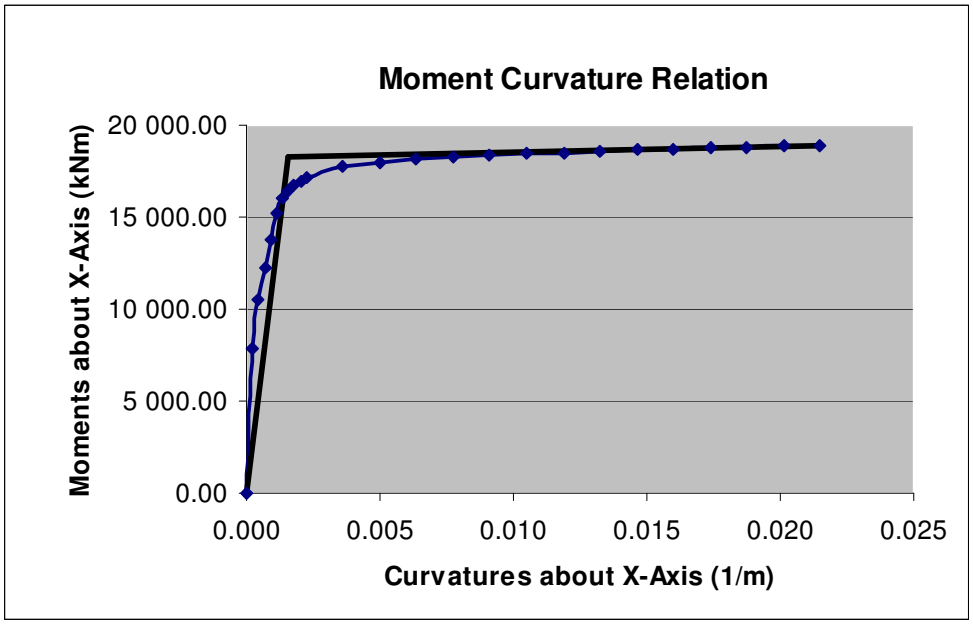

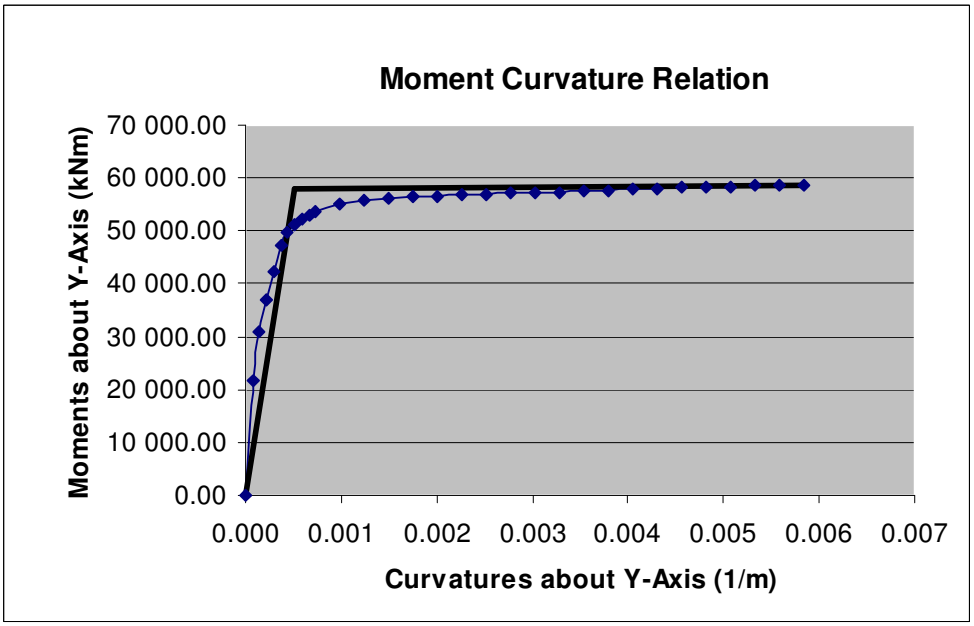

Figure A.6.1. Moment-Curvature relations at the bottom part of Pier 6 in x and y directions

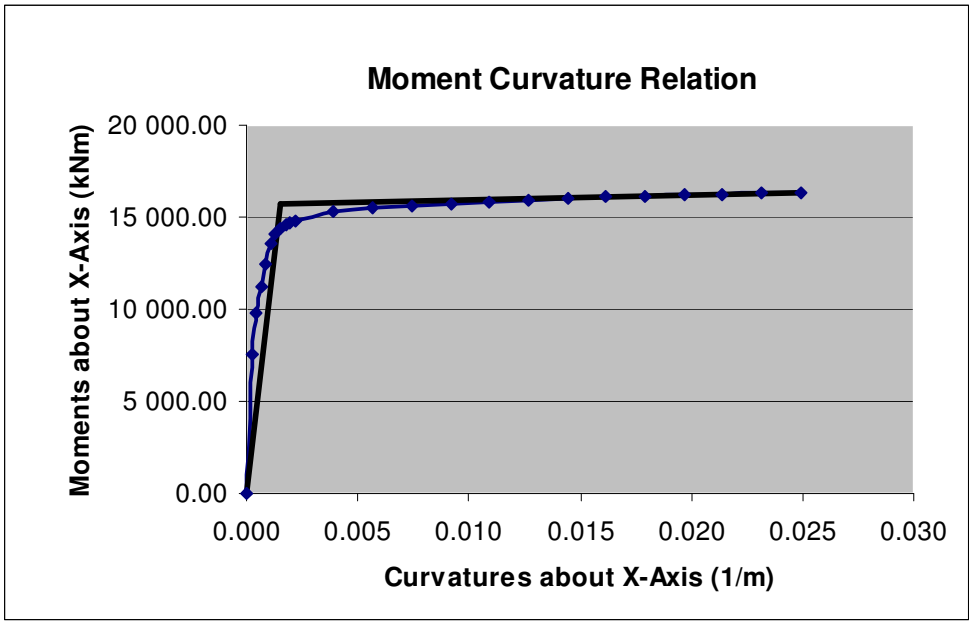

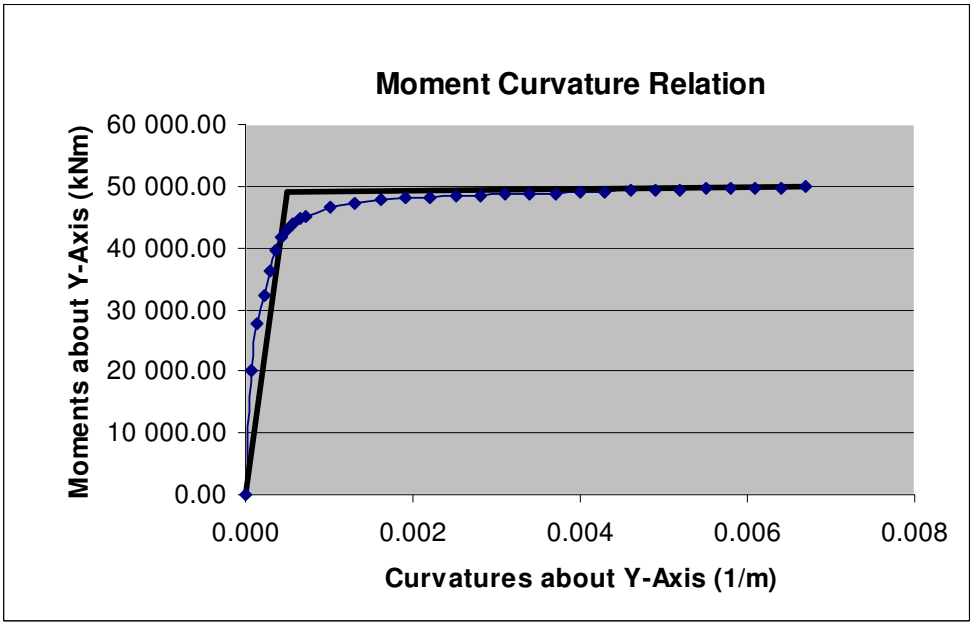

Figure A.6.2. Moment-Curvature relations at the top part of Pier 6 in x and y directions

A.7 Moment-Curvature Relationships of Pier 7

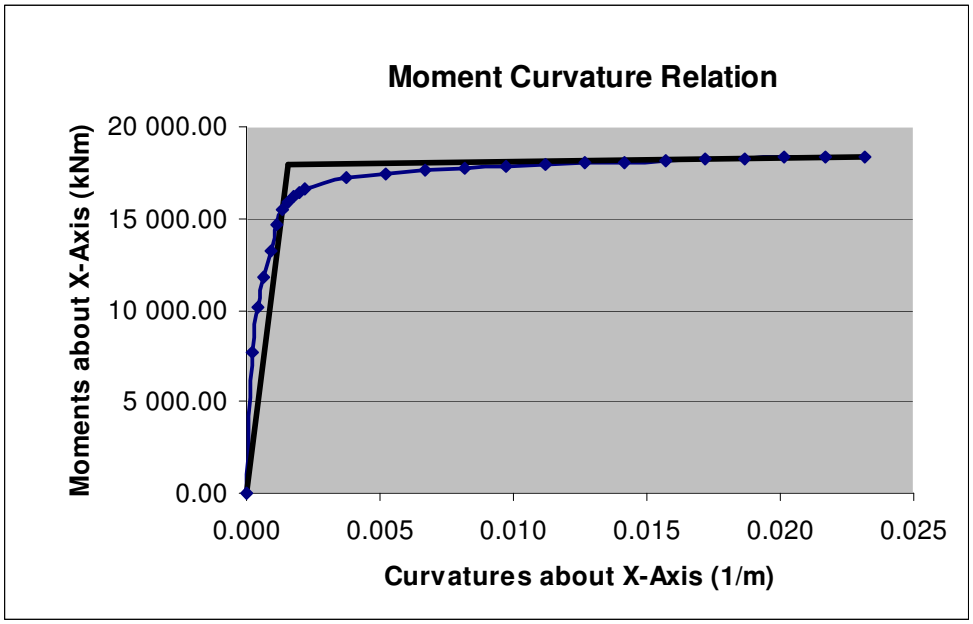

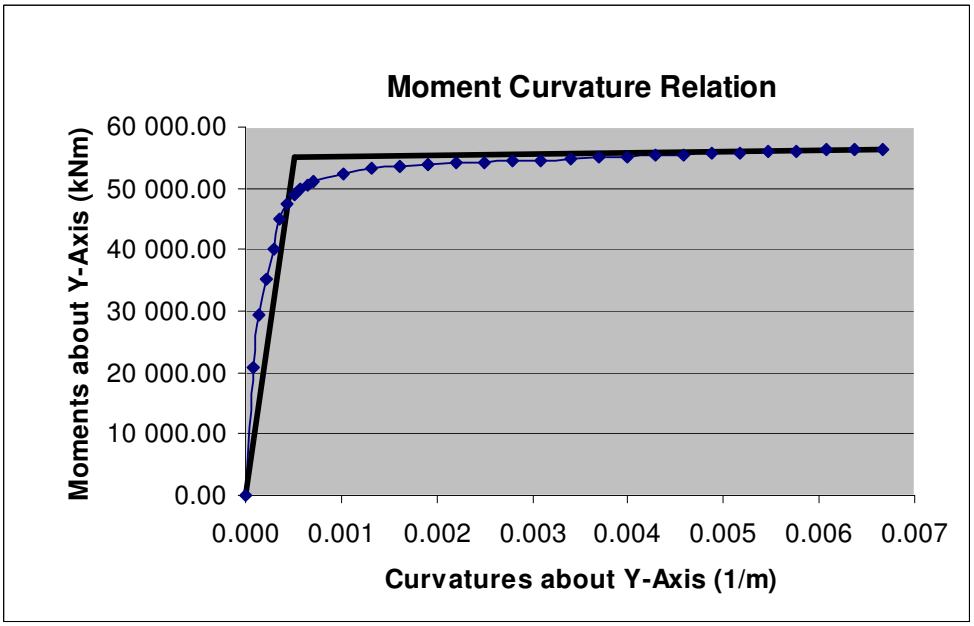

Figure A.7.1. Moment-Curvature relations at the bottom part of Pier 7 in x and y directions

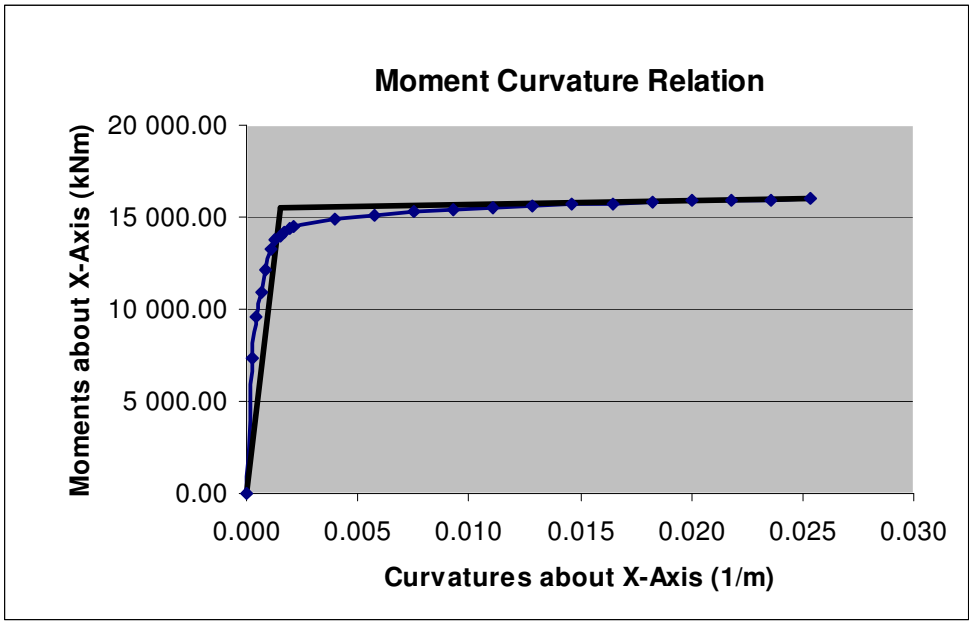

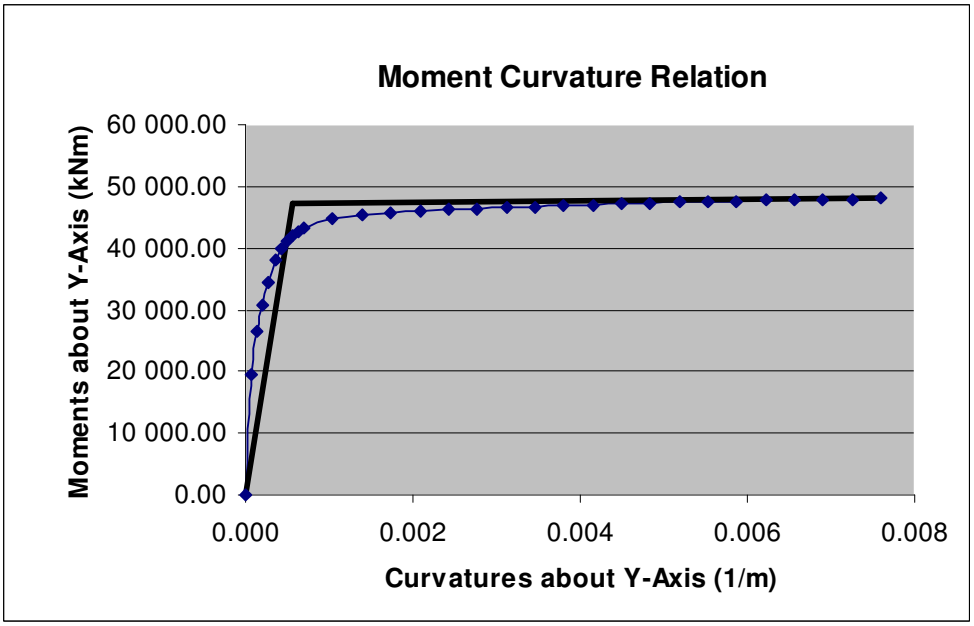

Figure A.7.2. Moment-Curvature relations at the top part of Pier 7 in x and y directions

APPENDIX B: P-M INTERACTIONS OF THE PIERS

B.1. P-M Interactions of Pier 1

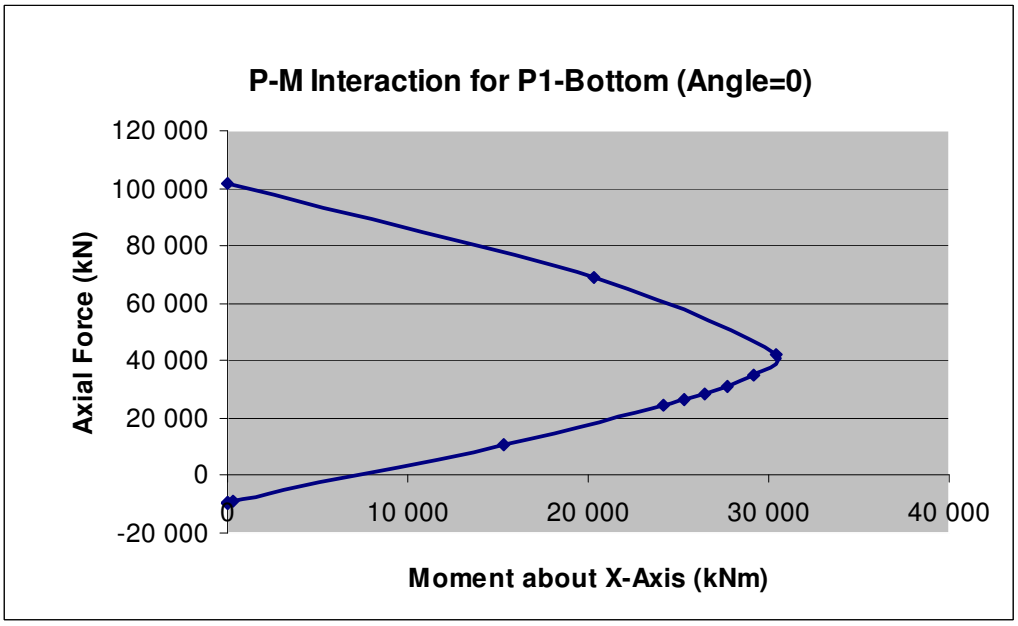

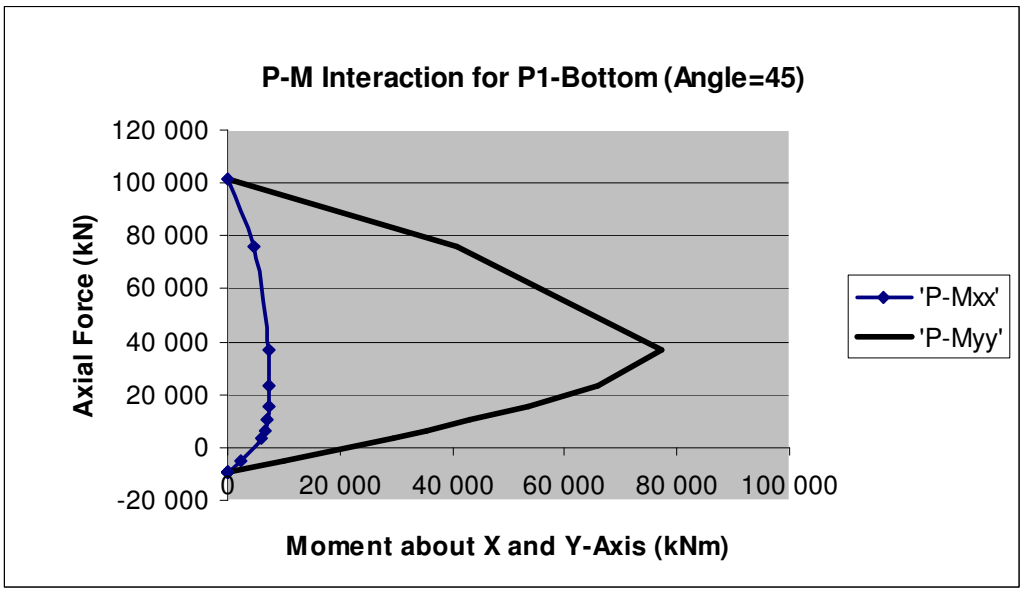

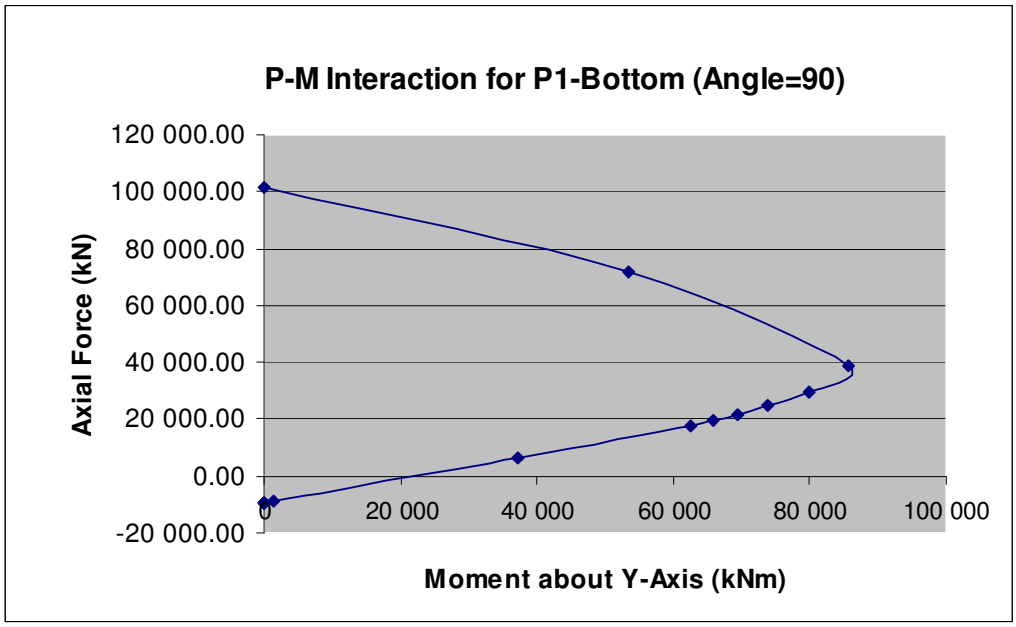

Figure B.1.1. P-M interactions at the bottom part of Pier 1 for angles 0, 45 and 90

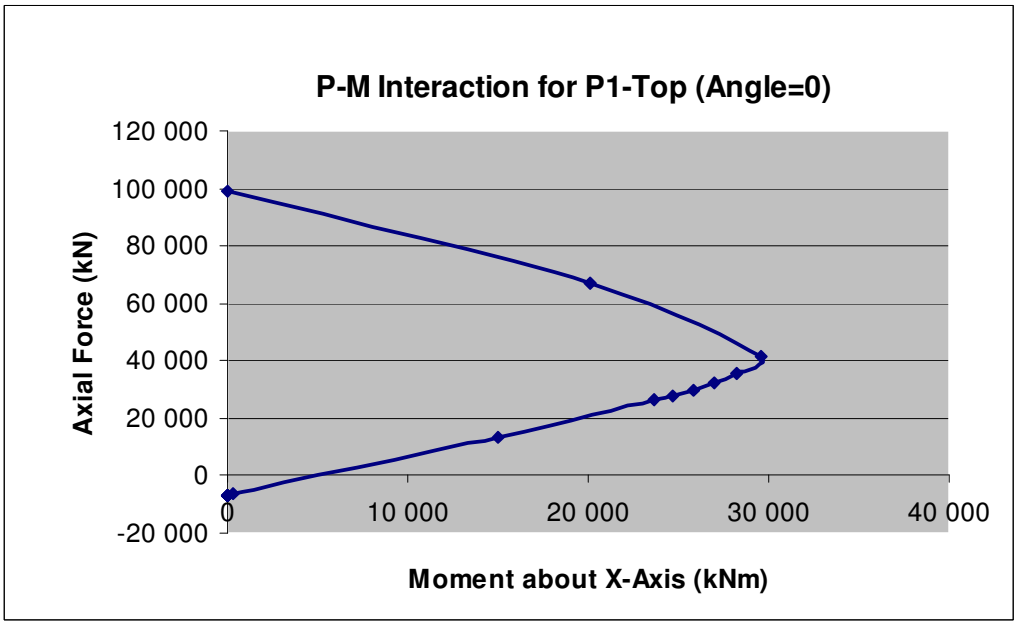

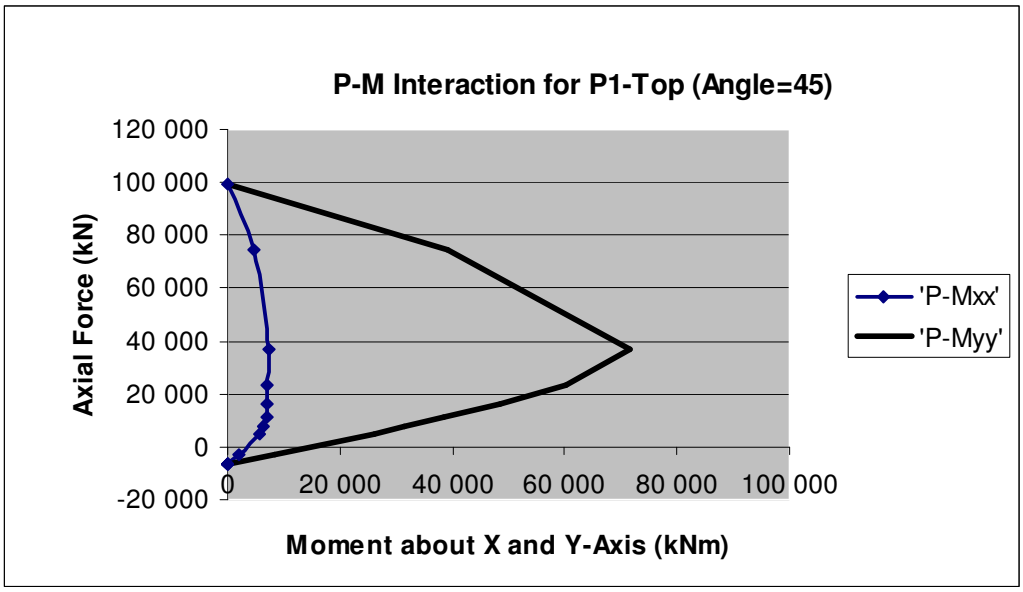

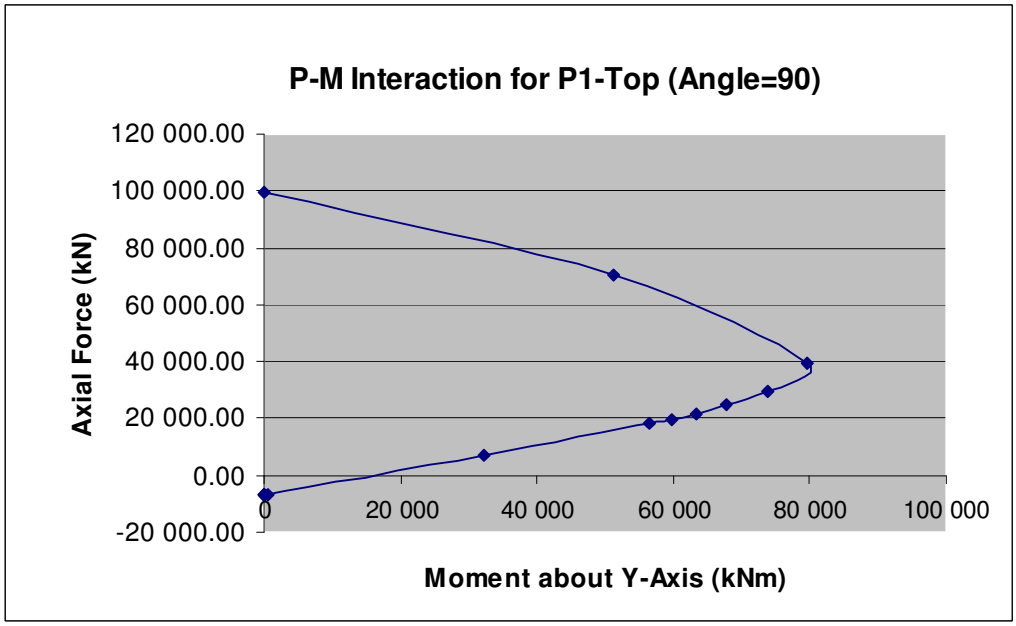

Figure B.1.2. P-M interactions at the top part of Pier 1 for angles 0, 45 and 90

B.2. P-M Interactions of Pier 2

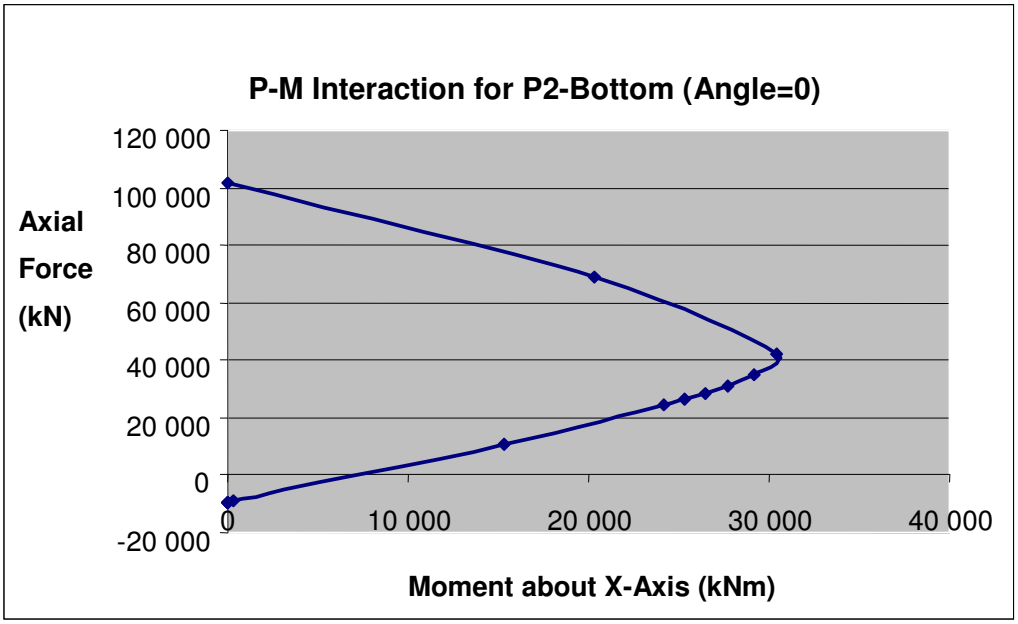

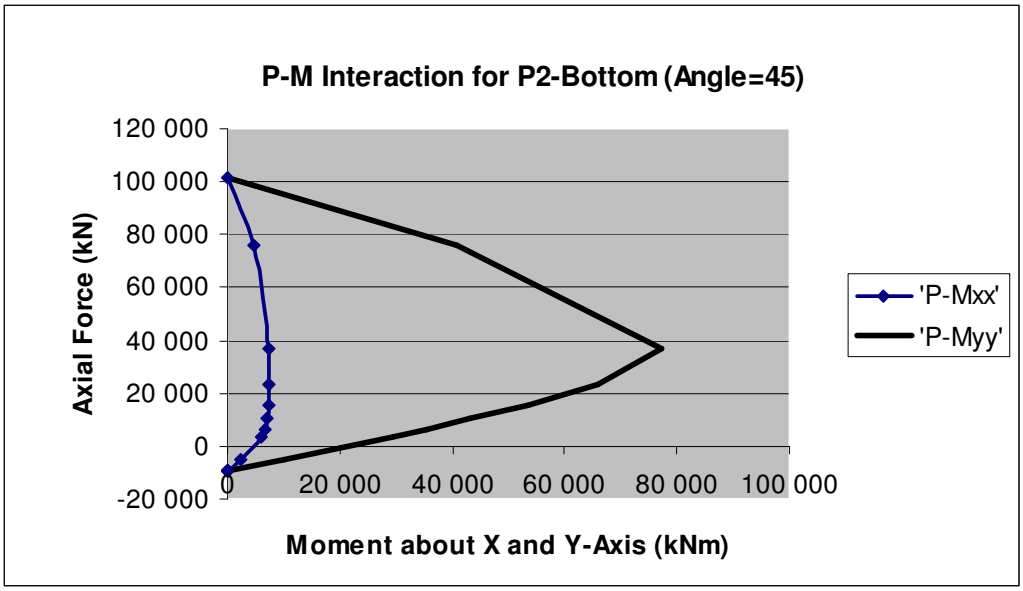

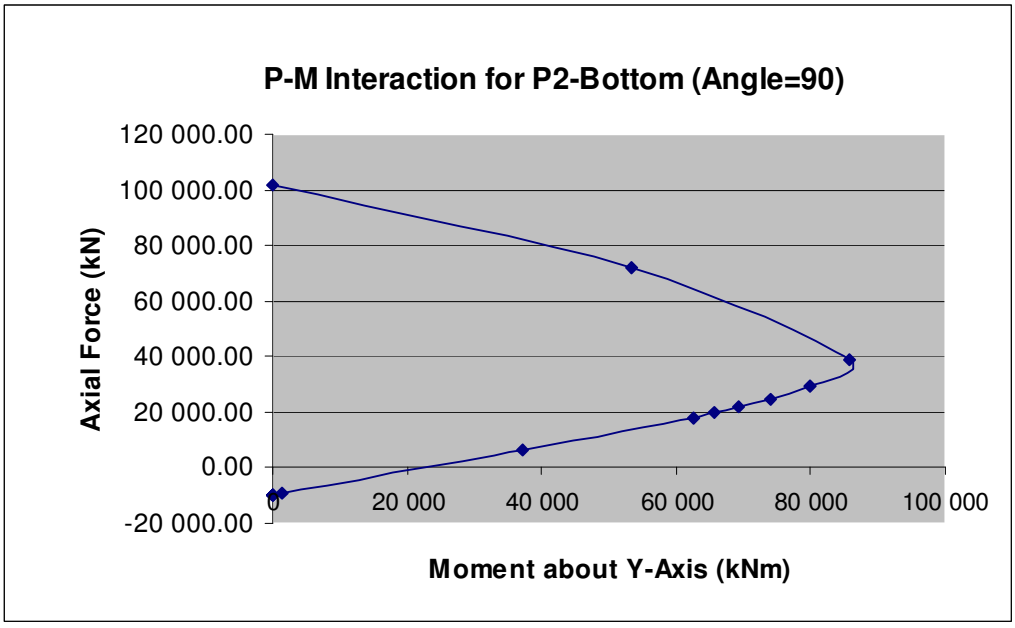

Figure B.2.1. P-M interactions at the bottom part of Pier 2 for angles 0, 45 and 90

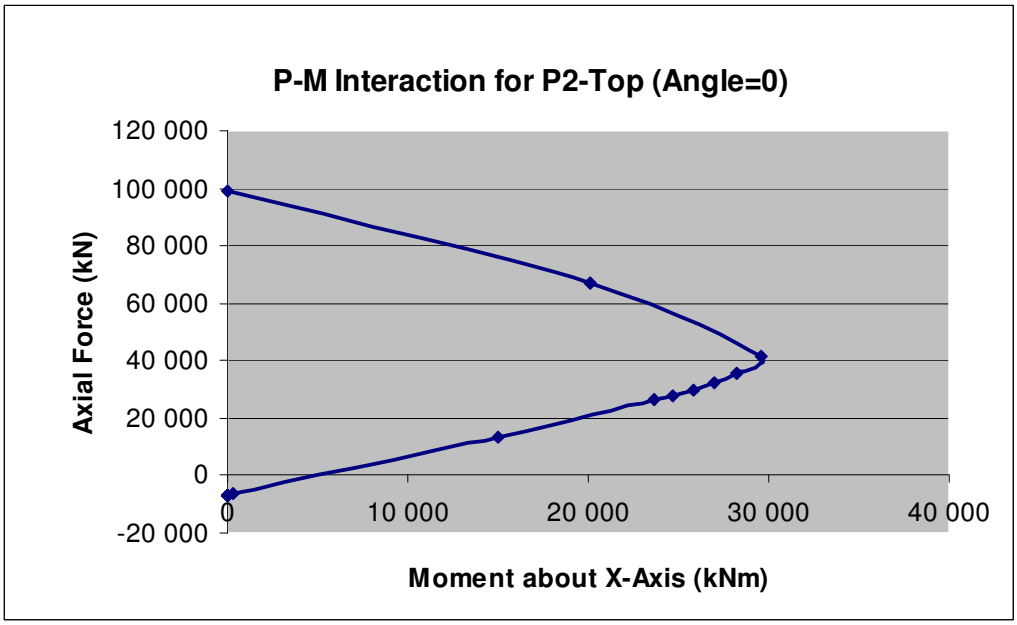

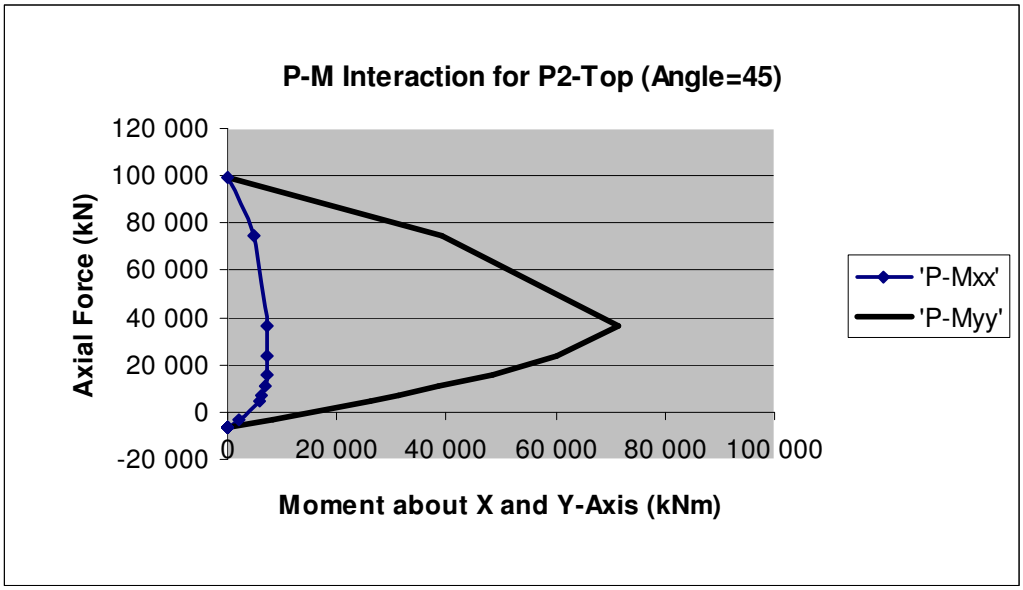

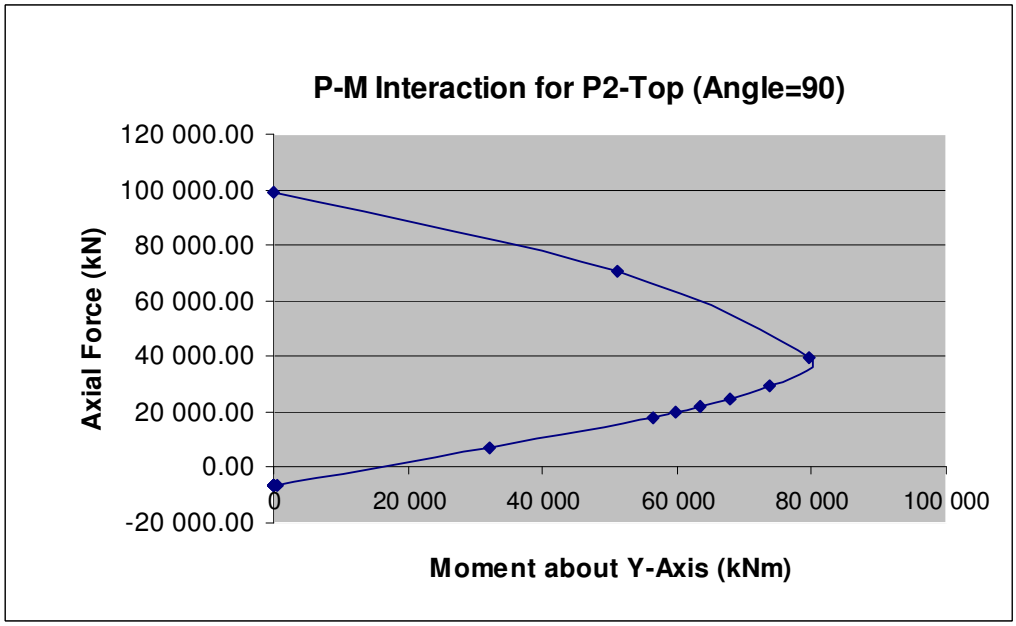

Figure B.2.2. P-M interactions at the top part of Pier 2 for angles 0, 45 and 90

B.3. P-M Interactions of Pier 3

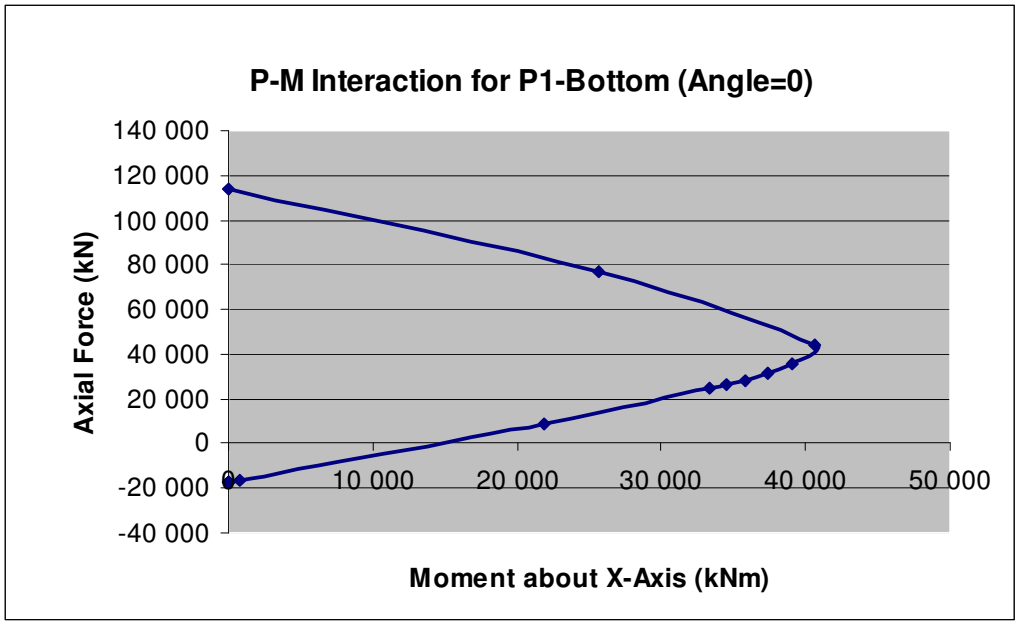

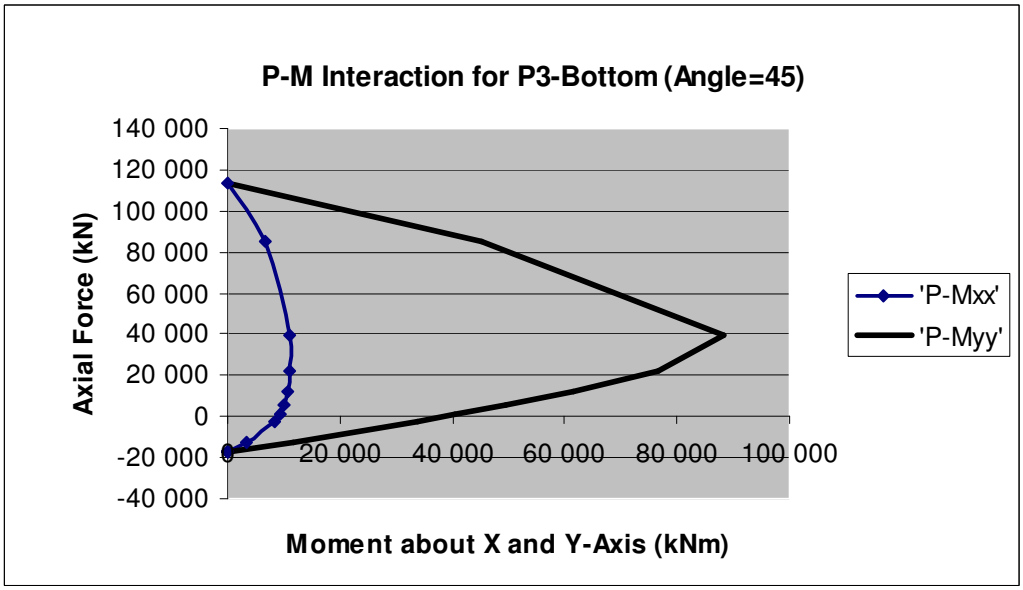

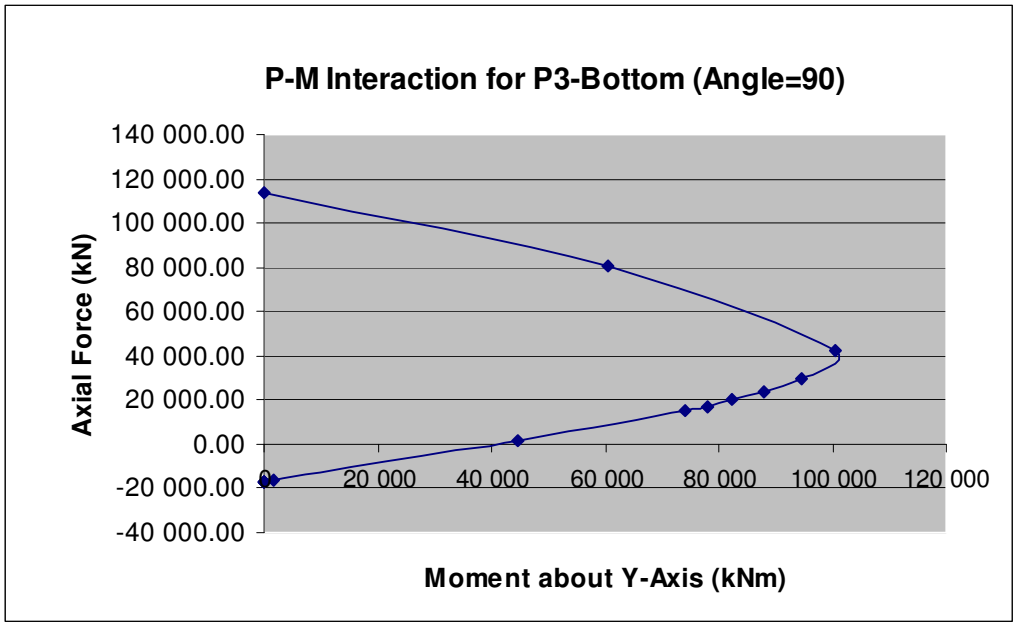

Figure B.3.1. P-M interactions at the bottom part of Pier 3 for angles 0, 45 and 90

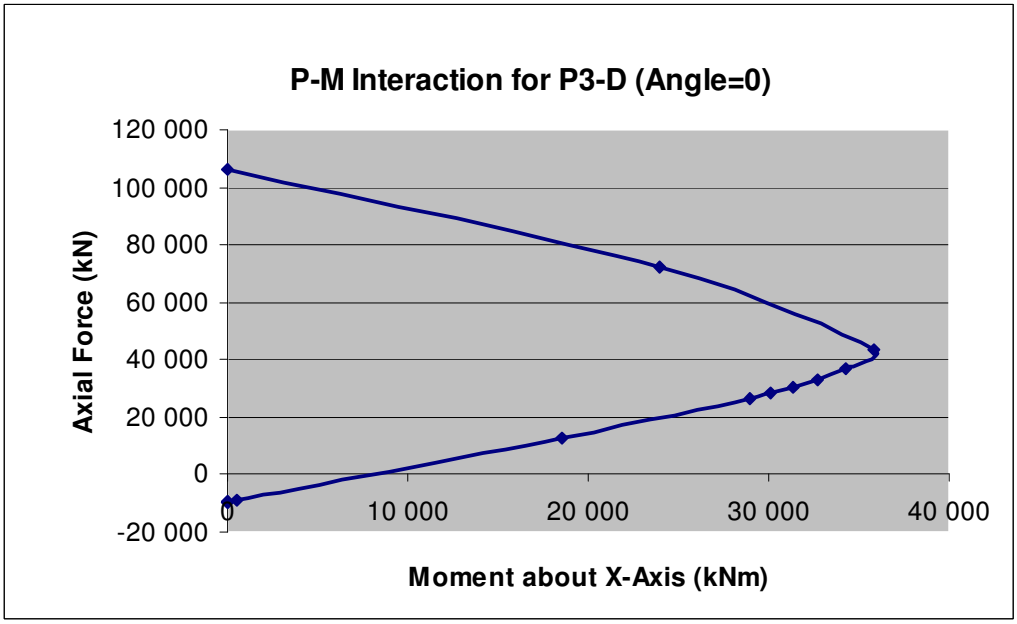

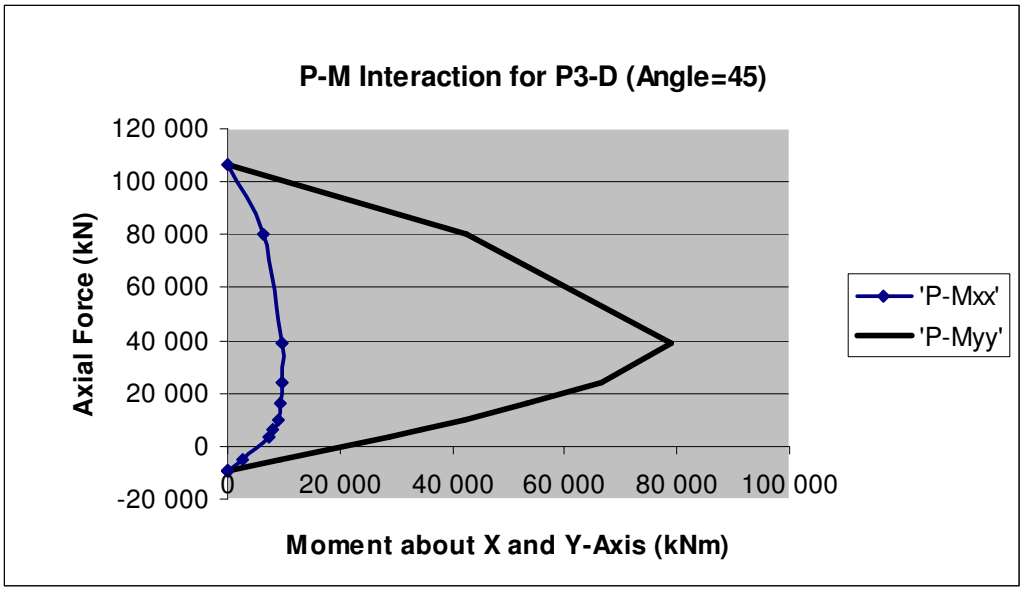

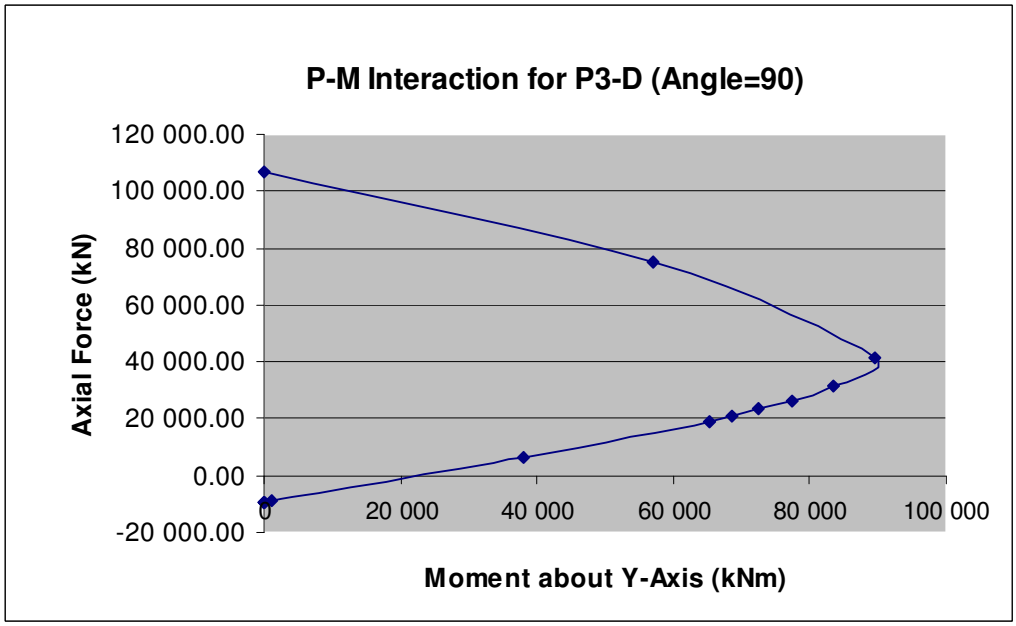

Figure B.3.2. P-M interactions at decreased part of Pier 3 for angles 0, 45 and 90

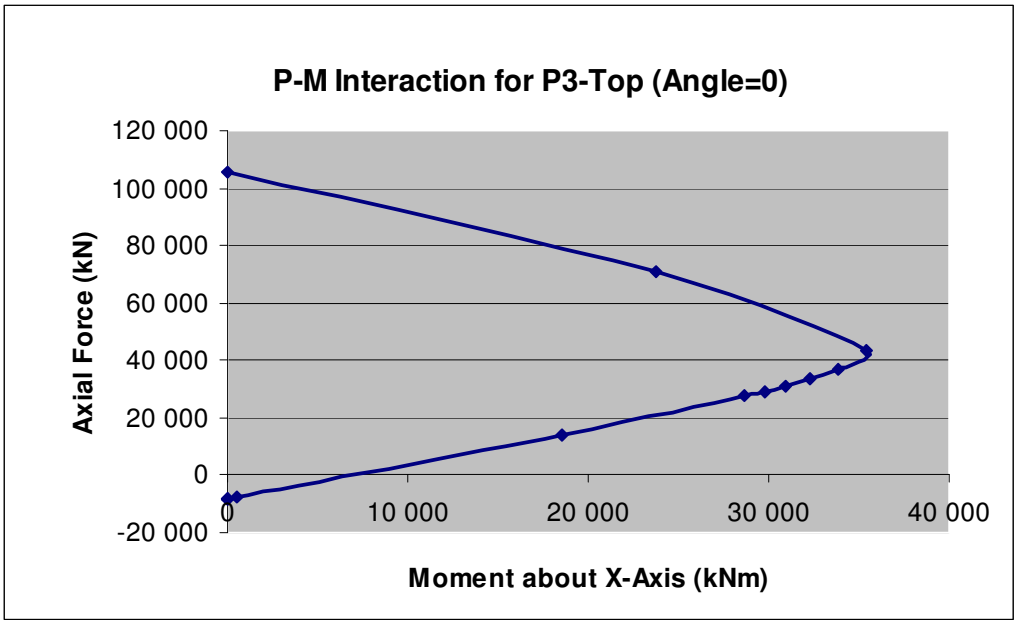
P-M Interaction for P3-Top (Angle=0)
120 000
100 000
80 000
60 000
40 000
20 000
0
-20 000
Axial Force (kN)
0
10 000
20 000
30 000
40 000
Moment about X-Axis (kNm)

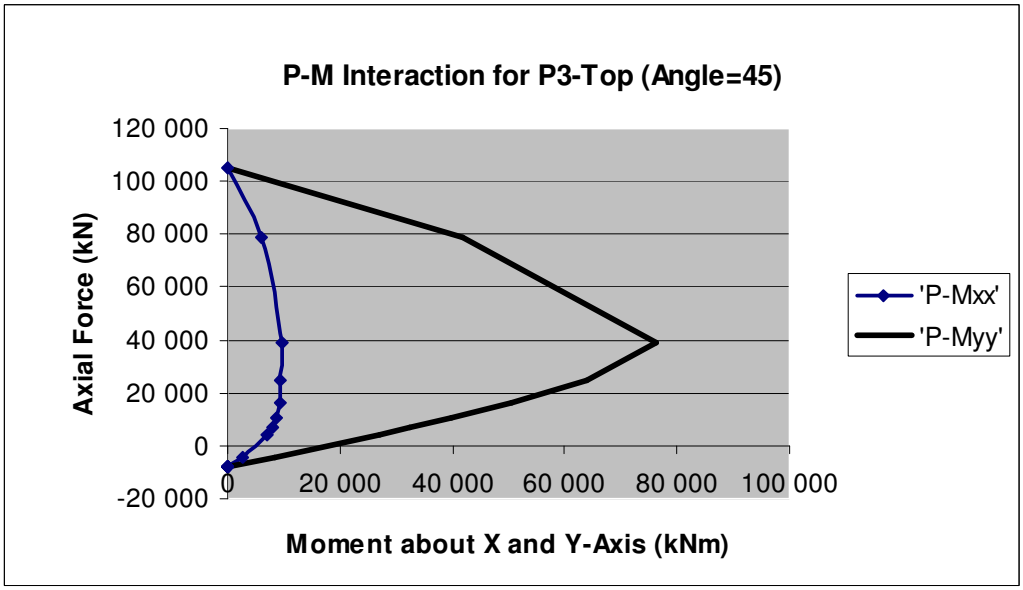
P-M Interaction for P3-Top (Angle=45)
120 000
100 000
80 000
60 000
40 000
20 000
0
-20 000
Axial Force (kN)
0
20 000
40 000
60 000
80 000
100 000
Moment about X and Y-Axis (kNm)
'P-Mxx'
'P-Myy'

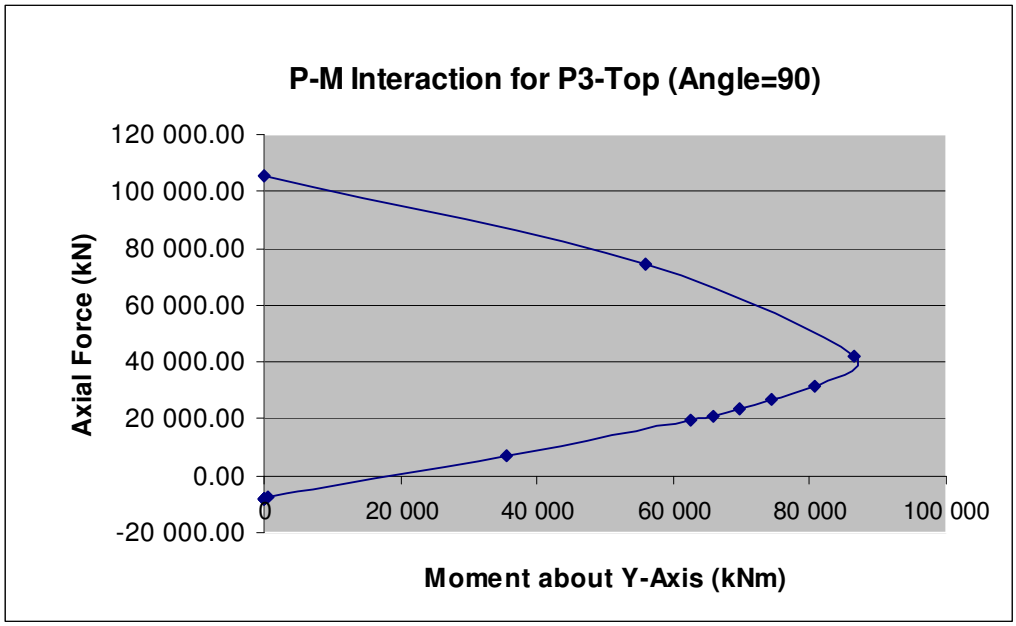

Figure B.3.3. P-M interactions at the top part of Pier 3 for angles 0, 45 and 90

B.4. P-M Interactions of Pier 4

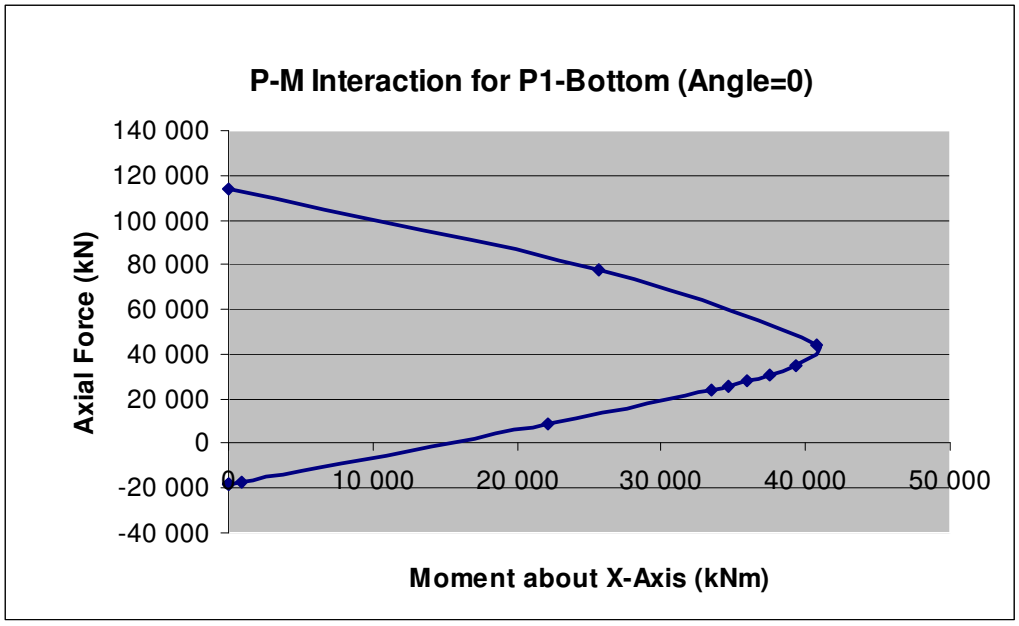

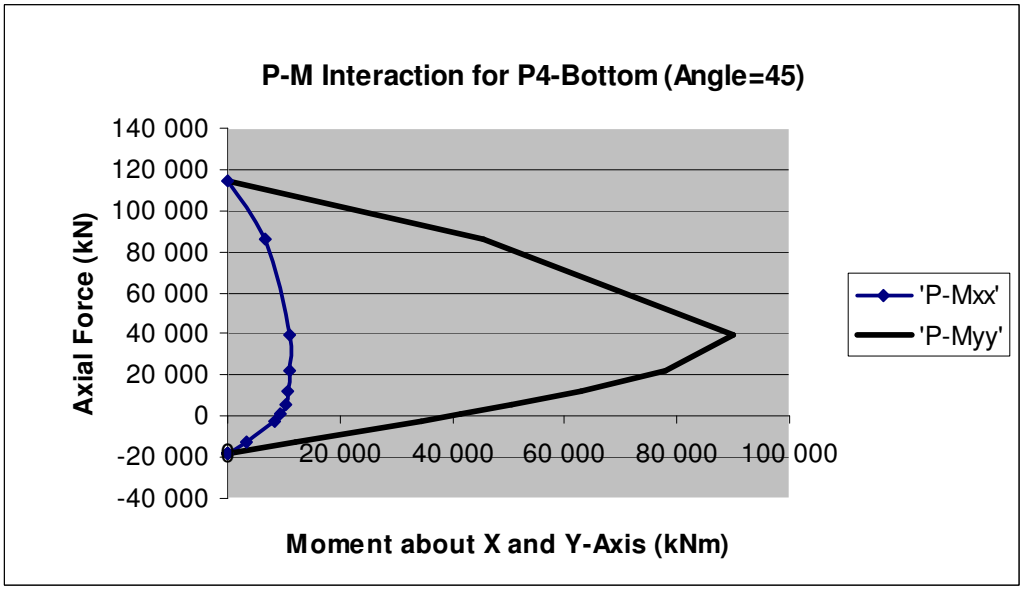

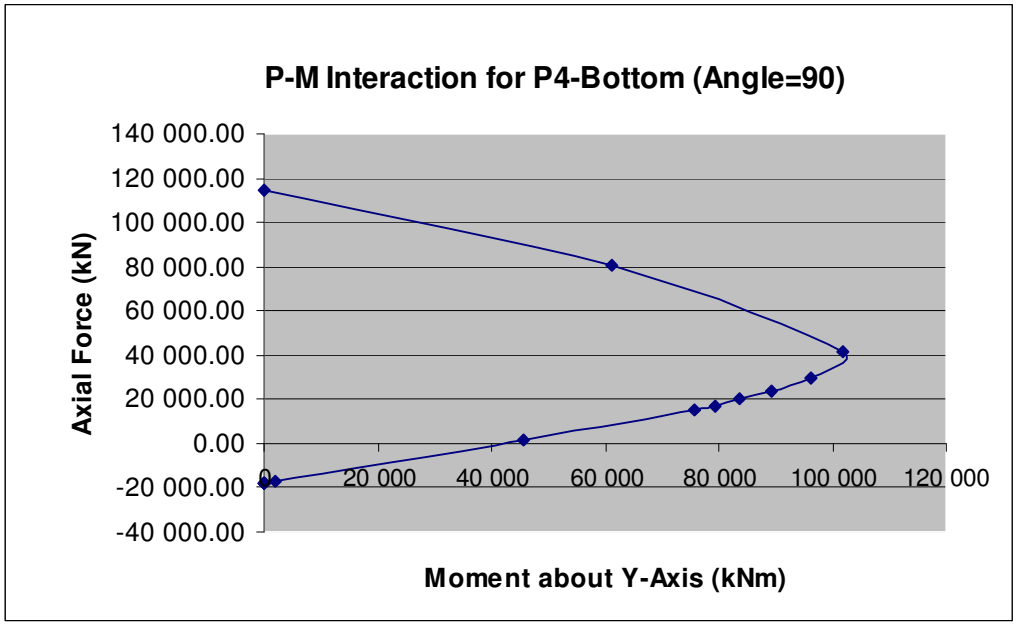

Figure B.4.1. P-M interactions at the bottom part of Pier 4 for angles 0, 45 and 90

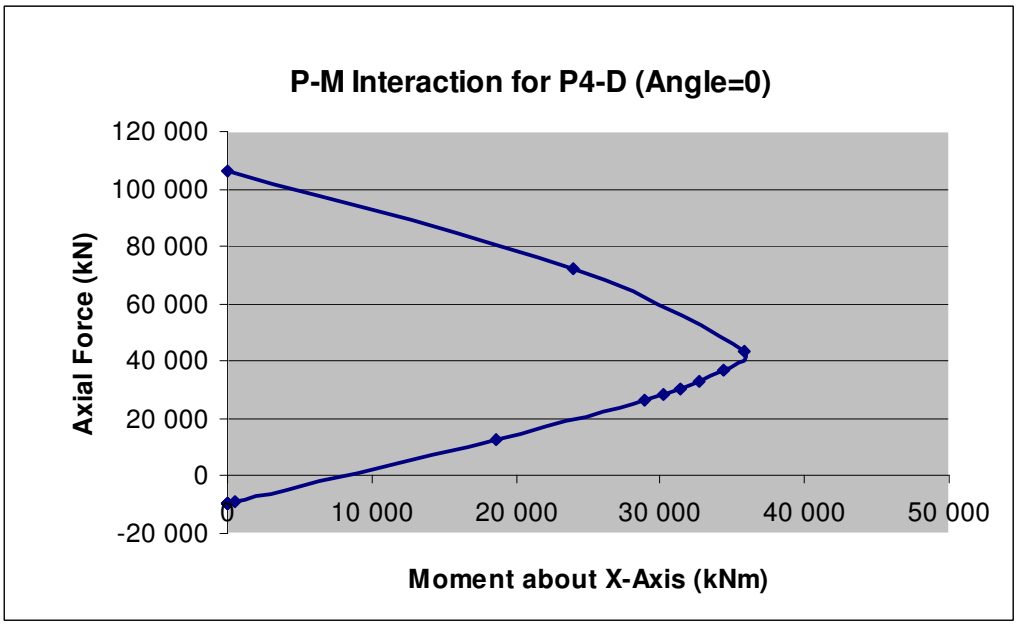

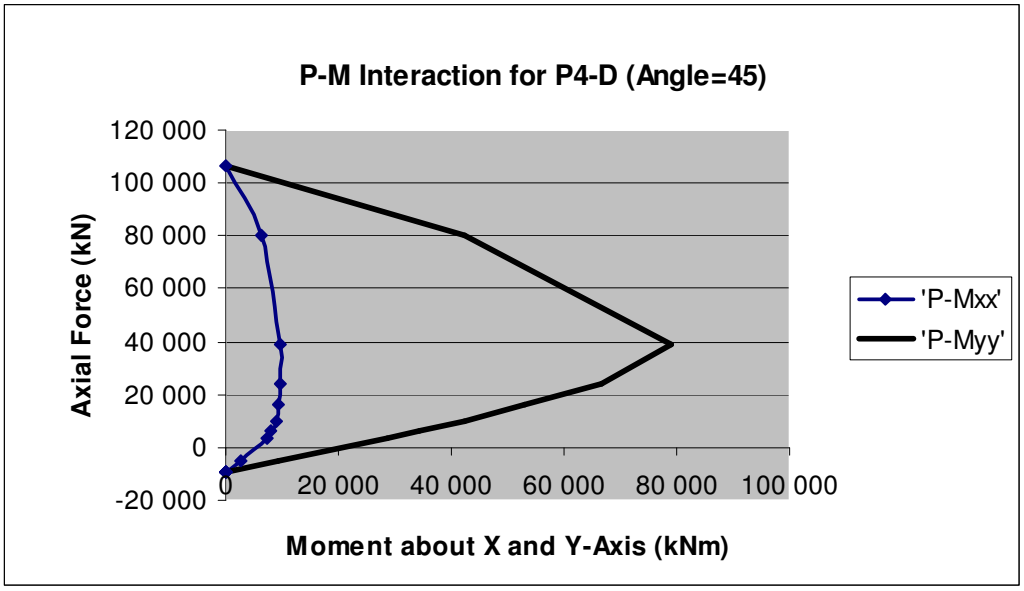

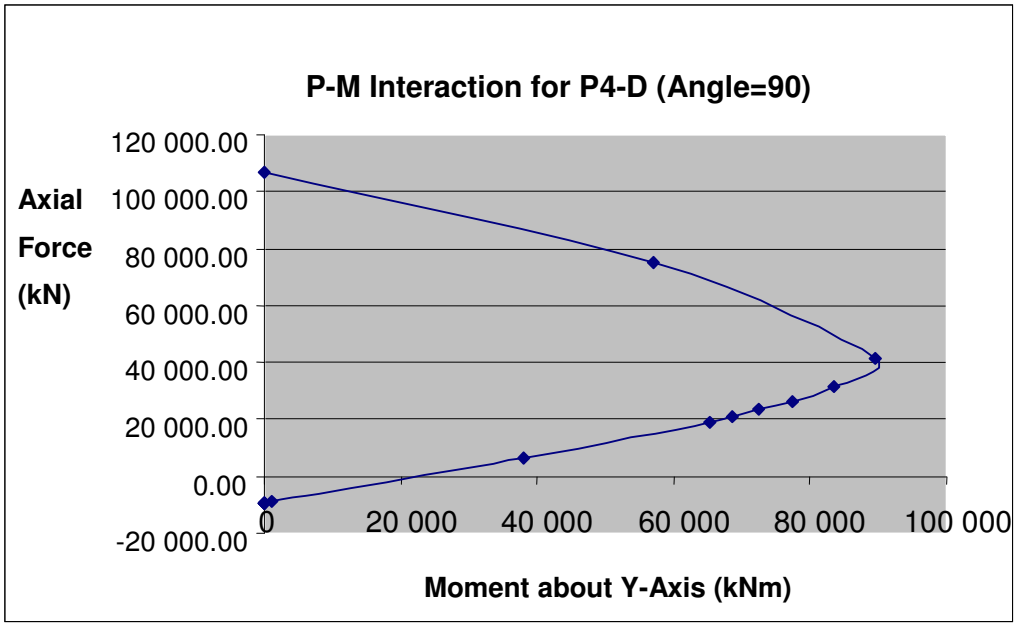

Figure B.4.2. P-M interactions at decreased part of Pier 4 for angles 0, 45 and 90

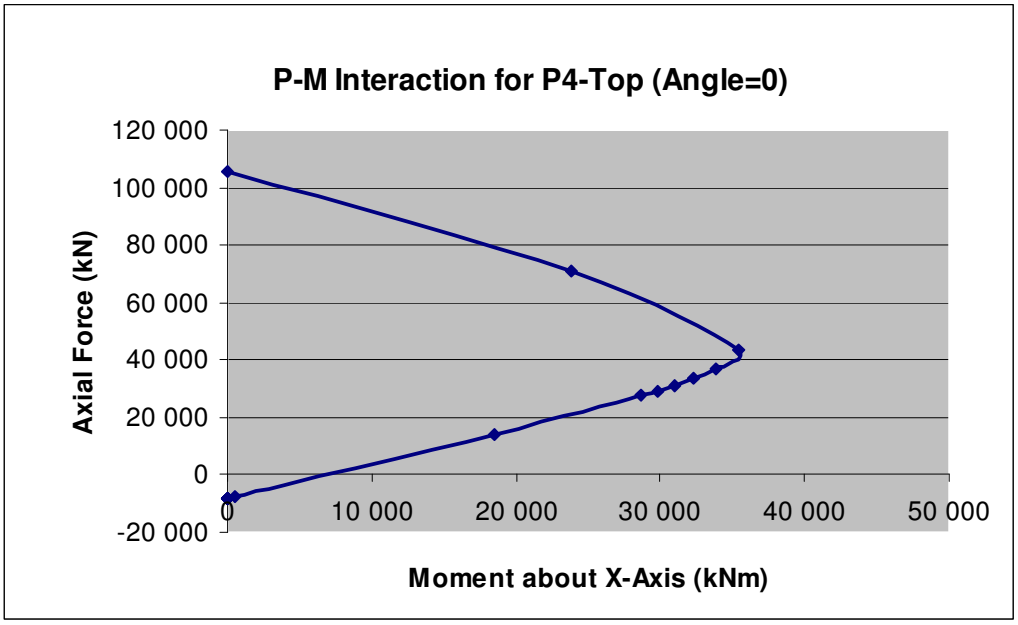
P-M Interaction for P4-Top (Angle=0)
Axial Force (kN)
120 000
100 000
80 000
60 000
40 000
20 000
0
-20 000
0
10 000
20 000
30 000
40 000
50 000
Moment about X-Axis (kNm)

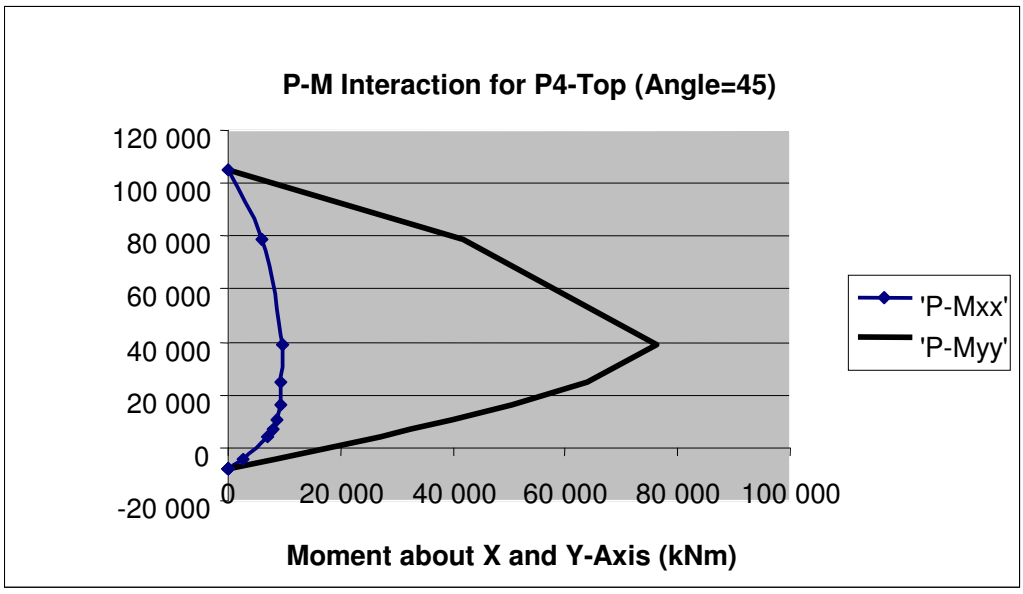
P-M Interaction for P4-Top (Angle=45)
120 000
100 000
80 000
60 000
40 000
20 000
0
-20 000
0
20 000
40 000
60 000
80 000
100 000
Moment about X and Y-Axis (kNm)
'P-Mxx'
'P-Myy'

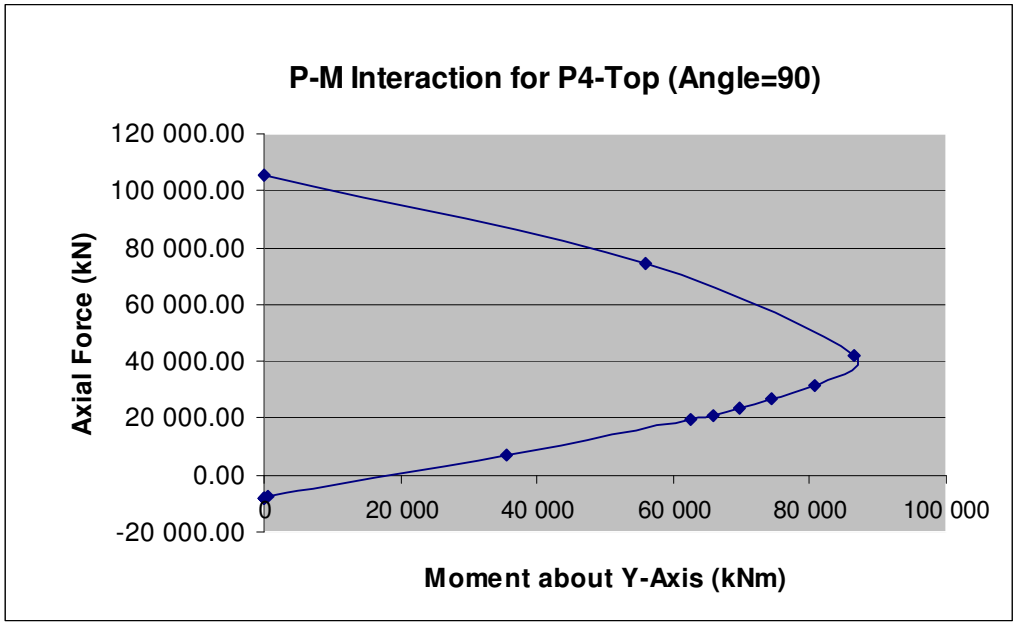

Figure B.4.3. P-M interactions at the top part of Pier 4 for angles 0, 45 and 90

B.5. P-M Interactions of Pier 5

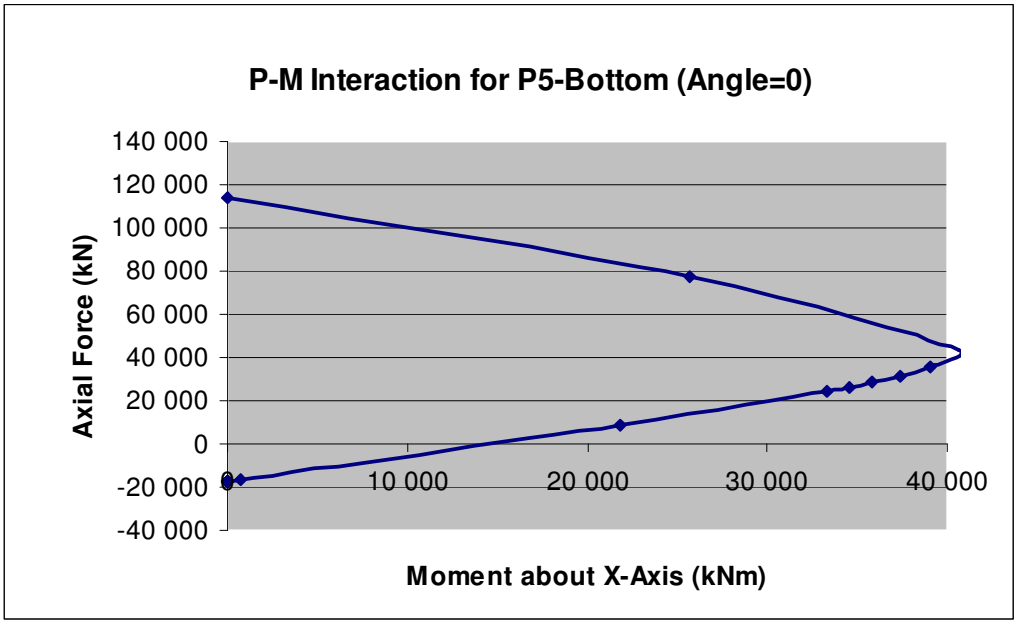

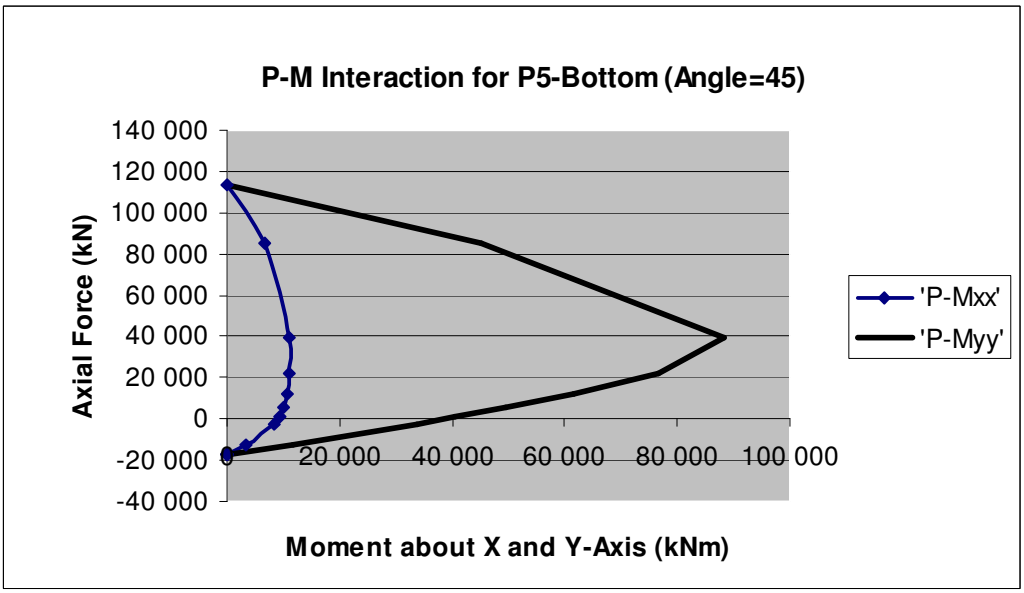

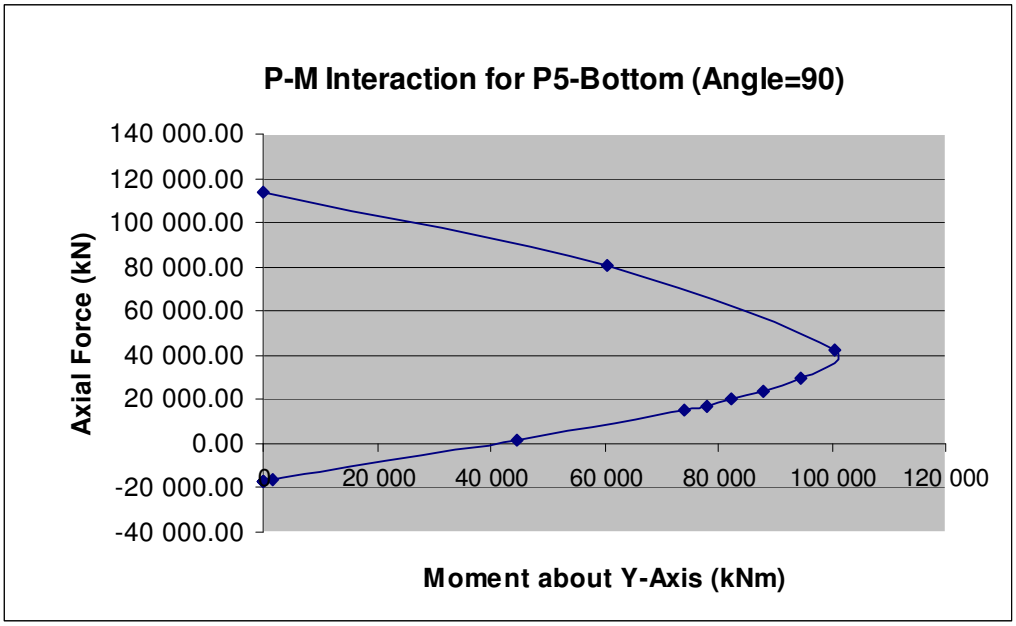

Figure B.5.1. P-M interactions at the bottom part of Pier 5 for angles 0, 45 and 90

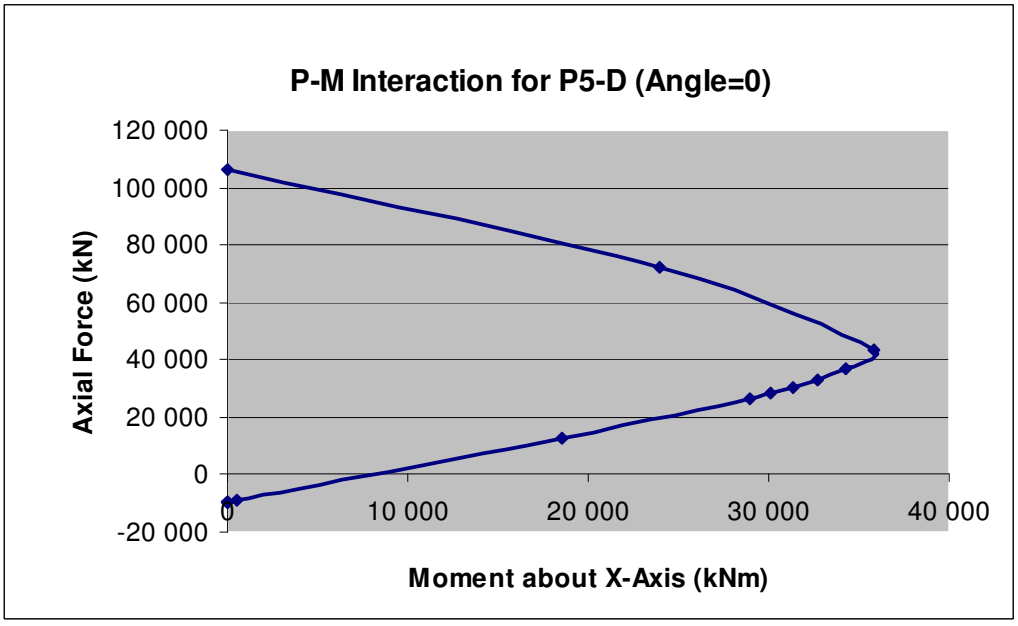

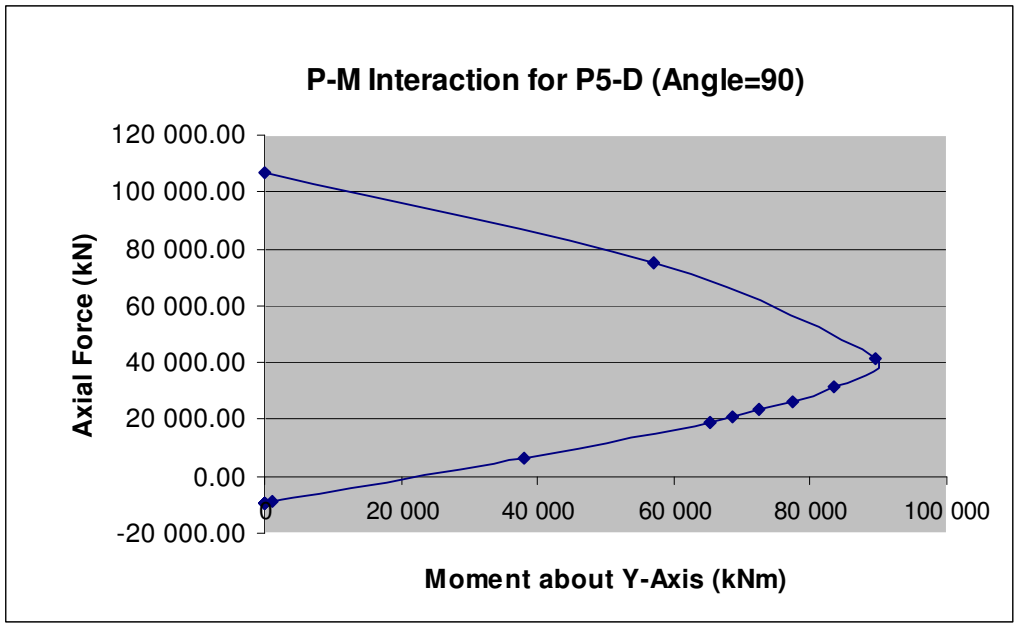

Figure B.5.2. P-M interactions at decreased part of Pier 5 for angles 0 and 90

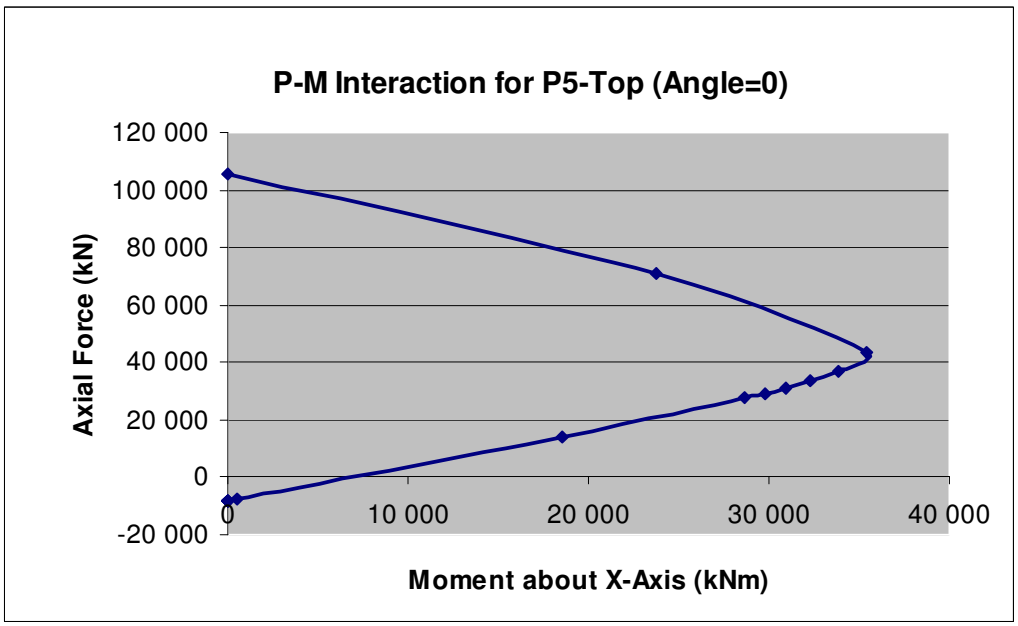

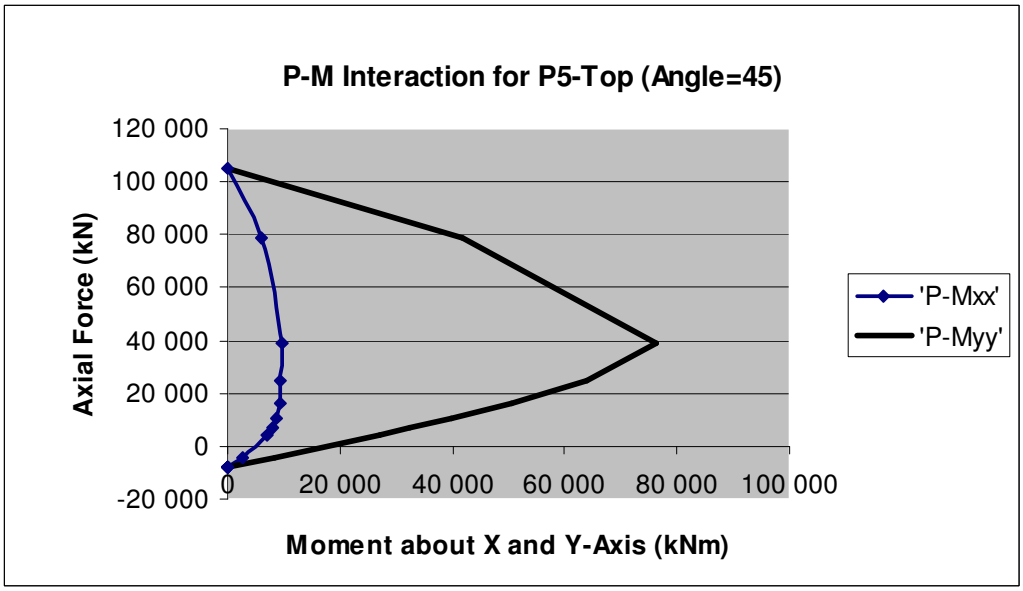

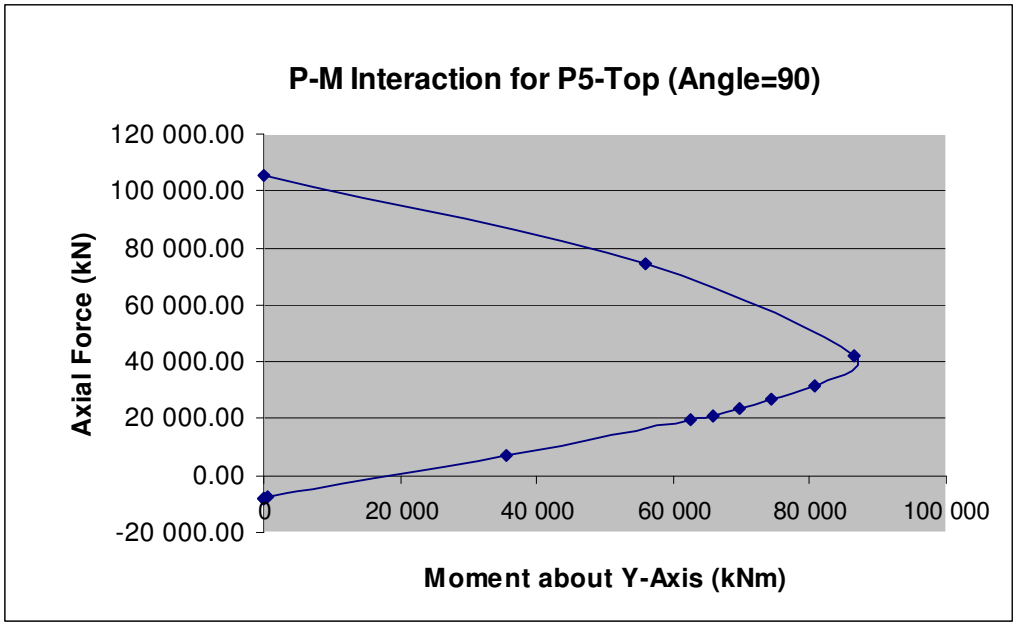

Figure B.5.3. P-M interactions at the top part of Pier 5 for angles 0, 45 and 90

B.6. P-M Interactions of Pier 6

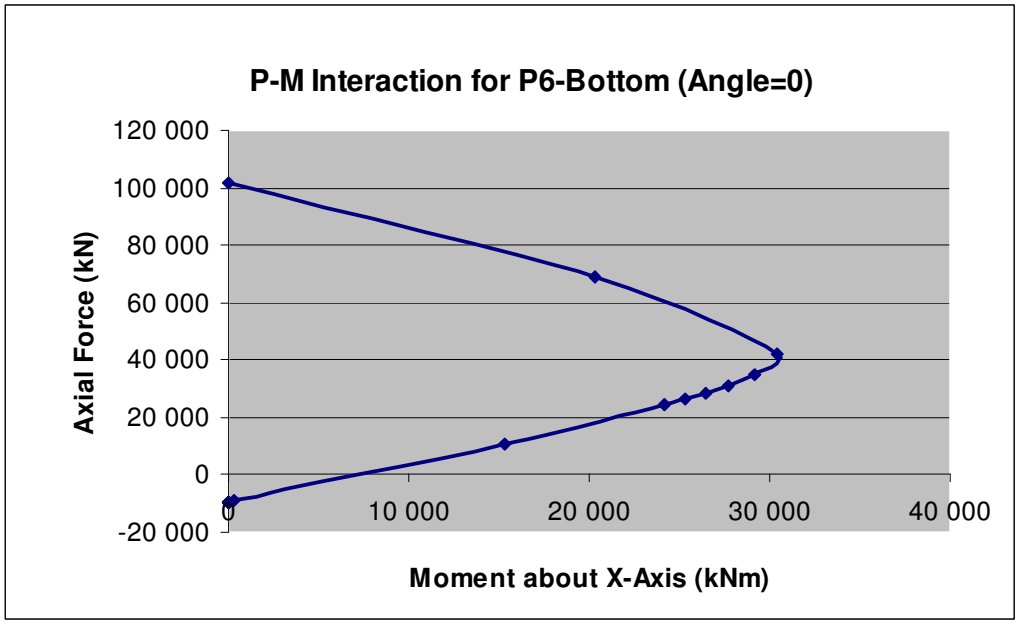

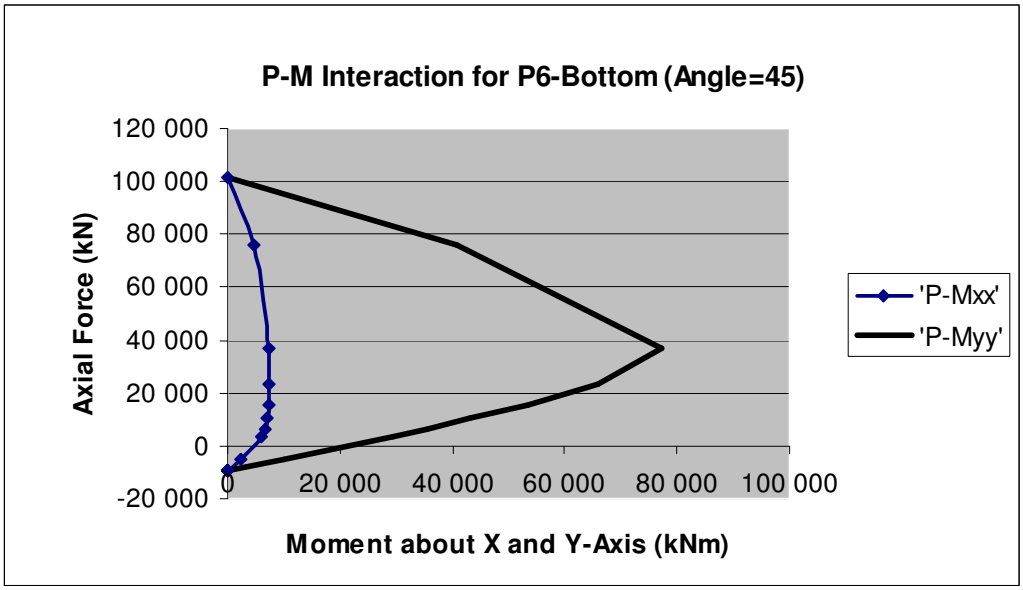

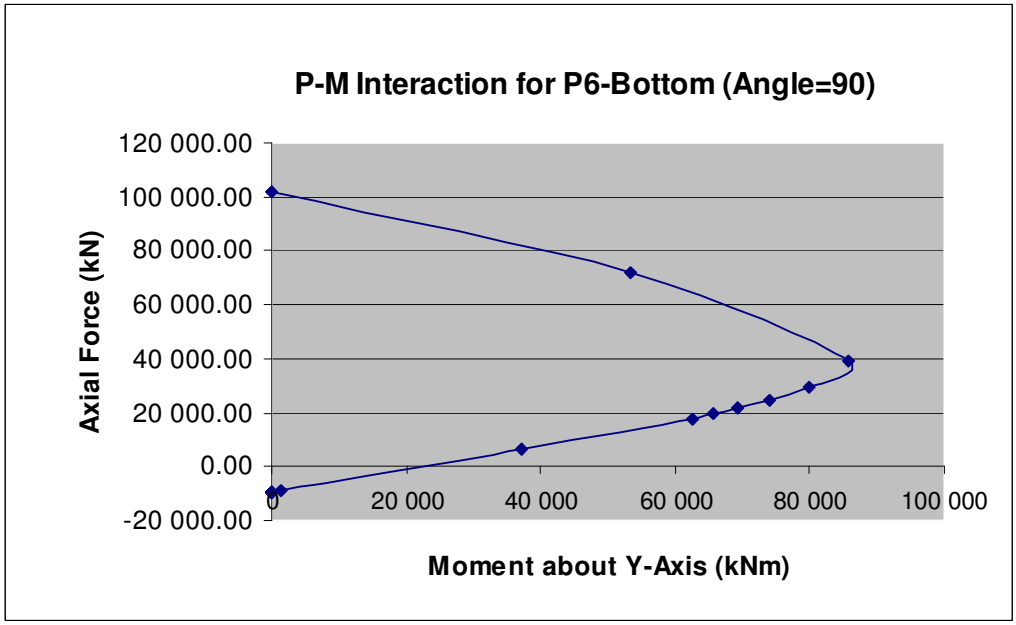

Figure B.6.1. P-M interactions at the bottom part of Pier 6 for angles 0, 45 and 90

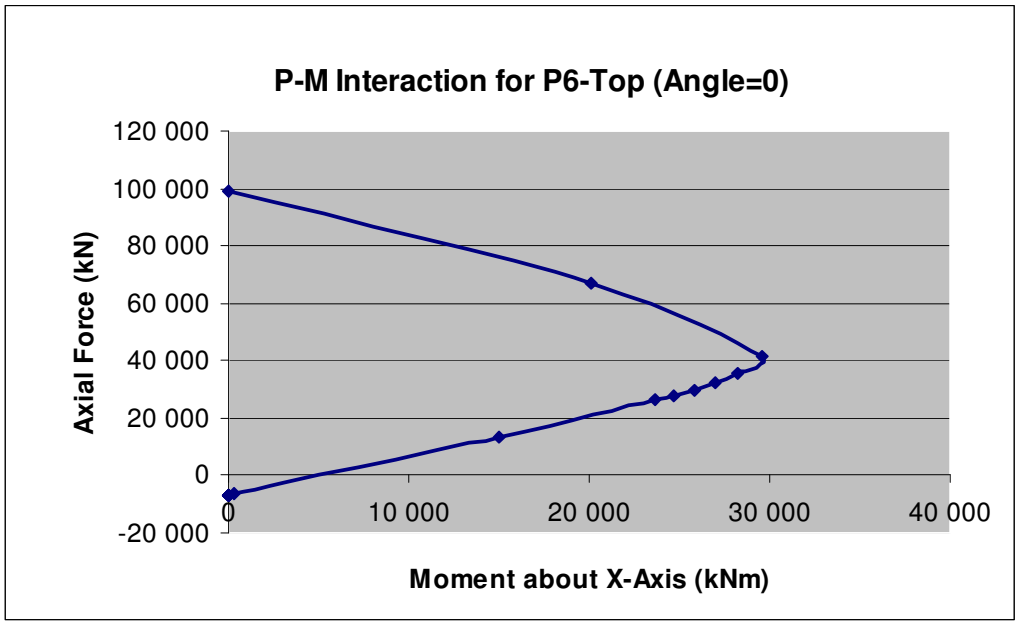
P-M Interaction for P6-Top (Angle=0)
120 000
100 000
80 000
60 000
40 000
20 000
0
-20 000
Axial Force (kN)
0
10 000
20 000
30 000
40 000
Moment about X-Axis (kNm)

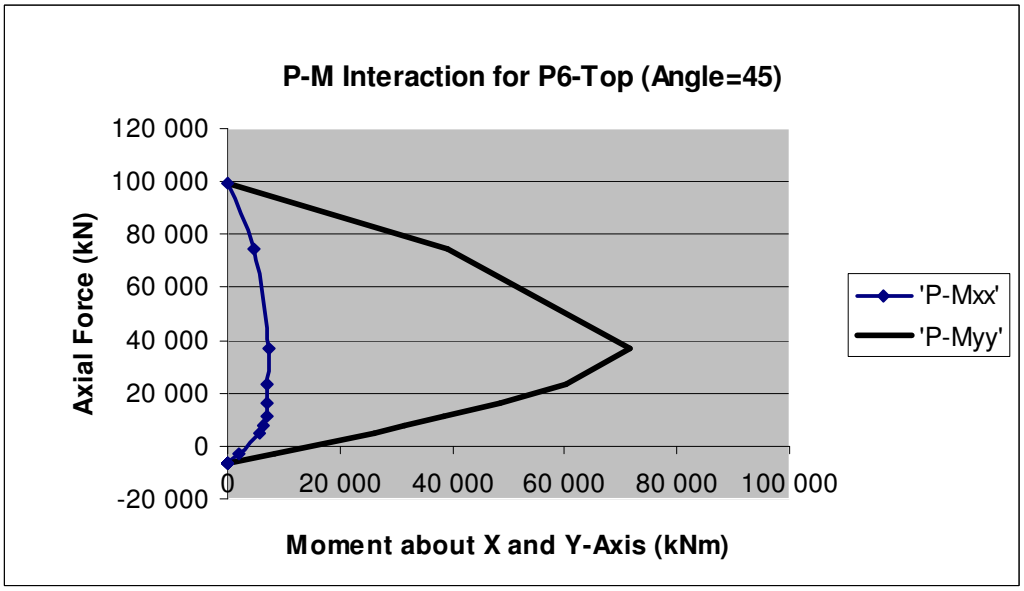
P-M Interaction for P6-Top (Angle=45)
120 000
100 000
80 000
60 000
40 000
20 000
0
-20 000
Axial Force (kN)
0
20 000
40 000
60 000
80 000
100 000
Moment about X and Y-Axis (kNm)
'P-Mxx'
'P-Myy'

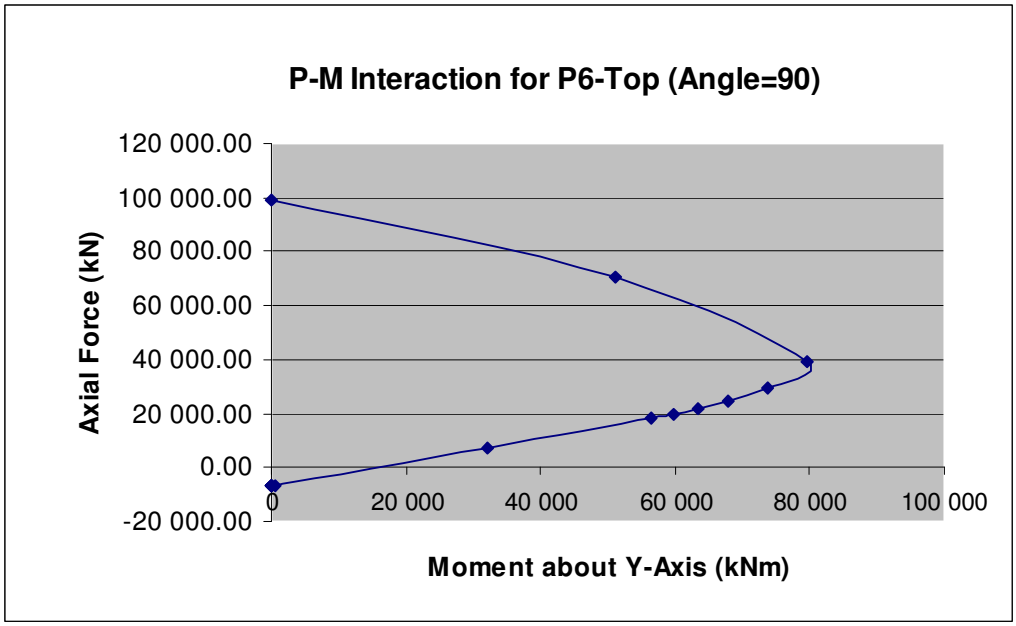

Figure B.6.2. P-M interactions at the top part of Pier 6 for angles 0, 45 and 90

B.7. P-M Interactions of Pier 7

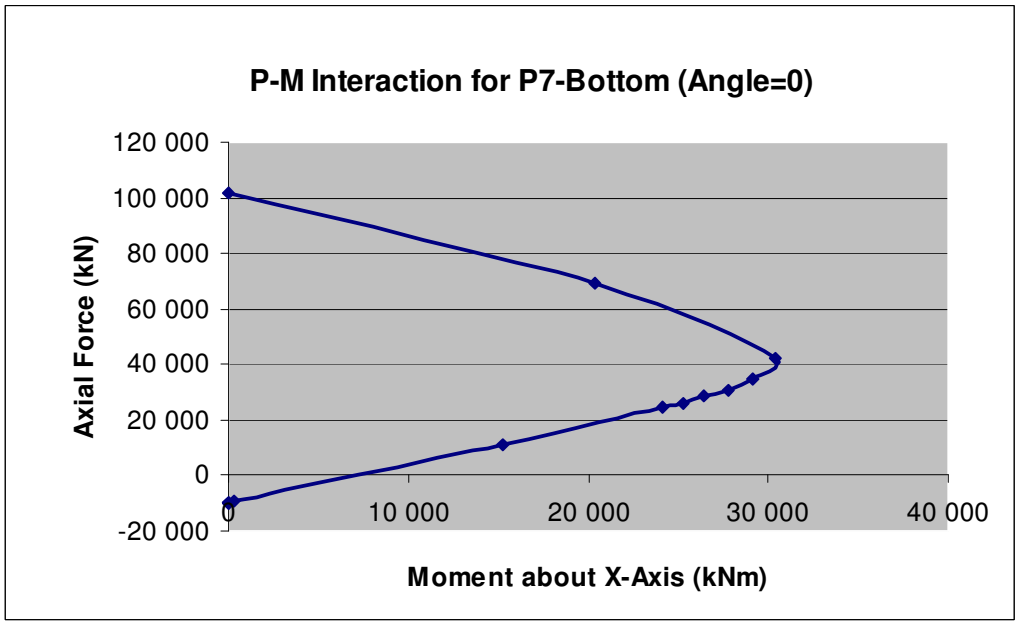

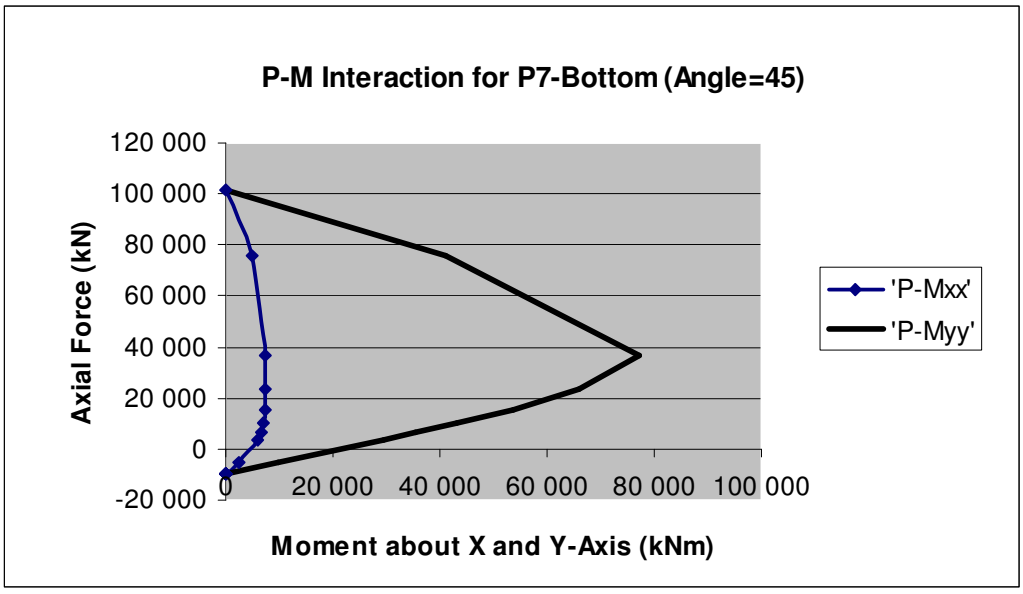

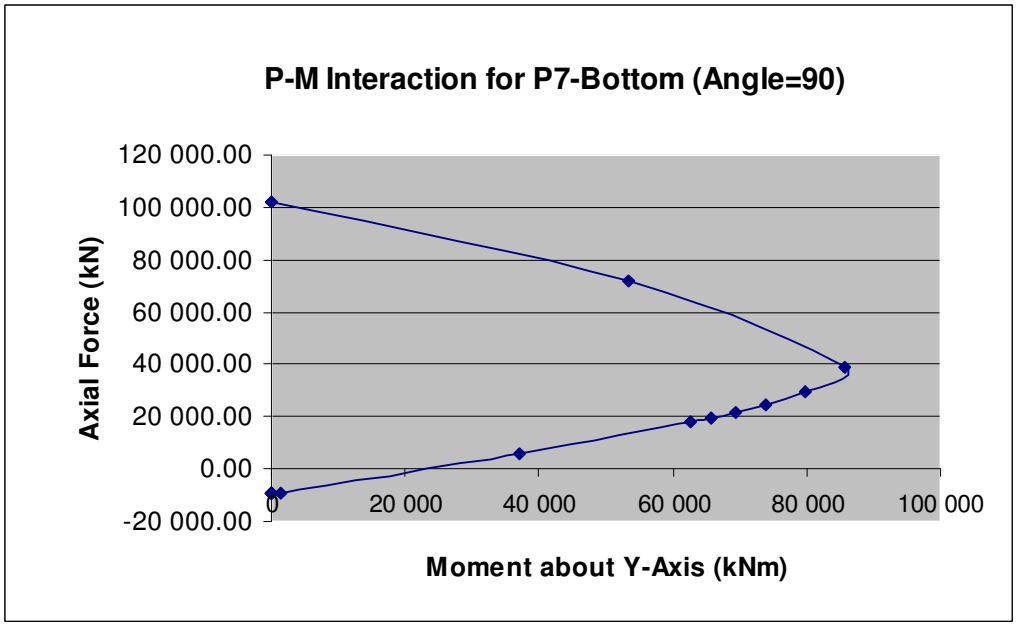

Figure B.7.1. P-M interactions at the bottom part of Pier 7 for angles 0, 45 and 90

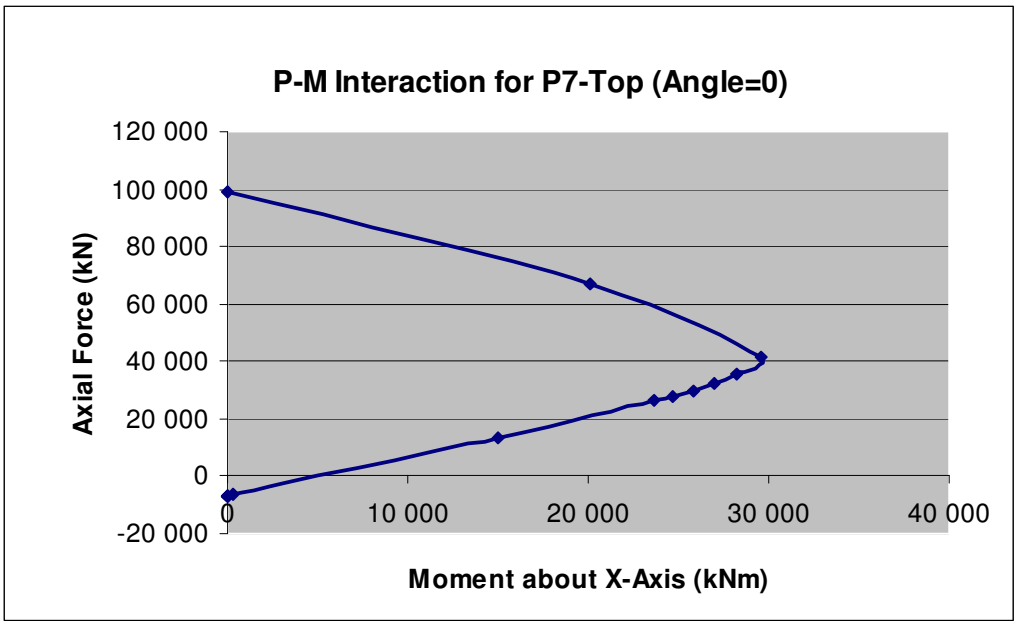

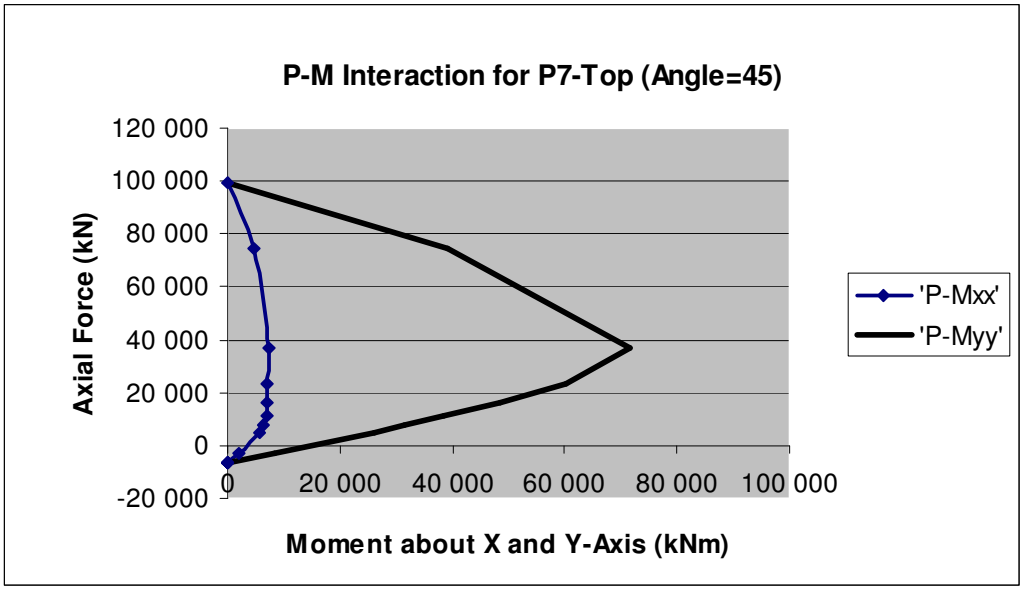

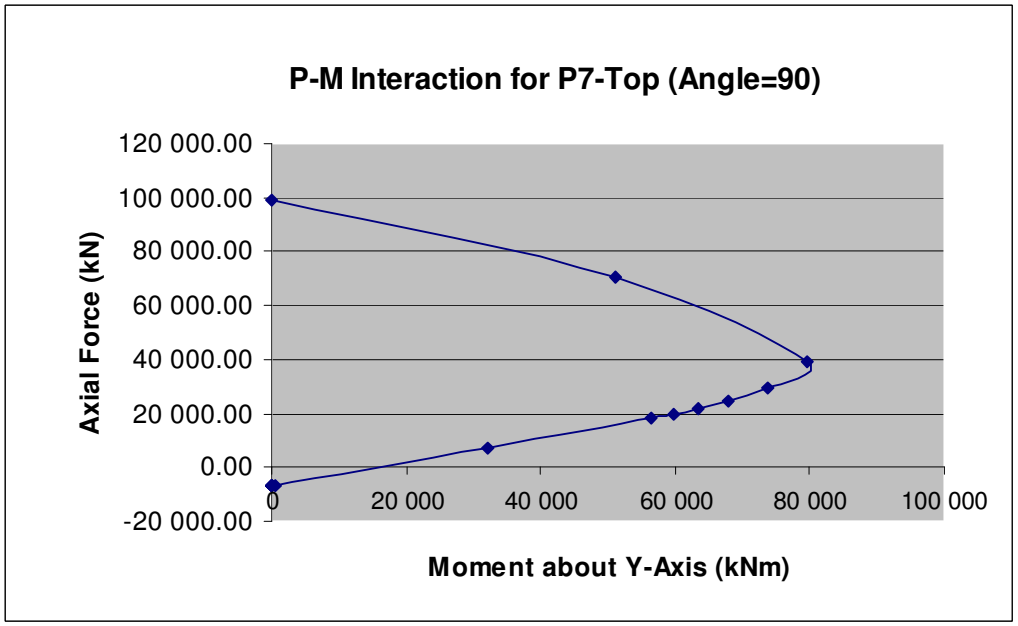

Figure B.7.2. P-M interactions at the top part of Pier 7 for angles 0, 45 and 90

APPENDIX C: EARTHQUAKE DATA IN TRANSVERSE DIRECTION

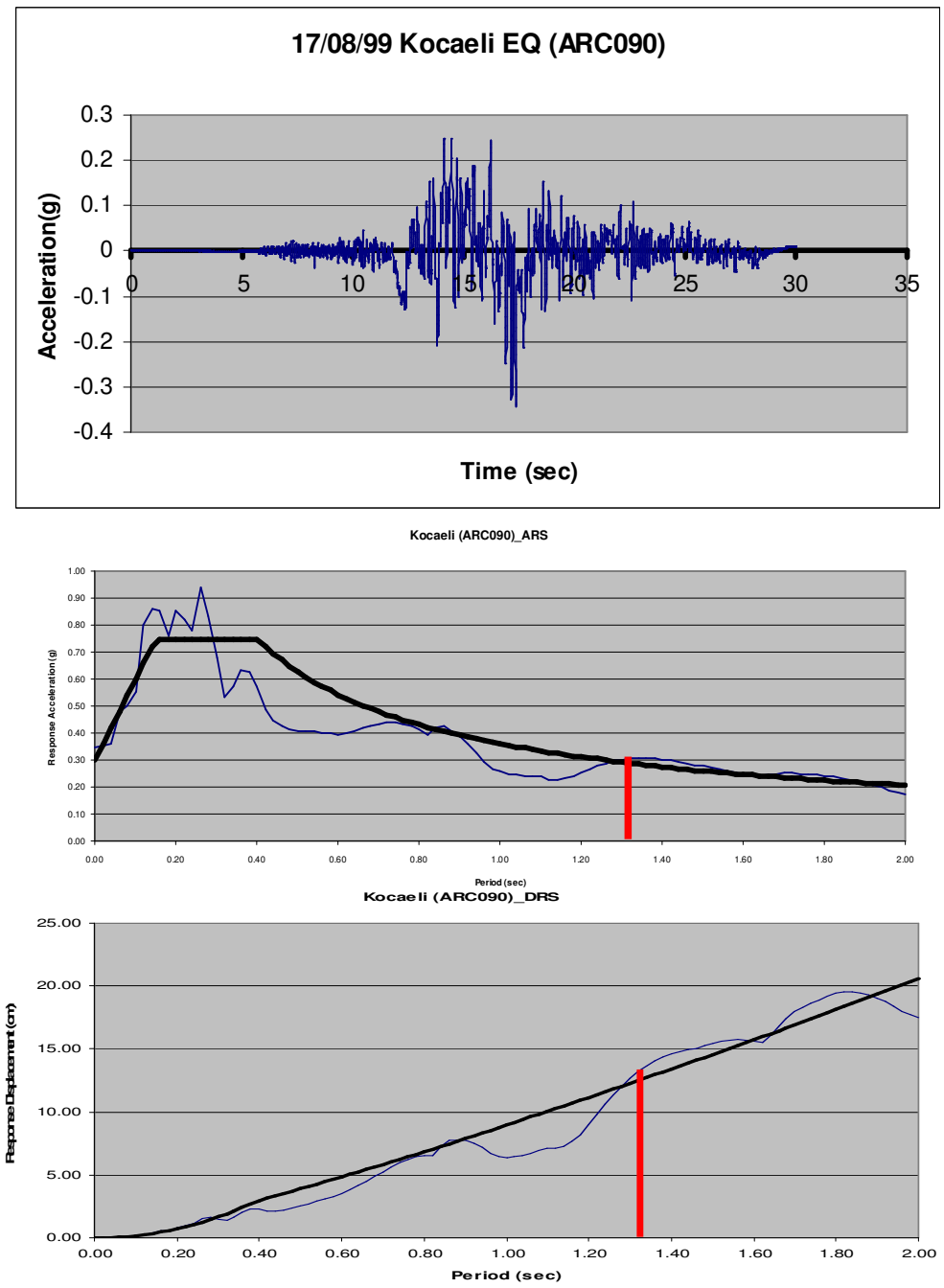

Figure C.1. Acceleration time h., ars and drs of kocaeli arcelik record

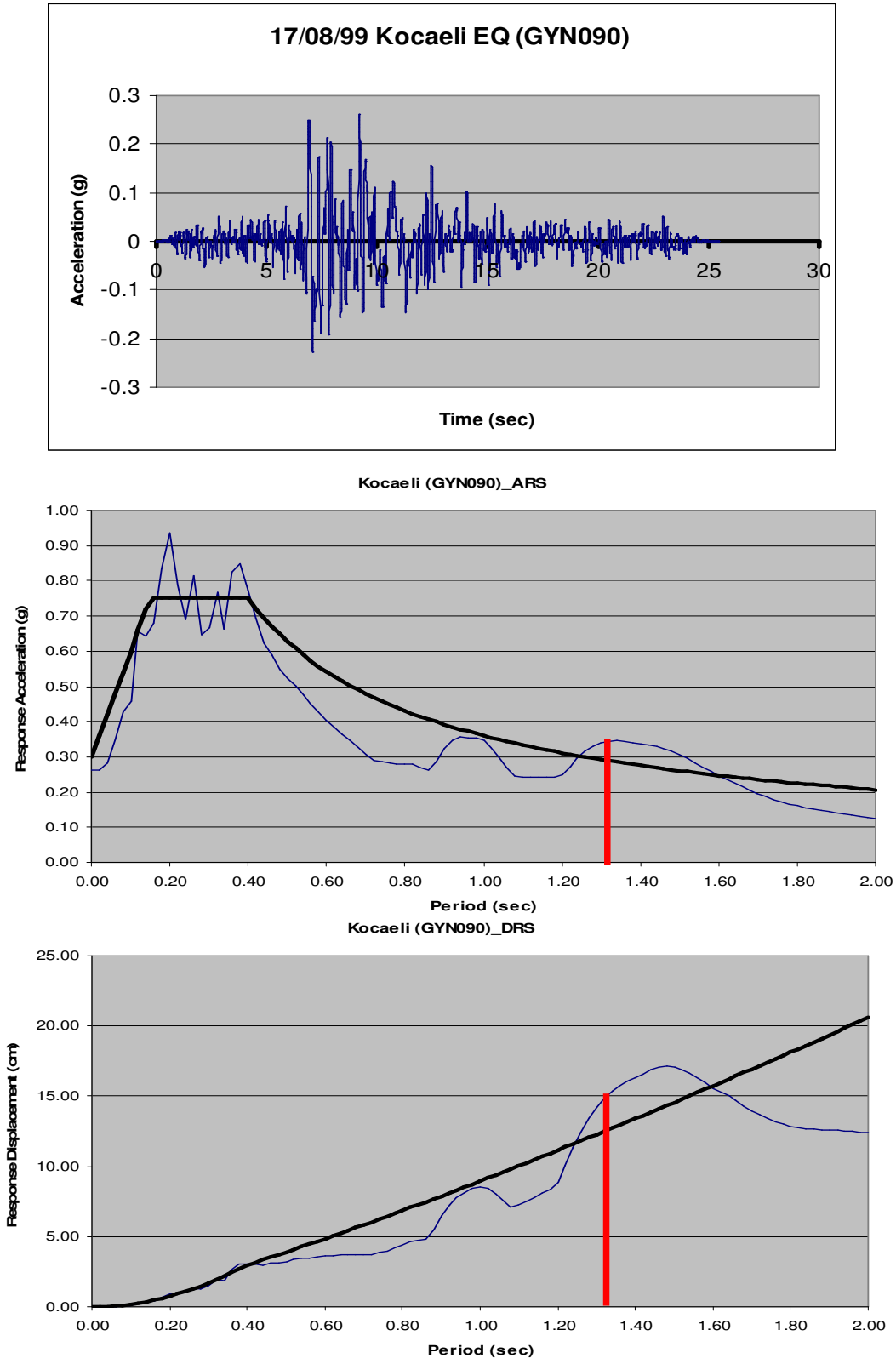

Figure C.2. Acceleration-time h., ars and drs of kocaeli goynuk record

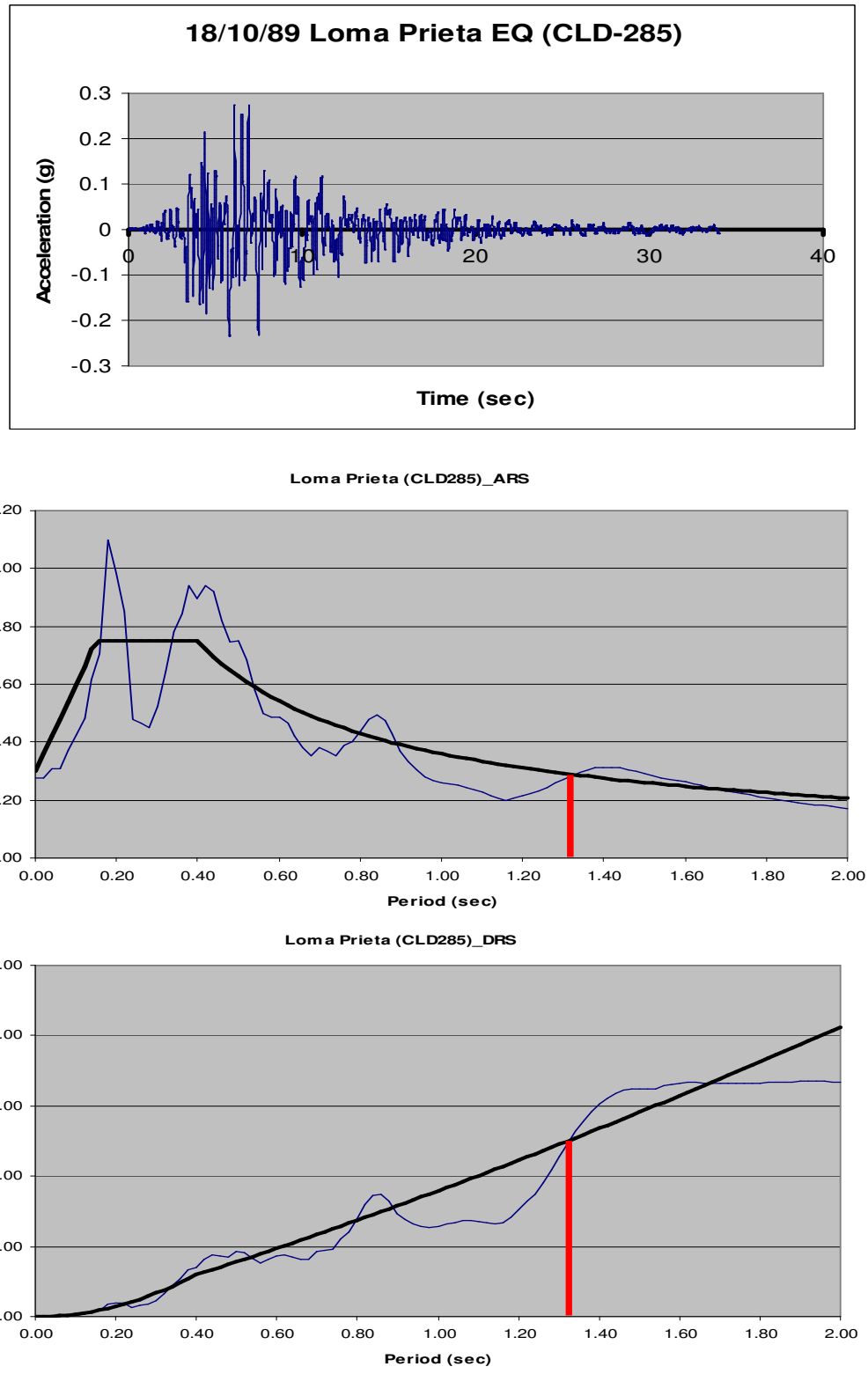

Figure C.3. Acceleration-time h., ars and drs of loma prieta (cld 285) record

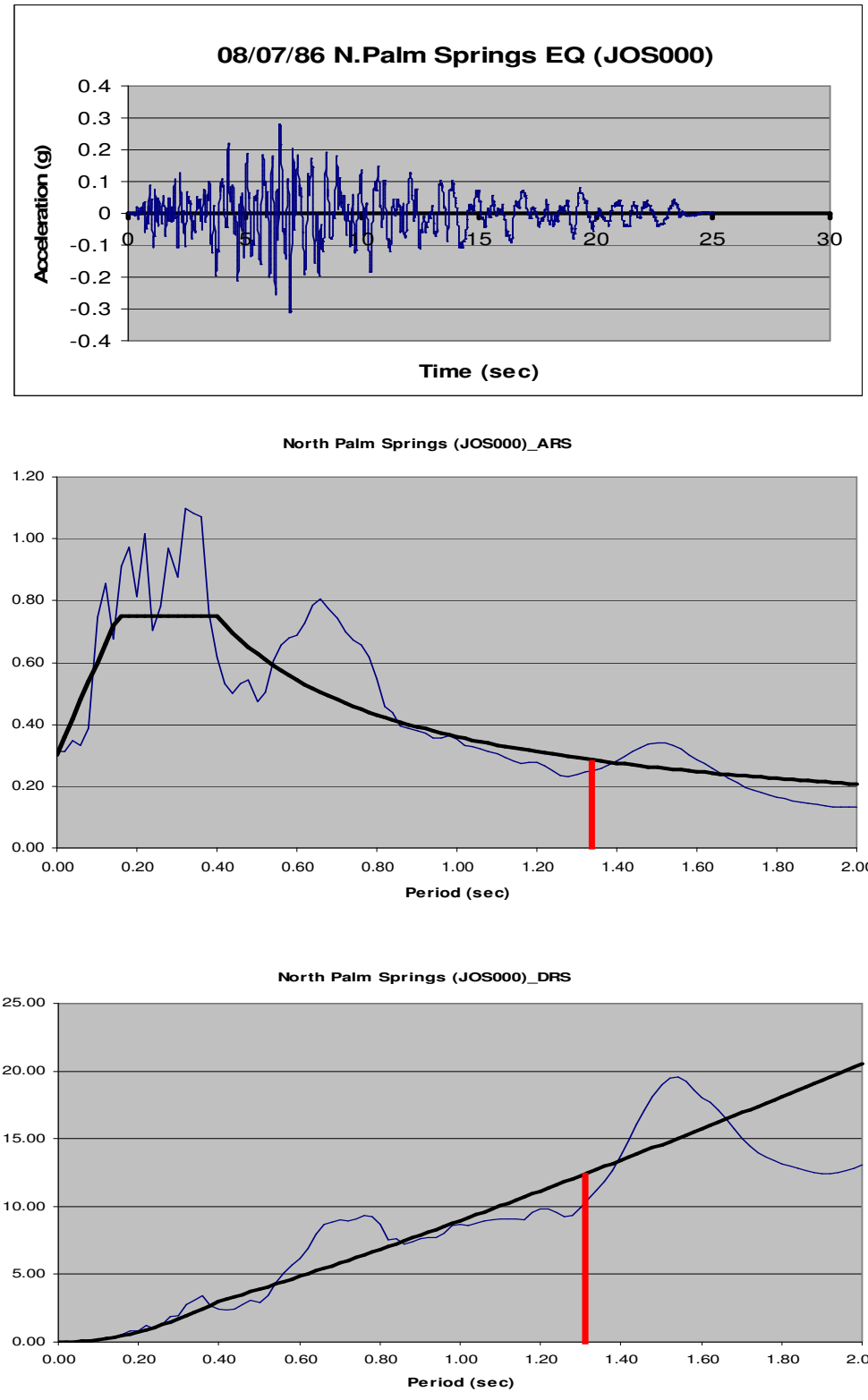

Figure C.4. Acceleration-time h., ars and drs of n.palm springs (jos 000) record

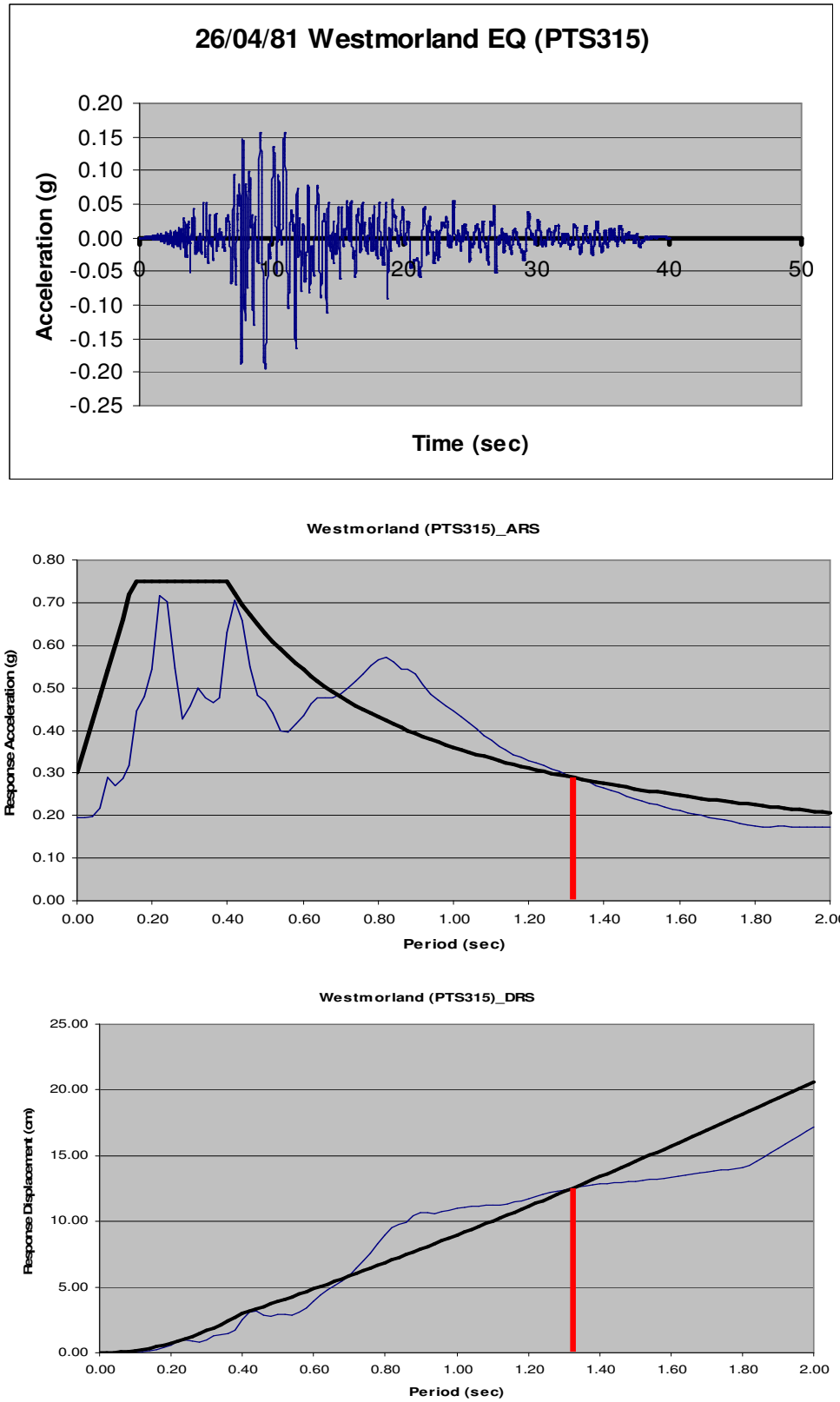

Figure C.5. Acceleration-time h., ars and drs of westmorland (pts315) record

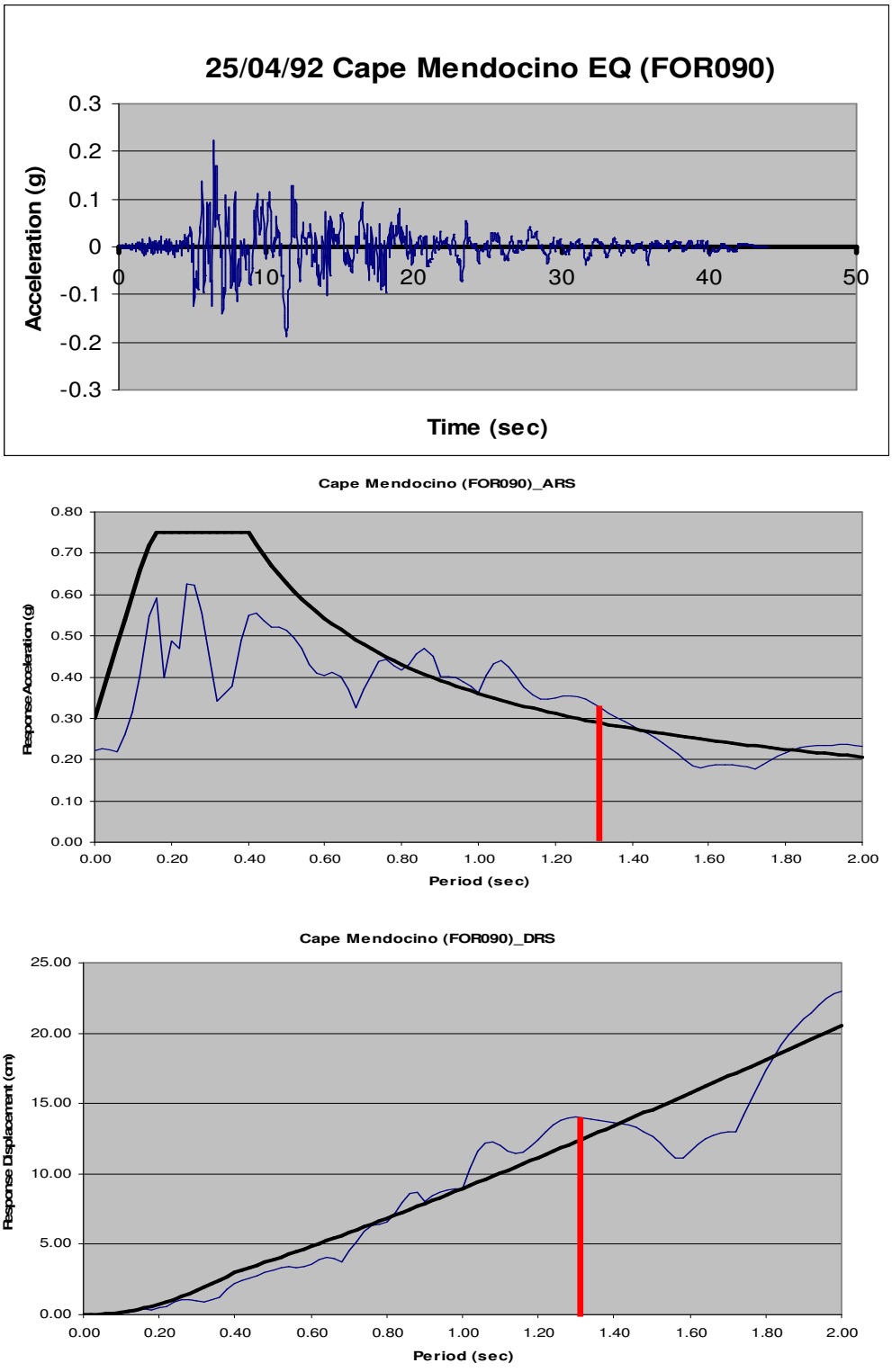

Figure C.6. Acceleration-time h., ars and drs of cape mendocino (for 090) record

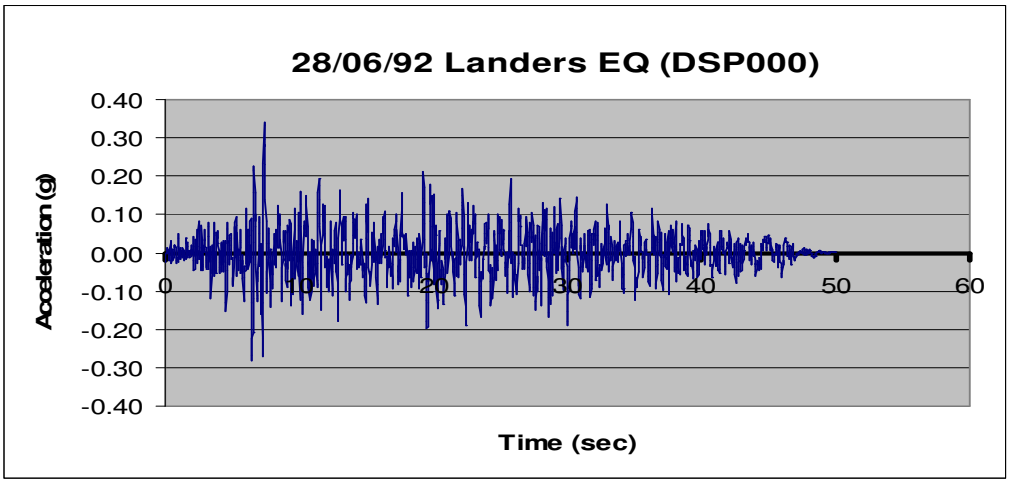

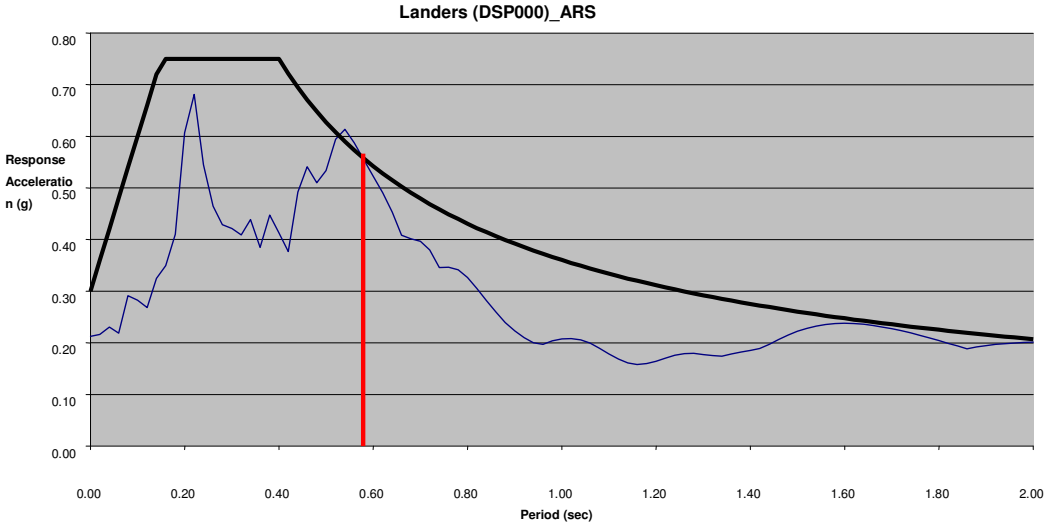

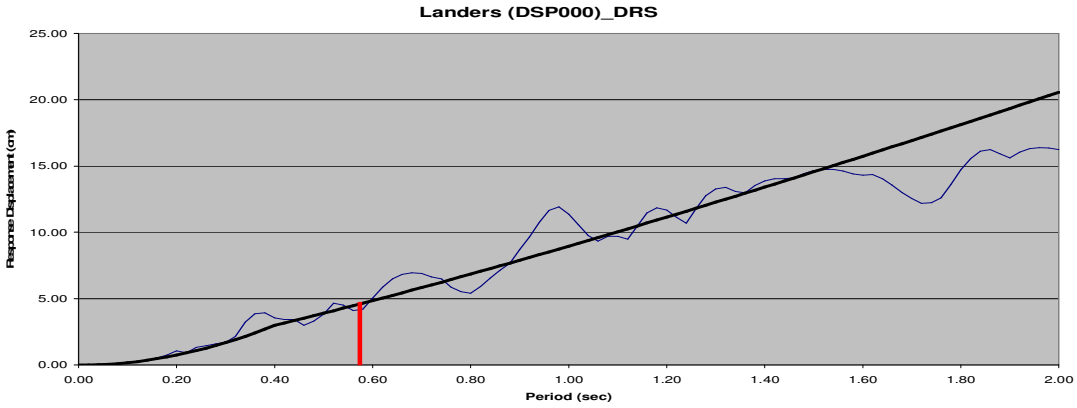

Figure C.7. acceleration-time h., ars and drs of landers (dsp 000) record

APPENDIX D: SAP2000 MODEL

D.1. General Model

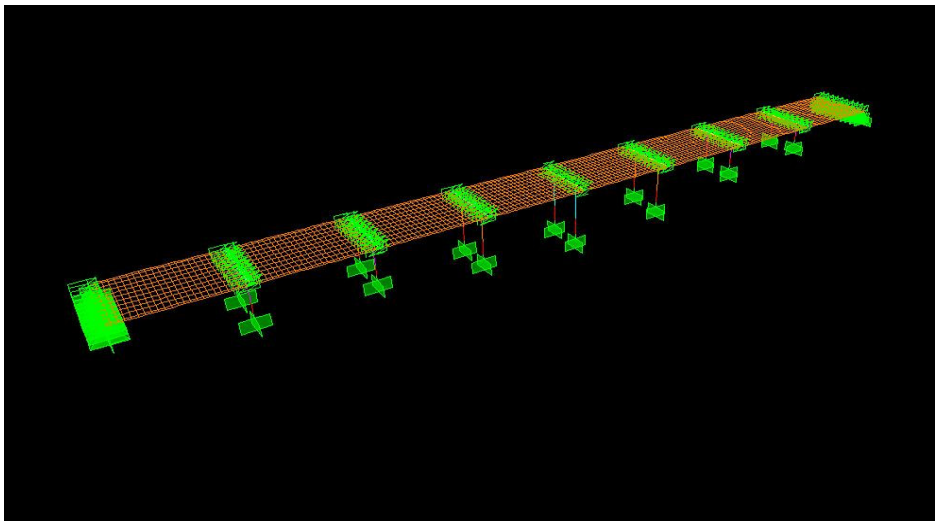

Figure D.1. Ortakoy v409 viaduct general model

D.2. Dominant Mode in Transverse Direction

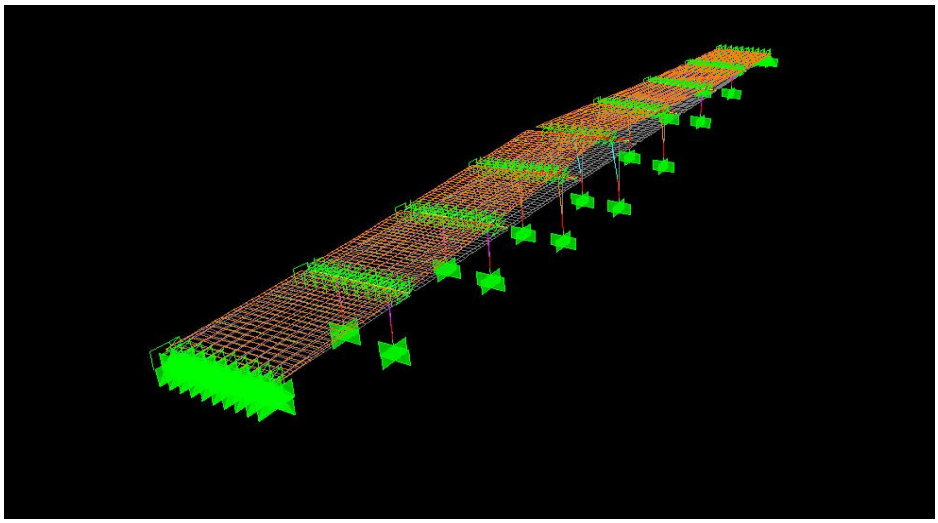

Figure D.2. T=1.365 second (dominant mode in transverse direction)

D3. Dominant Mode in Longitudinal Direction

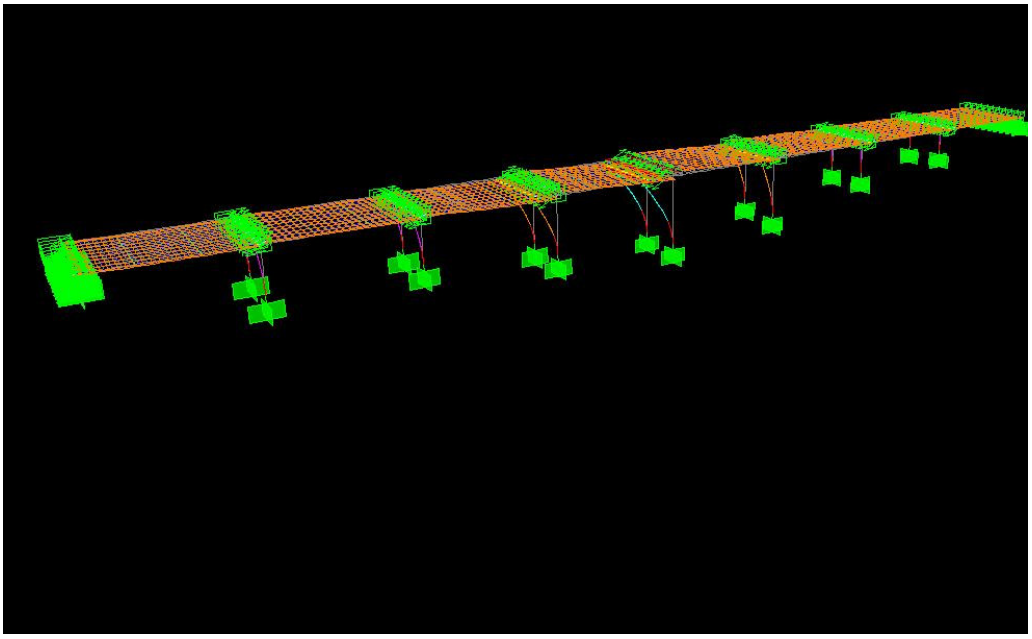

Figure D.3. T= 0.631 second (dominant mode in longitudinal direction)

REFERENCES

ABYYHY, 1998, *Afet Bölgelerinde Yapılacak Yapılar Hakkındaki Yönetmelik,* T.C. Bayındırlık ve İskan Bakanlığı, İlk Yayın Tarihi: 2.9.1997 – 23098 mükerrer sayılı Resmi Gazete, Değişiklik Tarihi: 2.7.1998 – 23390 sayılı Resmi Gazete.

Caltrans, 1999, *Bridge design specifications,* California Department of Transportation.

Celep, U., 2001, *Seismic Performance Assessment and Retrofit of the Ortaköy Viaduct (V408),* M.S. Thesis, Boğaziçi University.

Chopra, A.K., 1995, *Dynamics of Structures :Theory and Applications to Earthquake Engineering,* Prentice-Hall, New Jersey.

Elnashai, A.S. and McClure, D.C., 1996, "*Effect of modelling assumptions and input motion characteristics on seismic design parameters of RC bridge piers",* Earhquake Engineering and Structural Dynamics, Vol. 25, pp. 435-463.

Gumba GmbH, 2003, *Bearings for Bridges and Civil Engineering Structures,* Borken/Germany, http://www.gumba.de

Paulay, T. and Priestley, M.J.N., 1993, *Seismic Design of Concrete and Masonry Structures,* John Wiley and Sons Inc., New York

Priestley, M.J.N., 1995*, Myths and Fallacies in Earthquake Engineering,* John Wiley and Sons Inc., New York

Priestley, M.J.N., Mander, J.B. and Park,R., 1988, *Theoretical stres-strain model for confined concrete.* Journal of Structural Engineering,114(8):1804–1826, August.

Priestley, M.J.N., Seible, F. and Calvi, G.M., 1996, *Seismic Design and Retrofit of Bridges*, John Wiley and Sons Inc., New York

SAP 2000 Structural Analysis Program, 1998, *Integrated Finite Element Analysis and Design of Structures*, *Analysis Reference*, Vol.1, Berkeley, California.

Seismosignal Software, 2003, http:/ /www .seismosoft.com/Downloads / SeismoSignal.html

Wilson, E.L., 2002, *Three-Dimensional Static and Dynamic Analysis of Structures*, Computers and Structures Inc., Berkeley

XTRACT Cross Section Anaysis Program for Structure Engineers, 2002, Imbsen Software Systems, Sacramento.